Rician-K Factor Study for Temporal and Spatial Variations

Wadah Muneer

A Thesis

in

the

Department

of Electrical and Computer Engineering

Presented in Partial Fulfillment of the Requirements

For the Degree of Master of Applied Science (Electrical Engineering) at

Concordia University

Montreal, Quebec, Canada

December 2007

Your file Votre référence
ISBN: 978-0-494-40892-6
Our file Notre référence
ISBN: 978-0-494-40892-6

ABSTRACT

Rician-K Factor Study for Temporal and Spatial Variations

Wadah Mushriq Muneer

This thesis investigates indoor propagation by measurement and simulation using ray-tracing. An automated site survey measurement system is described. This site survey measurement system is used for measurements in two environments, a hallway and a microwave lab. Measurements were taken along a path at 1.5 cm intervals and at each point 30 time samples were taken, at 2 second intervals. Both the temporal and spatial variation of the signal strength are represented with Rician probability distribution functions. The Rician-K factor is computed by three methods found in the literature, called in this thesis the K_G / K_{24} method, the K_{12} method and the K_{MLE} method. The value of the Rician-K factor for the temporal data is investigated. Since the measured data revealed little time variation, high Rician-K factor values were found. The spatial variation of the received signal is investigated by taking the average of the temporal data at each distance point. The spatial variation of the Rician-K factor is investigated. The measured data showed rapid variation with distance, and thus small values of Rician-K factor were found. The two measurement environments are modeled for analysis by ray-tracing. The results obtained from the simulations are compared with the measured results. The comparison is based on four factors obtained from measured and simulated data: small–scale fading, path loss

index, large-scale fading and space-varying Rician K factor. The measured and simulated small-scale fading data matched poorly in the hallway. This is attributed to the wall model in the ray-tracing simulation, which is a poor representation of the actual wall construction. For the microwave lab, a more detailed representation and the location of the metal file cabinet and equipment gave good agreement between measured and simulated small-scale-fading. The path loss index indicates good agreement in the hallway and in the microwave lab between the large scale fading of the measurements and the simulations. Of the three methods for calculating the Rician-K factor, K_G / K_{24} is found to be the best for the large Rician-K factor values determined for time variations. However, the K_{MLE} method is the best to find the much smaller Rician-K factor values in space variations.

Acknowledgements

I would like to thank **Dr. C.W. Trueman** for his professional help and guidance throughout my thesis work, and **Dr. Davis** for his help in reviewing the thesis and for advising me.

The help of the following students is very much appreciated: **Russell Lobo, Meenakshi Venkat,** and **Imran Afzal** for building the prototype of the moving platform as part of their ELEC490 project. Lots of thanks again to **Russell Lobo,** who helped me even after the ELEC490 project was finished. And thanks to **Spyro Koukis** who provided me with the proper manuals to learn LabVIEW. Thanks to my friends, **Alaa Salman, Rafid Mendwei, Faris Jasem, Abdallah Al-Shehri, Esam Elsheh, Jason Casimir, Abdulhadi Abdulhadi, Ahmed Abumezwed** and **Jacques Athow**.

Finally I would like to thank my family, especially my parents **Dr. Mushriq Muneer** and **Dr. Manal Amin** for their support and their prayers to be a successful student. I would also like to express my gratitude to my **wife** for her support, and my **sister** and my **brothers** for their encouragement.

TABLE OF CONTENTS

Chapter Three

Chapter Four

Chapter Five

List of Figures

Figure

Abbreviations

EMC	Electromagnetic compatibility
Tx	Transmitter
Rx	Receiver
PDF	Probability Density Function
CDF	Cumulative Density Function
LOS	Line of Sight Path
NLOS	None line-of-sight path
GUI	General User Interface
EMI	Electromagnetic Interference
LabVIEW	Laboratory Virtual Instrumentation Engineering Workbench
VI	Virtual Instrument
GPIB	General Purpose Interface Board
GO_3D	Geometrical Optics Three Dimensional
ISM	Industrial Scientific Medical unlicensed band
RF	Radio Frequency
PC	Personal Computer
ASCII	American Standard Code for Information Interchange
KS test	Kolmogorov-Smirnov Test
PLL	Phased-Locked Loop
VCO	Voltage controlled Oscillator

List of Symbols

K	Rician value
K_{24}	K found from second and fourth moment
K_{12}	K found from first and second moment
K_{MLE}	K found from method of least square estimator
K_{CDF}	K found from the Cumulative distribution function
K_G	K found using the Greenstein method
PL	Path loss
P_t	Transmitted power
P_r	Received power
n	Path loss exponent
X_σ	Zero-mean Gaussian random variable
v	Receiver measured voltage.
Ω	Mean of the measured power
$I_0(\ )$	Modified Bessel function of the first kind, zero order
$I_1(\ )$	Modified Bessel function of the first kind, first order
v_m	The voltage value (peak)
σ^2	Variance of the measured voltage
μ_1	First moment of the measured voltage.
μ_2	Second moment of the measured voltage.
μ_4	Fourth moment of the measured voltage.

Chapter One

Background and Literature Survey

1.1 Applications and Motivations

For wireless communications and for electromagnetic compatibility, it is essential to characterize electromagnetic fields within buildings. Electric field behavior is highly dependent on the propagation environment [1]. Indoors, waves will experience reflection and absorption by walls, floors, ceilings and people. The resultant field pattern is unpredictable and complex [1]. Factors such as the materials of the walls, the frequency and power will affect the resultant field pattern.

To characterize indoor wireless fields for a certain indoor geometry, the values of the received field as a function both of distance and time must be known. These values can be found by two methods: actual measurements or simulation programs. Actual measurements are done by physically implementing a wireless channel (transmitter (Tx) with known frequency and transmitted power and a receiver (Rx)), recording the received field for variations in distance or time. This is called "site surveying". Simulation programs are based on site-specific propagation models [2]. These models in turn are based on detailed knowledge of the environment. Ray tracing, based on Geometrical Optics, is one of these models and is used in this thesis as our simulation program – specifically the GO_3D program [3][4].

The Rician probability distribution is often used in communications to model the fading of the signal strength in a wireless channel in an indoor context. It is used to evaluate that the probability that the signal strength is above the minimum needed for good communication. In EMC it is used to determine if the signal strength is so strong that it exceeds the immunity level of equipment. The immunity level of a device is defined as the maximum value of electric field strength that an electronic device can be exposed to without malfunctioning. A major objective of this thesis is to determine the value of the Rician-K factor that characterizes a room or a corridor, both by measurement and by simulation. For temporal variations of the signal strength, it will be shown that typical Rician-K factor values are comparable to 60 dB. For spatial variation, typical values are 10 to 20 dB.

The following Sections give a summary of radio propagation mechanisms and parameters. Model classifications are explained, and an empirical model, specifically "the Rician distribution" and its characterizing factor "Rician-K factor", are explained in detail. Four methods from the literature for evaluating the Rician-K factor are mentioned. Site specific models are also explained, including the thesis site specific model of interest the "ray tracing method". An abbreviated summary of previous indoor propagation measurements and measurement systems is presented, followed by the detailed objectives of this thesis.

1.2 Basic Radio Propagation Mechanisms

Reflection, diffraction and scattering are the three basic propagation mechanisms that govern radio propagation [1]. Reflection occurs when an electromagnetic wave hits an object that has large dimensions compared to the wavelength of the wave. The reflection coefficient is the parameter that relates the incident wave to the reflected wave. This coefficient is a function of the material properties and construction of the surface that the wave reflects from. It also depends on the wave polarization, the angle of incidence and the frequency of the propagating wave [5].

Diffraction occurs when the radio path between the transmitter and the receiver is obstructed by a surface that has a sharp edge [6][7]. Diffraction is based on the concept of Huygens' principle [5], which states that all points on the waveform are sub sources for the production of secondary wavelets and that these wavelets combine to produce a new wavefront. Other references [8] explain Huygens' principle as a method for finding subsequent positions of an advancing wavefront.

Scattering occurs when an object in the radio path has dimensions much smaller than the wavelength. Scattering can be described as disorganized reflection from a rough surface. Scattering sometimes adds extra strength to the received signal in a mobile environment. Objects such as lampposts and trees tend to scatter energy in all directions [5][8]. Scattering can make the actual received signal stronger than was predicted by reflection and diffraction alone. It occurs when the reflected signal impinges upon a

rough surface; the reflected energy is spread out (diffused) in all directions due to scattering [5]. A scattered signal is a multipath signal since the signal traveling from the Tx to the Rx will undergo multiple paths [9].

The resulting field obtained from the use of the propagation models is often very complex. It is a common practice to make a simplified model for a particular application. The next Section will discuss some of the more popular models and their associated parameters.

1.2.1 Radio Propagation Parameters

Path loss (PL) is one of the important parameters needed for the analysis of indoor radio-wave propagation. It is a measure of the losses the signal suffers when it reaches the receiver [6][7][10][11]. It is given as

$$PL(dB) = 10 \log \frac{P_t}{P_r} \tag{1.1}$$

where P_t is the power transmitted from the transmitting antenna and P_r is the power received at the receiving antenna. This measured parameter will help to determine the models used for the mobile channel. Some other studies [5][6][11] express path loss as a function of distance (d) and with the following formula

$$PL(d) = PL(d_0) + 10n\log(d/d_0) + X_\sigma \quad (1.2)$$

where n is called the path loss exponent [5] n is equal to 2 for free space. The value of n is less than 2 for indoor wireless channels. For indoor wireless channels this value depends on the frequency being transmitted, the geometrical shape of the environment being measured, the materials used in the indoor environments and the antenna height[12]. X_σ is a zero mean Gaussian random variable which accounts for the variation in average received power that happens when this type of model is used.

1.3 Model Classification

All models used in the indoor propagation channel are either empirical models or site-specific models. The main difference is that empirical models are easier to implement, whereas site specific models are more accurate but require a large amount of input data and considerable computation [7]. These models could be used on two types of data format for the received signal strength. "Large scale propagation" characterizes the received signal strength over large distances. It is also called "large scale fading". "Small scale propagation" accounts for the rapid fluctuation of the received signal over short distances. It is also called "small scale fading" or "Rayleigh fading" because if the multiple reflective paths are large in number and there is no LOS component the received signal is described by the Rayleigh probability distribution [5]. To show the "large scale fading" behavior of a signal with "small scale fading" behavior, the "small scale fading" will be averaged using a sliding window. The sliding window starts with the first

distance point and combines the number of points required to change the scale of the measured data from small to large distances. The next window starts by dropping one point on the left and adding one on the right, keeping the same window size, and so on. The next step is to average the data values for each window. The average value corresponds to the middle of the size of the sliding window. The next Section will speak about the Rician distribution as an empirical model example for a wireless channel, the empirical model used in this thesis.

1.3.1 The Rician Distribution "Empirical Model" and the Rician-K Factor

One of the important parameters that must be known for the wireless channels that follow the Rice distribution is the Rician-K factor. The Rician-K factor is a parameter that characterizes the Rician probability distribution and which is also called the Rice distribution. A wireless channel can be statistically characterized to follow a Rician distribution when there is a dominant signal present such as the (LOS) propagation path between the transmitter and the receiver. Some studies [14] suggest that for extensive temporal variations or fast fading analysis when there was no LOS between the Tx and the Rx, the distribution of the measured data was also Rician and it fits the measured data inside office and university buildings. The Rician distribution probability density function (PDF) is given by [1][17].

$$f(v)=\frac{2(K+1)v}{\Omega}\exp\left(-K-\frac{(K+1)v^2}{\Omega}\right)I_0\left(2v\sqrt{\frac{K(K+1)}{\Omega}}\right) \tag{1.4}$$

where v is the measured voltage at the receiver of the wireless link, K is the Rician-K factor which is given by $v_m^2/2\sigma^2$, v_m is the voltage value (peak) of the LOS path between the Tx and the Rx of the channel, σ^2 is the variance of the measured voltage of the receiver of the wireless link, Ω is the mean of the measured power of the receiver at the wireless link, and $I_0(\ )$ is the modified Bessel function of the first kind and zero order.

The cumulative distribution function (CDF) of the Rice distribution is given by[18]

$$F(v) = 1 - \exp\left[-\left(K + \frac{v^2}{2\sigma^2}\right)\right]\sum_{m=0}^{\infty}\left(\frac{\sigma\sqrt{2.K}}{v}\right)\cdot I_m\left(\frac{v\sqrt{2.K}}{\sigma}\right) \tag{1.5}$$

where $I_m(\ )$ is the modified Bessel function of the first kind and m order

The Rician probability distribution is used to model wireless channels where there is a strong deterministic signal component and a lower-level random signal component. In this thesis, the strong signal component is associated with a line-of-sight (LOS) path joining the transmitter to the observer. The random signal component models the many reflections from the walls, floor and ceiling. The phase of the field associated with each reflection path is modeled as uniformly distributed, and the various reflected fields combine to form a random variable with a Rayleigh distribution. The Rician K factor is the ratio of the power in the direct field to the power in the reflected field. When the direct field strength is much larger than the reflected field strength, K is large, such

as 60 dB, and the Rician distribution can be approximated as a Gaussian distribution with a small spread of values around the mean, corresponding to a low standard deviation [7]. The field strength deviates very little from the mean value and is almost deterministic. When the direct field strength is not very much greater than the reflected field strength, K is not large, such as 10 dB, and the Rician probability density shows a large spread of values around the mean, corresponding to a large standard deviation, and the Rician distribution can be approximated with a Rayleigh distribution [7]. The field strength has a large random component and varies over a wide range.

1.3.2 Rician K Factor Evaluation

Given a set of measured voltage data in linear scale $\{v_l : l = 1 : N\}$ where N is the number of samples being measured, and this set, which is the square root of the set of power measured data in linear scale $\{p_l : l = 1 : N\}$, then from the set of measured voltage data, the Rician-K factor can be estimated. Four methods to estimate the Rician-K factor are found in the literature. In [19], the Rician-K factor found from this method will be called here K_G in honor of first author Greenstein. In [20][21] the Rician-K factor is found from two methods. One is called here K_{24} because it is based on finding the second and fourth moment. The other method is called here K_{12} because it is based on finding the first and second moment. In [20][22] the Rician-K factor found from this method is called here K_{MLE} because it is based on the method of least square estimator. Each method will be described in detail in Chapter 3.

1.3.3 Ray Tracing "Site Specific Model"

One of the site specific models used in radio propagation is the ray tracing method, based on geometrical optics. It assumes that energy from the EM wave can be considered in terms of rays. This is a simple representation of the EM wave mechanisms [2]. One type of ray tracing is the image method. It assumes that when the ray is reflected from a wall, an image of the source is generated behind that wall, which gives back the reflected wave with an attenuation factor. This concept is the basis of the GO_3D program used in this thesis [3][7][9]. In this thesis the GO_3D Ray Tracing program will be used [3][4]. The GO_3D Ray Tracing program shows the field behavior when radiating from the transmitter source; at each wall rays are incident on, and then each image source acts as another transmitter and transmits the ray again. This is equivalent to a ray that is incident on the wall and then reflected from the wall again, the number of reflections to be considered on each wall gives the number of levels on the image tree. More details about the image tree concept can be found in [3].The next Section will speak about previous studies on indoor propagation measurement systems.

1.4 Indoor Propagation Measurement Systems

When any measurement campaign is performed, the need for a measurement system arises. In all measurement campaigns, although the measurement systems differ from each other, they all have common parts. Each system consists of a transmitting unit with known parameters such as the gain of the transmitting antenna, transmitting

frequency, output power, polarization, and radiation pattern. The receiving antenna, also with known antenna parameters and the added value of the antenna factor to transform the voltage measured to an electric field, and measuring devices such as a spectrum analyzer for CW wave single tone frequency or a vector network analyzer for broad band frequencies connected to a computer, and the receiver antenna moving on a predefined path with known steps and via different tools all combine to make up the measurement system. This Section describes measurement systems found in the literature for indoor propagation.

In [23] an automated guided vehicle (AGV) was developed to use in indoor propagation measurements. This AGV provides an accurate estimate of position, which is very useful in measurements. Many types of AGV's rely on what is called dead reckoning, where distances are computed by integrating the distance traveled by one or more vehicle wheel. Here the AGV carries the microwave receiver, including the receiving antenna and spectrum analyzer used in measurements. It has a front wheel containing a steering motor and a drive motor. Each rear wheel has an optical shaft encoder that is translated into distance and path curvature information .

In [24], the AGV is called a robot. The concept has it following a predefined path on the ground. Two sensors on the front of the robot follow a predefined path, made with black electrical tape on the floor. The receiver was mounted on the top of the robot using a PVC pipe, holding a calibrated dipole antenna connected to a spectrum analyzer. The robot platform had one fixed front wheel with an optical encoder to determine the

distance moved by the robot, and two rear wheels. The transmitter in the system was an analog cellular telephone with 850 MHz frequency and 600 mW output power or an RF signal generator at 1900 MHz.

In [25] the measurement approach was quite different. The measurement was to detect electromagnetic interference (EMI) in a hospital environment and at fixed locations. The approach has more to do a with a computer system, which had a general user interface (GUI) to take readings in various hospital environments, and to show if any cases of EMI occurred in the hospital environment. The computer program used in measurements uses LabVIEW programming language. It is the state-of-the-art program in measurements, and it enables the computer to take readings from a spectrum analyzer connected to the computer via a GPIB card. LabVIEW is a visual programming language provided by National Instruments company and it is a very useful tool in data acquisition. LabVIEW version 8.0 has been used in this thesis [26][27].

In [28] a mobile robot platform was developed to provide a mechanism to determine the accurate position of the robot using odometry equations. These are easy to implement but there is the drawback of error accumulation as the travel distance increases. The general concept of the robot mechanism is the same as in [24] but with different design layouts and different microcontrollers. The next Section provides information about indoor propagation measurement results.

1.5 Indoor Propagation Measurement Results

In any measurement campaign, after the data has been collected a meaningful interpretation must be given. This meaningful interpretation is done by statistical interpretation. One method to interpret the data is to characterize it using certain statistical parameters. This Section gives a survey of the characterization of measured data from measurement campaigns using the Rician-K factor.

In [29] measurements were performed to investigate the Rician K Factor (in dB) for four different measurement environments, and for LOS and NLOS cases. The four different measurement environments were: small room, hallway, stairwell and a lecture theatre. The small room had work benches heavily equipped with computer equipment. The hallway was free of any obstructions and had doors both sides closed during the measurements The hallway was open at one end. The stairwell had two set of stairs going downwards and one doorway. The lecture theater was a typical lecture theater environment. For all environments the Tx antenna was moved to eight locations and the Rx antenna was at a fixed location. For the small room the K value was the highest for a LOS case and the lowest for the NLOS case, for the hallway the K value was approximately the same for all positions. For the stairs, the lowest value was in a location that had an obstructed line of sight, and the highest one was for the location that had a clear LOS . In the lecture theatre all values of K were virtually the same. The values of Rician-K factor obtained ranged from 1.8-4.7 dB.

Another indoor measurement study in a hospital environment [25] used completely automated software in analyzing and taking measurements. The software was produced using LabVIEW. The software, known as PRISM, was designed for ease of use and can be monitored from remote areas. Measurements were done for the electric field at the same points for different times in the 2.4 GHz ISM frequency band. Results showed some constant behavior for the electric field during the different times of measurements.

Another study [30] was done in Spain at the University of Cantabria campus. Three measurement scenarios were performed. Each scenario corresponds to a different environment. The measurement system was totally automated. The receiver was moving and the transmitter was fixed. The movement of the receiver was controlled by the computer via a serial port, and at the same time the computer recorded the readings from the spectrum analyzer using the GPIB interface. LOS path scenario measurements for 1.8 and 2.5 GHz were made. The same scenarios were also simulated using a GO computer-based program. For the results of measurements and simulations the values of the Rician-K factor that were calculated showed a good agreement . The Rician-K factor was found for the entire path, denoted as Kwhole, and for windows along the path which were represented by their maximum, minimum, and mean value denoted by Kmax, Kmin, and Kmean. The values of Rician-K factor found ranged from 0 - 3.45.

In [31] measurements were performed at 2.4 GHz, in a large engineering lab at the University of Oxford. The Rician- K factor was investigated, and it showed that it has constant and small values for NLOS conditions along the path being measured. For the LOS conditions, the Rician-K factor goes up to 170, for a corresponding Tx, Rx separation of 2 meters, and then is varies After the 2 meter Tx, Rx distance the Rician-K factor value varies, down to a minimum value of approximately 10 at a distance of 30 meters. Also, the value of K for LOS conditions shows a decreasing behavior as the Tx, Rx distance increases. The values of the Rician-K factor found ranged from 0-200.

The Rician-K factor values were evaluated from a large set of wireless indoor propagation measurements in [32]. The data collection procedure was organized in the following manner: both the transmitting and the receiving antennas were mounted on an arm that rotated in the horizontal plane. Narrowband RF power was measured at 1.92 GHz and recorded. One thousand data points were calculated as both the Tx and the Rx were moving. This procedures was repeated at 400 locations. Some locations were line of sight and others were obstructed locations. The author calculates the Rician-K factor based on finding the mean and variance from the 1000 data samples calculated at each location. The author does not state the reference he relied on for the method used to calculate the Rician-K factor. His calculated Rician-K factors for the measurements he performed showed peaks and nulls, the values ranged from 20 to -25 dB. The Rician-K factor plotted graph shows that the high values were for line of sight locations, while the low values were for obstructed locations.

In [33], measurements were performed at 2.4 GHz, at the cooperative research center for broadband telecommunications and networking laboratory at Curtin University of Technology, Australia. They used a typical laboratory environment, with a middle work bench, two right and left side benches and a door open to the hallway. The measurement scenarios had the Rx antenna fixed and ten different locations for the Tx antenna were considered. One was an LOS condition facing the open door at the hallway, and the remaining nine others were NLOS conditions. At each of the ten Tx, Rx, fixed wireless link there were three scenarios when measuring the received power, no movement, three people moving, and six people moving in a similar manner within a two meter radius around the Rx. Four representative Rician-K factor value results are shown from the previous arrangement made for measurements. Three values of K from the four shown were for the three people moving around the Rx antenna. The highest value of K was obtained for the largest NLOS Tx, Rx separation. The fourth value was for six people moving around the antenna, which gave a the smallest value of the Rician K factor for the whole four which is 1.3. The four values for the Rician K factor shown were 1.3, 2.0,2.0 and 8.7.This shows the Rician-K factor is higher when less people are moving around the measurement setup and higher at larger Rx, Tx separation for NLOS conditions.

Rician-K factor measurements were performed in a multi-storied building in [16]. These survey results were used to find the Rician-K factor for a spatial variation of the received power. Here it was determined that higher values of K are found in LOS conditions while low values of K are found in NLOS conditions, and typical values for

the Rician-K factor were from 0 – 6.6. In [34], the Rician-K factor for the temporal variations of the RF received power was found. Estimating the Rician-K factor value was based on the best fit of the measured data empirical CDF with the CDF found from applying the Rician CDF formula. The highest value of K was for a short LOS path and the lowest value of K was for a location of the Tx where the multipath signals dominated the main path. The measured Rician-K factor ranged between 0-20. In [35], measurements were done in a tunnel with different scenarios. The results show that slow fading did not match the lognormal distribution as sometimes anticipated by other references. Also shown was that the fast fading of measurements in straight Sections in a tunnel correlates well with the Rician distribution while fast fading signals for curved Sections does not closely fit the Rayleigh distribution, and higher frequency signals exhibit more fluctuations for the received signal versus distance. The comparison criteria was developed by comparing the CDF for the measured data with a theoretical Rician or Rayleigh CDF. The next Section presents the objective sets for this thesis.

1.6 Objectives

The objective of this thesis is to study the behavior of the Rician-K factor for an indoor wireless channel. Four methods from the literature are used to calculate the Rician-K factor from the measured received power. Two environments are used as case studies: a hallway and a lab. Measurements are performed using a site survey system designed to be an automated system and that accounts for spatial and temporal variation of the received signal power. Simulations for the same environments are done using a ray tracing program, in order to have a simulated version of the measured data that accounts for spatial variation only. The simulated data version is compared with the measured data to see if the ray tracing models generated for the two environments provide a good match with measured data. The comparison between measured and simulated data is based on comparing the following: small scale fading, path loss index n, the space varying Rician-K factor and the large scale fading for both measured and simulated data.

1.7 Overview of Thesis

Chapter 2 describes the site survey measurement system. For the hardware, survey supporting block diagrams and pictures are given with full explanation of each part. For the software, flowcharts are given for the programs used to operate the robot and for the control unit. The flow chart of the control unit program also shows the communication between the control unit and the robot's microcontroller.

Chapter 3 investigates the temporal variation of the received power. Measured data was obtained for two environments, the hallway and the microwave lab. Four representative distance points between the transmitter and the receiver were chosen, and the time varying received voltage level is graphed. The difference on a linear scale between the maximum and the minimum values for time varying voltages at each distance point are graphed in dB and are called as the range of variation of voltages. Four methods for calculating the Rician-K factor from measured sampled data from the literature are presented, and the time varying Rician-K factor values are calculated using all four methods.

Chapter 4 investigates the spatial variation of the Rician-K factor for two environments, the hallway and the microwave lab. At each receiver, transmitter separation of the average value of the time varying received voltage is found. The average value is graphed as a function of the distance between the transmitter and the receiver. This is also known as the small scale fading of the measured data. A sliding

window is moved along the small scale fading measured data. The large scale fading for the measured data is found by averaging each sliding window set of data and corresponding this value to the middle point of the size of the window. Then the space varying Rician-K Factor values are calculated for each set of data of the sliding window, using the methods presented in Chapter 3.

Chapter 5 shows how ray-tracing method is used to simulate two environments, the hallway and the microwave lab. The ray-tracing based GO_3D program calculates the received electrical field. A method to calculate the received voltage across a 50 ohm load from electric field strength is presented. comparison between measured and simulated voltages is based on four factors, small-scale fading, path loss index, large scale fading and space-varying Rician-K factor.

Chapter 6 summarizes the thesis and presents the conclusions. The best method to calculate the Rician-K factor is described, based on comparison between measured and simulated data, and the agreement and disagreement they present based on the comparison criteria used. Some recommendations for future work are presented.

Chapter 2

The Measurement System

2.1 Introduction

In this Chapter the complete site survey system will be described, including the hardware utilized and the software programs that were developed.

2.2 The Site Survey System

Figure 2.1 shows a block diagram of the site survey system, which has three main parts: the transmitting unit; the robot; the receiving unit and the control unit. The transmitting unit transmits between 2.3 to 2.5 GHz in the ISM band. The robot is a microcontroller-based moving platform that is equipped with a 900 MHz wireless link to communicate with the control unit. The receiving unit consists of a calibrated dipole antenna connected to the HP8569B spectrum analyzer, and the control unit is composed of a desktop PC equipped with a GPIB card and a 900 MHz wireless communication link to the robot. Figure 2.2 shows the actual site survey system used in measurements, the robot carries the transmitting unit and moves following the white tape on the floor.

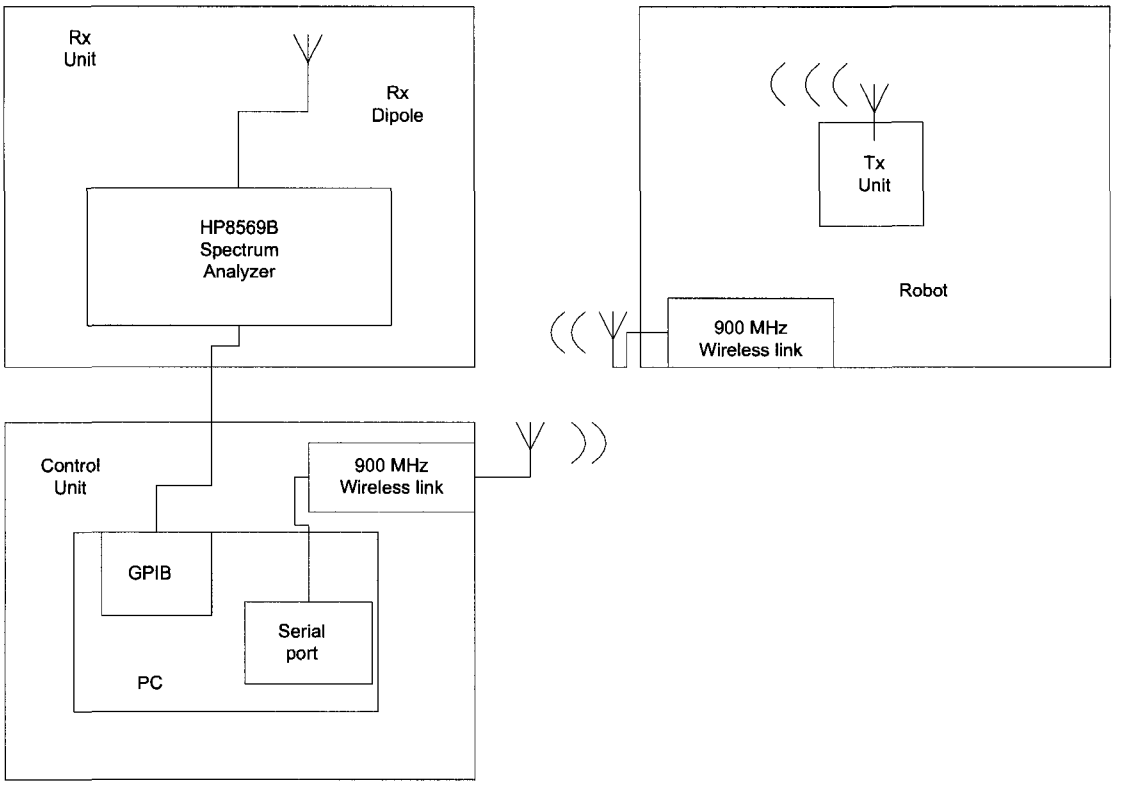

Figure 2.1 Block diagram of the site survey measurement system.

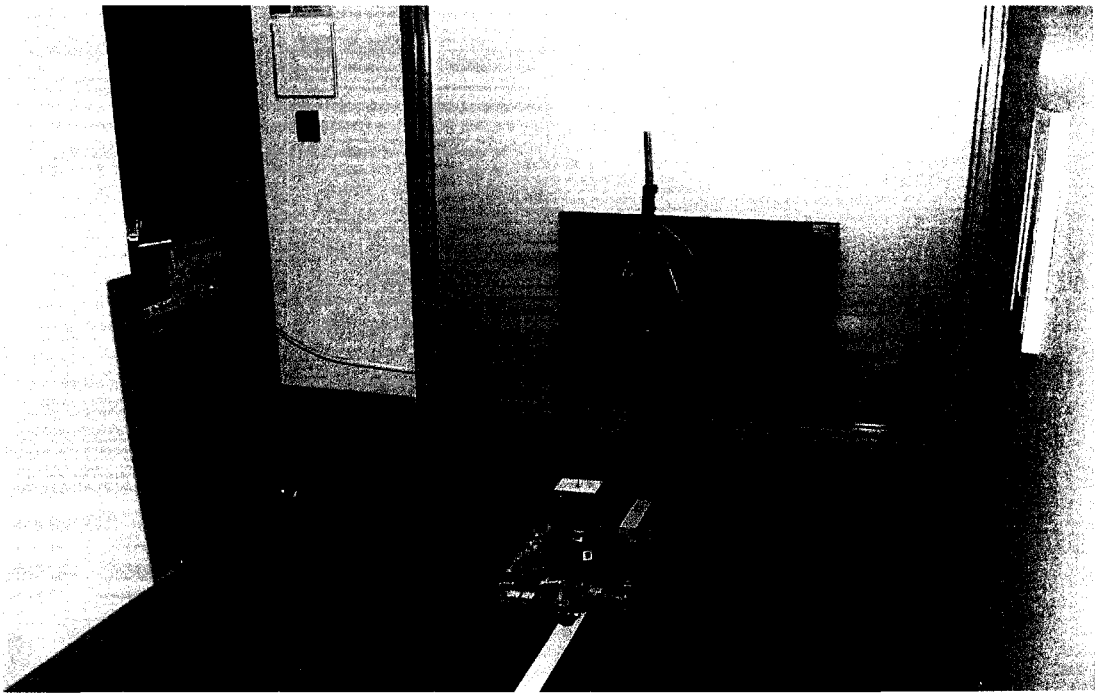

Figure 2.2 The site survey system.

The site survey measurement system was designed to measure the spatial and temporal variations of the received RF signal power level, and then write them to a text file on the computer in a predefined format. This text file will work as an input file for post processing applications. This site survey measurement system has already gone through two versions[12][36]. The first was only a prototype of a moving platform with the Tx unit [36], and the second version, semi-automated, has a moving platform as described here [12]. The control unit (PC) has a LabVIEW program that captures data from the spectrum analyzer using a GPIB card for communication. Control of the robot's movement is done using a 900 MHz wireless link between the control unit and the robot. The current version of the site survey system is fully-automated using a LabVIEW program. This program has a control part and a measurement part work with each other in a correlated manner to provide this automation property.

The automated concept of this system which is the communication between the robot and the control unit is explained in Section 2.6 of this Chapter. Each part of the site survey system will be described in detail in the following Sections. The earlier steps taken to make the prototype of the mobile platform and some measurements related to it can be found in [12][36].

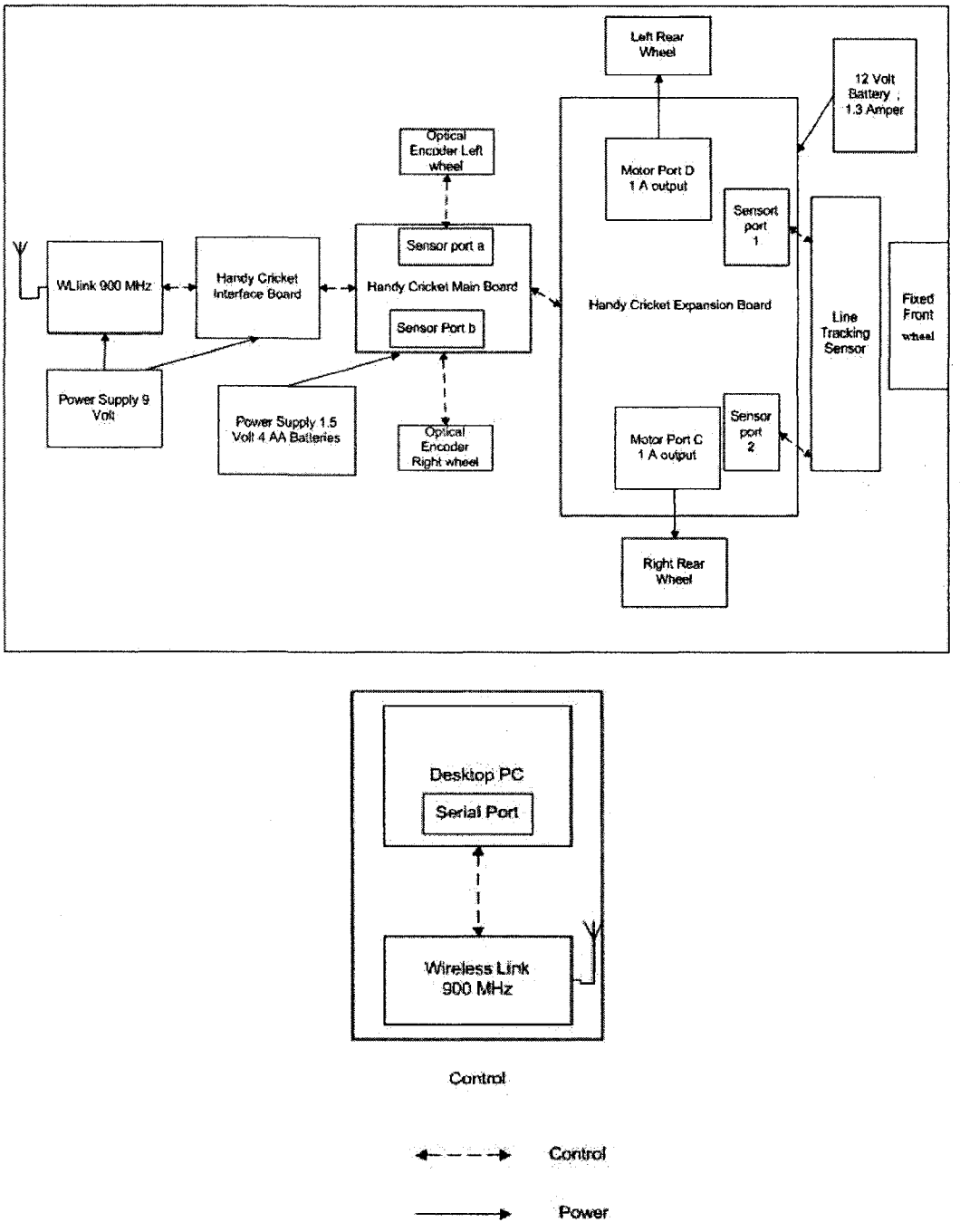

Figure 2.3 Block diagram of the robot and the control unit.

2.3 The Robot

Figure 2.3 is a block diagram of the robot and the control unit, and Figures 2.4 and 2.5 show photographs of the robot from the top and the bottom, respectively. The "Handy Cricket Board" controls the operation of the robot [12][36], shown as a block diagram in Figure 2.3, and close to the right rear wheel of the robot in Figures 2.4 and 2.5. It has two sensor ports, connected to the optical encoders that are coupled to the rear wheels, and which are operated by two DC motors. These two DC motors are shown as block diagrams in Figure 2.3 and are facing the two rear wheels in Figures 2.4 and 2.5. The two DC Motors need to draw a high current to operate, and this high current is provided to them via the Handy Cricket extension board, shown as a block diagram in Figure 2.3 and located near the front wheel in Figures 2.4 and 2.5. This board is powered by a 12 volt battery with 1.3 ampere, as shown as a block diagram in Figure 2.3 and located between the two rear wheels in Figures 2.4 and 2.5. The Handy Cricket extension board has two motor ports and four sensor ports: two of these sensor ports are connected to the line tracking sensor board, shown as a block diagram in Figure 2.3 and mounted on two supporting metal stands behind the front wheel, as can be seen in Figures 2.4 and 2.5. The line tracking sensor board facilitates the movement of the platform on a predefined path, which is a masked tape that is applied to the floor where the robot will be moving. The tape must be black if the floor is light-colored and white if the floor is black or dark- colored. More details can be found in [12].

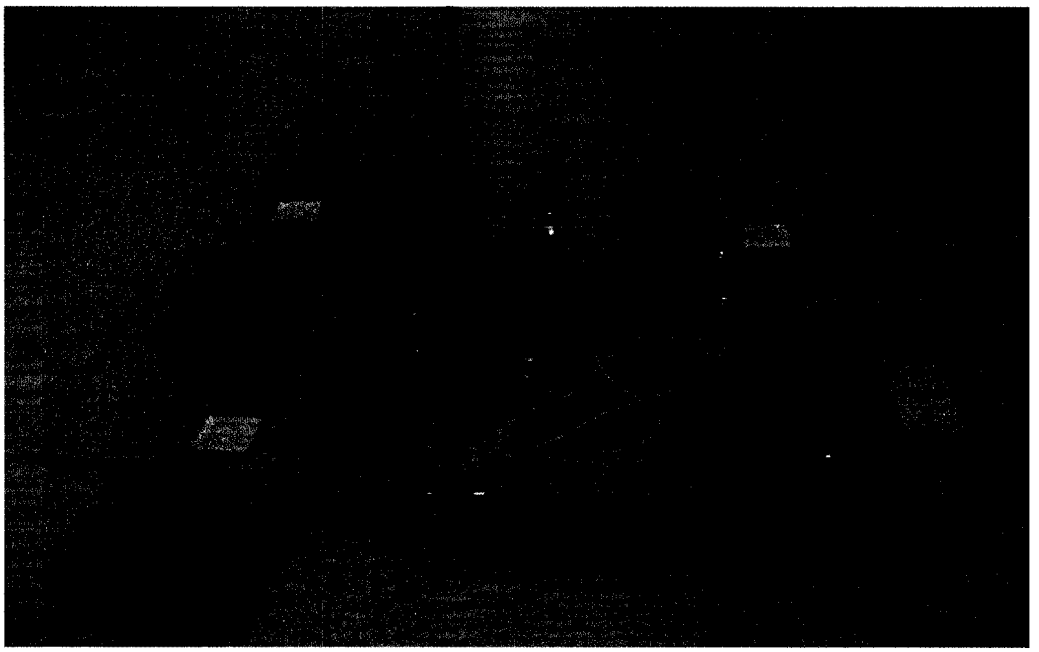

Figure 2.4 Top view of the robot.

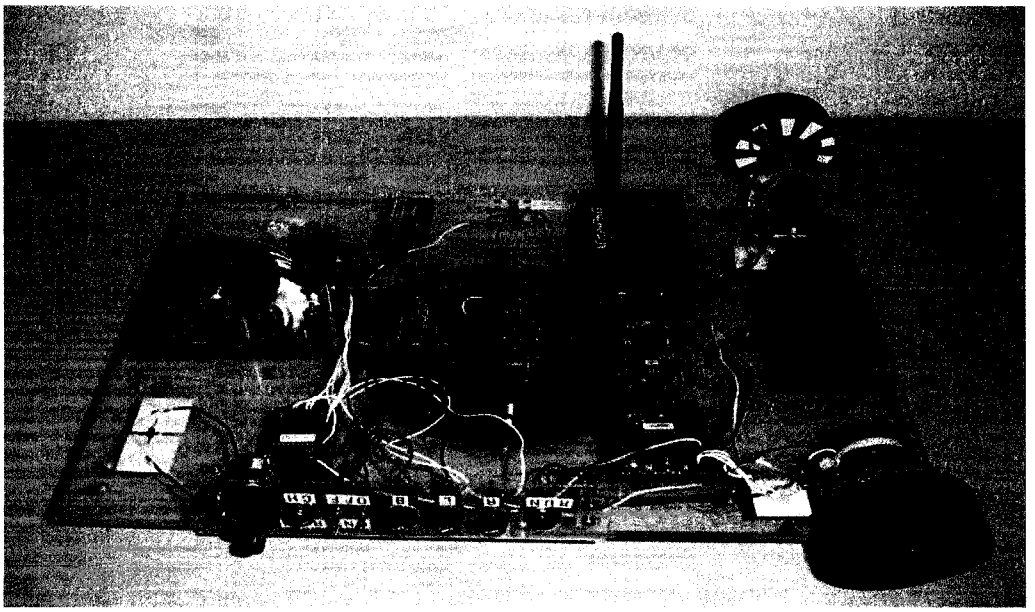

Figure 2.5 Bottom view of the robot.

2.3.1 The Cricket Logo Software

The robot is controlled by the Handy Cricket board, which uses a programming language called “Cricket logo”. This cricket board includes a "Cricket logo" interpreter. Programs in "logo" are downloaded from a PC to the cricket board via the infra-red (IR) cricket serial interface and then executed independently on the microcomputer cricket board. In other words, once the "logo" program is downloaded to the robot's computer, it can be executed on the Cricket board.

2.3.2 Programming the Handy Cricket Board

The flow chart for the "logo" program used for the robot's microcontroller is shown in Figure 2.6. When the robot is powered up, the microcontroller is in ‘wait’ mode. The microcontroller waits for an ASCII character to be received via the serial port from the PC that controls the measurement system. When an ASCII character "A" is received, this signals the start of the measurement campaign, and in reply the microcontroller sends an ASCII character "AB" to the control unit. When an ASCII character "C" is received, the robot follows the tape on the ground for a distance of 1.5 cm and then stops. Then an ASCII character "D" is sent to the control PC. If an ASCII character "E" is received by the microcontroller, this signals the end of the measurement campaign. Further details can be found in [12][36] and a listing of the "Cricket logo" program is in Appendix B.

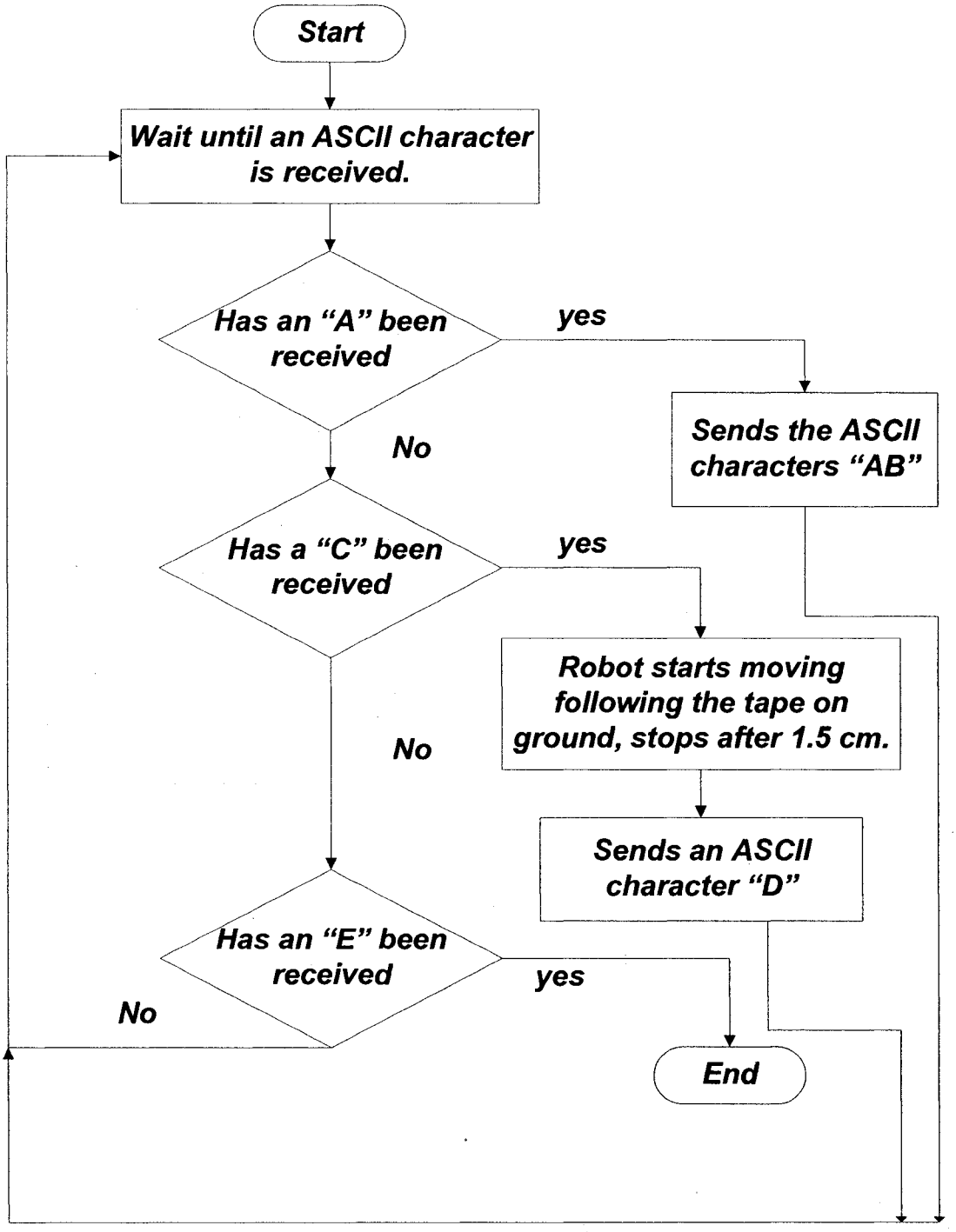

Figure 2.6 Flow chart of programming the Handy Cricket board.

2.4 The RF Transmitting Unit

The RF transmitting unit of the site survey system is a battery-operated CW transmitter. It is mounted on the robot, which moves it along the path of the tape on the floor in the microwave lab or hallway. Figure 2.7 shows the RF transmitting unit mounted on the robot moving platform. The theory behind how the RF Transmitter works is based on the concept of Phased-Locked Loop (PLL) [11][36][37]. Figure 2.8 shows the circuit of the RF transmitter, the board on the right is the PLL circuit. It contains a voltage-controlled oscillator (VCO) and a loop filter (LF). This board has one input, a crystal oscillator (XO) on the lower left part of the board, used to stabilize the frequency for the transmitting unit. The output of the PLL circuit is on the upper left part of the board and is used as an input to an amplifying board, which amplifies the input frequency power level from 0 dBm to 10 dBm. The frequency range of the RF transmitter is the ISM band from 2.4 to 2.5 GHz.

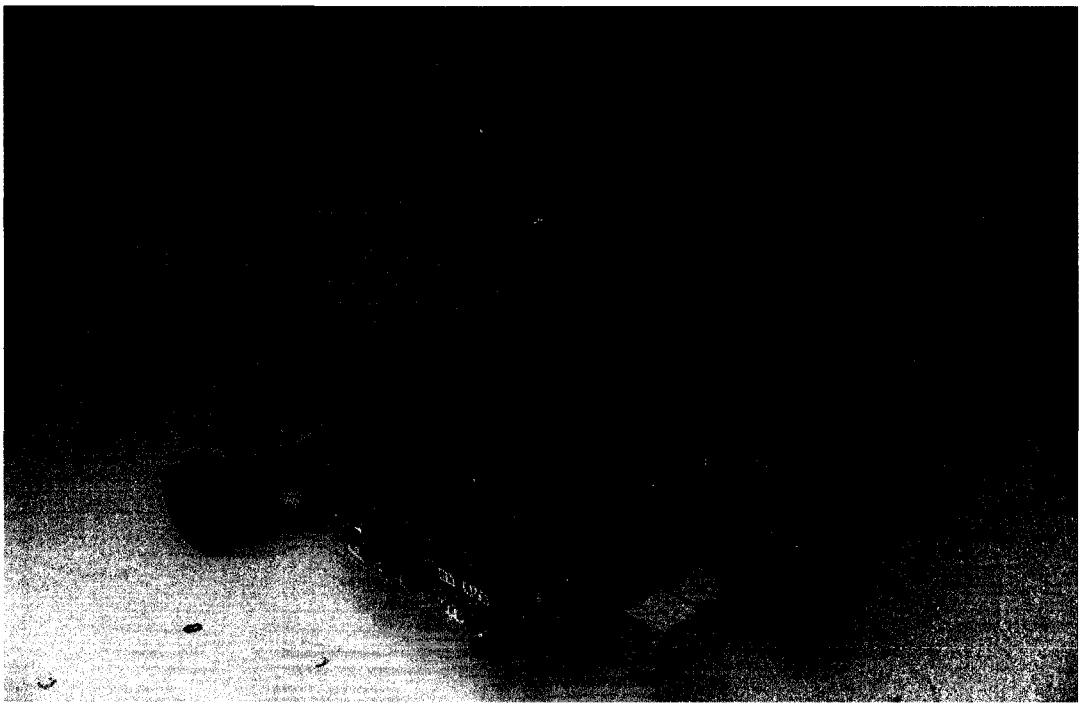

Figure 2.7 The transmitting unit showing the RF Transmitter mounted on the robot.

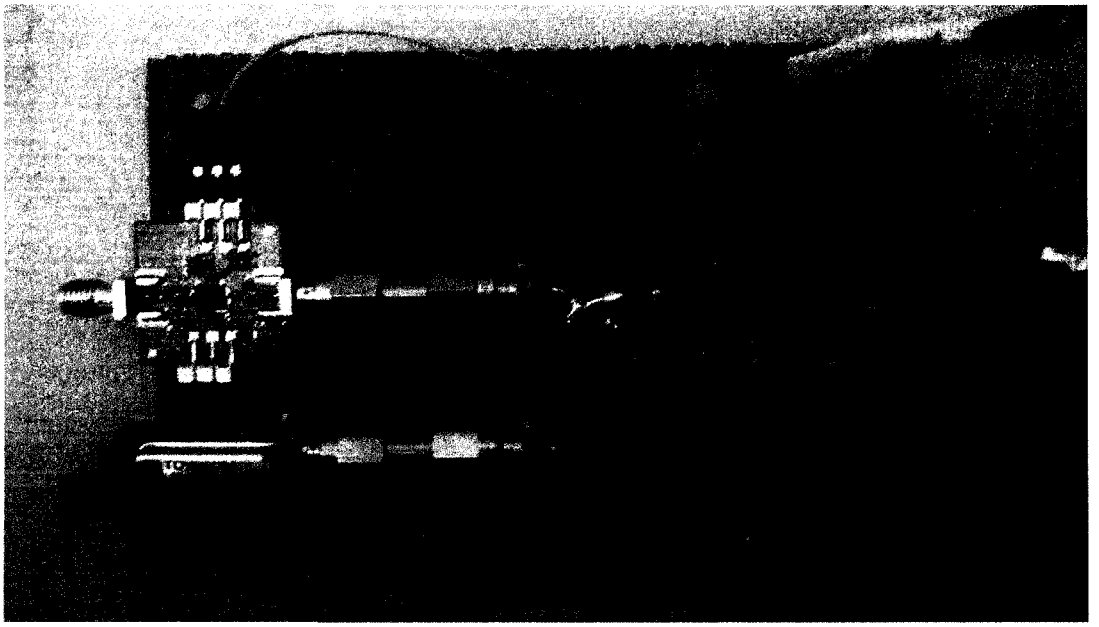

Figure 2.8 The inside of the RF transmitter.

The antenna mounted on the Tx unit is a monopole. The length of the monopole was trimmed to have a return loss at the input port better than -10dBm for the frequency range from 2.4 to 2.5 GHz, as shown in Figure 2.9. The return loss was measured using an HP8720 Network Analyzer.

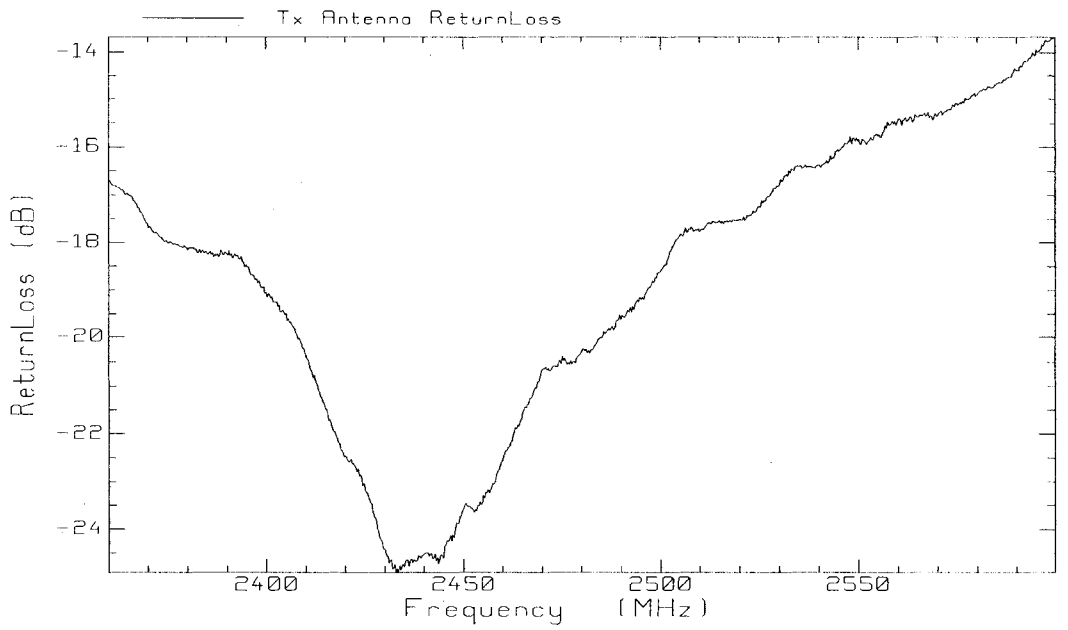

Figure 2.9 The return loss at the input port of the antenna of the Tx Unit.

2.5 The Receiving Unit

The receiving unit shown in Figure 2.10 consists of a calibrated sleeve dipole provided by ETS, LINDGREN Model # 3126. It is connected to an HP8569B spectrum analyzer. The spectrum analyzer is used to measure the RF power received by the sleeve

dipole working into a 50 ohm load. With the robot and the transmitter at a fixed location, the power received by the spectrum analyzer is measured at 30 two-second time intervals, in order to measure the temporal variation of the signal. To measure the spatial variation, the robot follows a path along the floor defined by applying a masking tape to the floor. At each position on the path, 30 time samples of the received power are taken and written to the output data file.

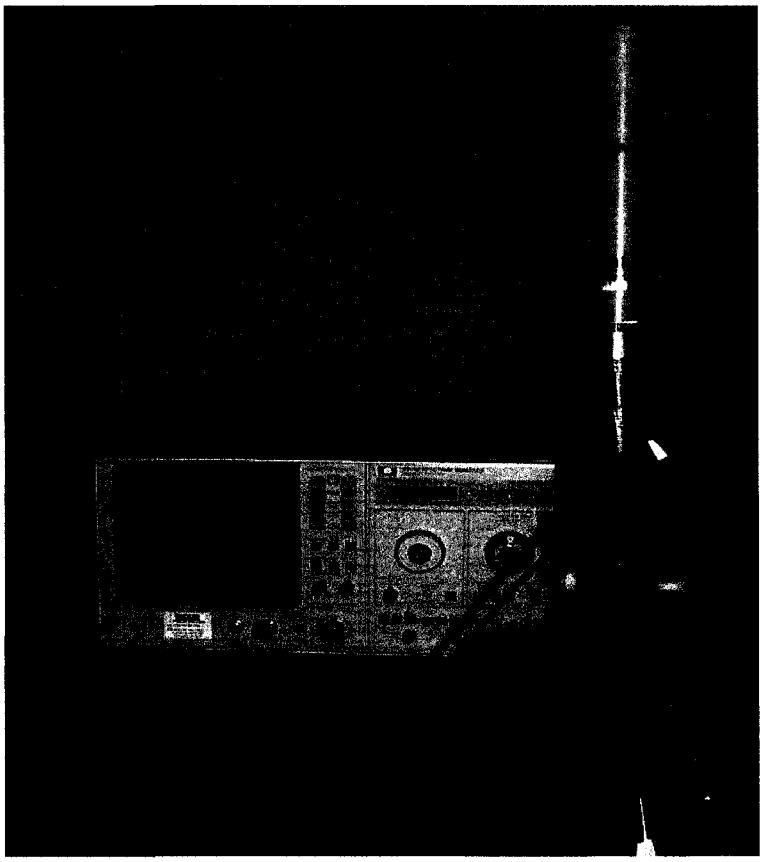

Figure 2.10 The Rx unit showing the Rx Antenna Model # 3126 and the HP8569B spectrum analyzer.

2.5.1 The Rx Antenna

The Rx Antenna is a calibrated sleeve dipole. It is an omni-directional antenna in a plane perpendicular to the dipole axis. The antenna design allows it to be end fed to avoid feed point and cable interactions that affect the radiation pattern. This antenna covers the frequency range from 2.3 to 2.6 GHz. The antenna is mounted on a tripod during measurements. The return loss for the Rx sleeve dipole antenna for both a vertical and a horizontal orientation are shown in Figure 2.11. This was measured using the HP8720 network analyzer. The return loss is somewhat different for the two orientations because the measurements were taken on a lab bench, rather than in an anechoic room. The antenna interacts with the nearby objects.

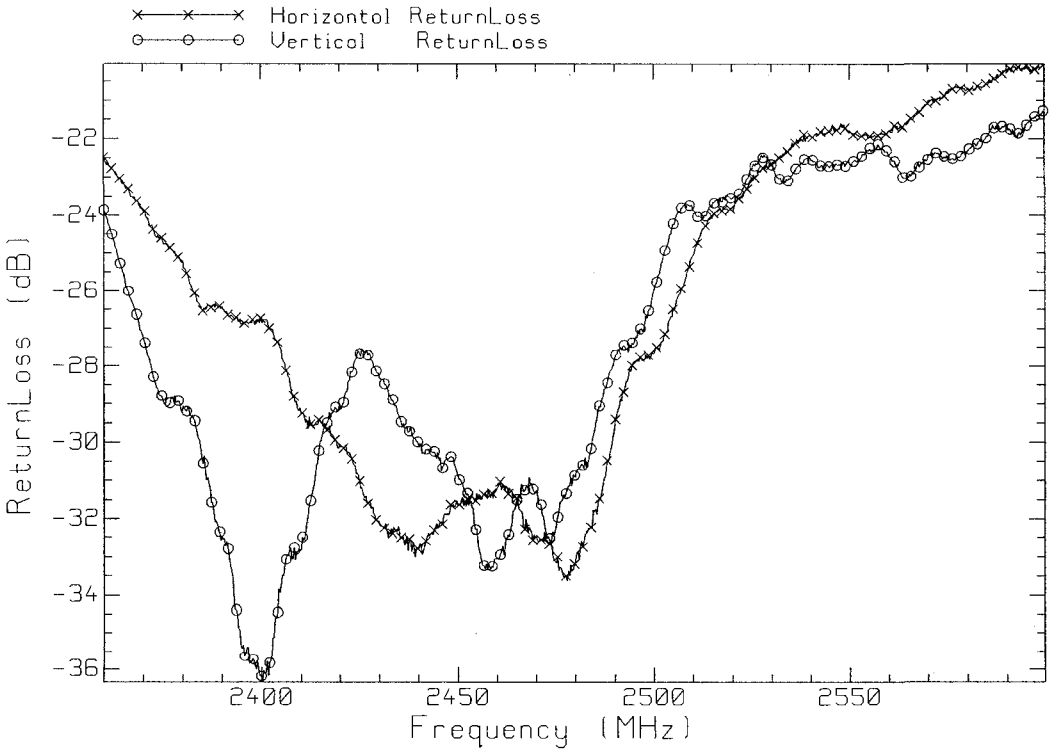

Figure 2.11 Horizontal and vertical return loss of the Rx antenna.

2.6 The Control Unit

The control unit consists of a desktop PC equipped with a GPIB card and a 900-MHz wireless link connected to the serial port of the PC. The GPIB card connects the PC to the HP8569B spectrum analyzer of the Rx Unit and is used to capture data from the spectrum analyzer. The 900-MHz wireless link is used to communicate between the Mobile platform and the Control Unit using ASCII characters. The program used to control the robot movement and take spatial and temporal RF received power level measurements is written in LabVIEW. The programming flow chart is shown in Figure 2.12, and the description of each block diagram of the flow chart is given below.

1. System Setup and Execution: the robot is powered on, the controlling program in the Handy Cricket board is started, and then the LabVIEW program is started after all its input parameters are defined.

2. First Serial Port Communication: the LabVIEW program is started on the controlling PC, and starts serial port communication between the controlling PC and the robot's cricket board. The PC sends an ASCII character "A" and the robot responds with "AB".

3. Initial Distance Position: the initial distance is checked and the initial position is written to the text file on the controlling PC.

4. Time Varying Measurements: the LabVIEW program reads the spectrum analyzer 30 times, at a time interval of 2 seconds between readings. The received power is determined at the operating frequency and then the time and received power are written to the output text file.

5. Second Serial Port Communication: the LabVIEW program sends the ASCII character "C" to the robot. The robot responds by moving an increment of 1.5 cm. This distance is determined by the optical encoders attached to the wheels of the robot. Next, the platform sends the ASCII character "D" to the control unit to acknowledge moving and stopping.

6. Next Distance Position: the new position is written in the text file on a new line. The next distance position value is the previous position value plus the distance increment. The spectrum analyzer reads the received RF power at 30 time intervals and writes them to a text file. If there are more positions for measurements, the program goes to step 5.

7. Last Serial Port Communication: when all distance points have been reached and the corresponding RF power time-varying measurements have been recorded, the Control Unit sends the ASCII character "E" to the moving platform to terminate the measurements and the LabVIEW program shows the operator a message that indicates measurements have finished.

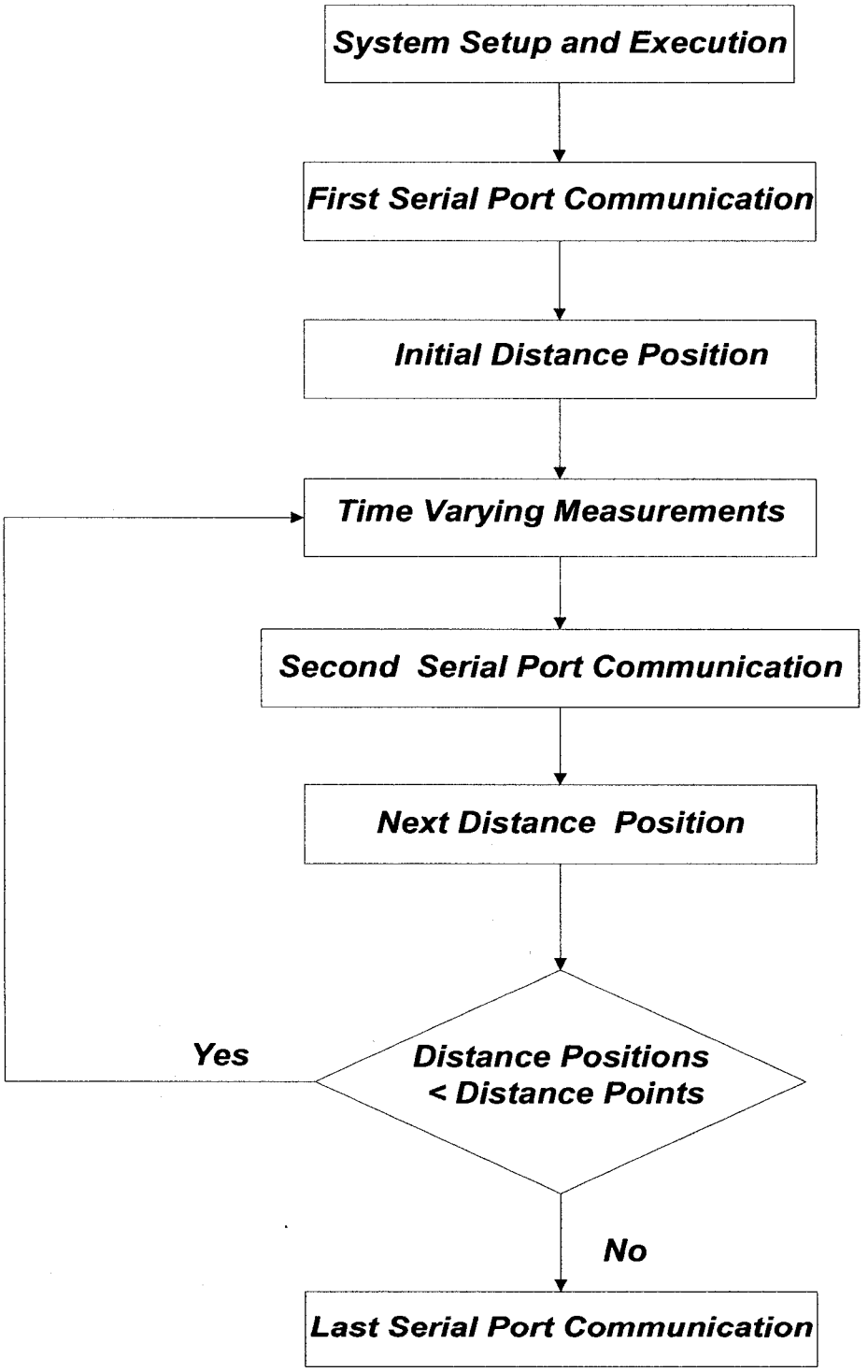

Figure 2.12 Control Unit and mobile platform communication (automation process).

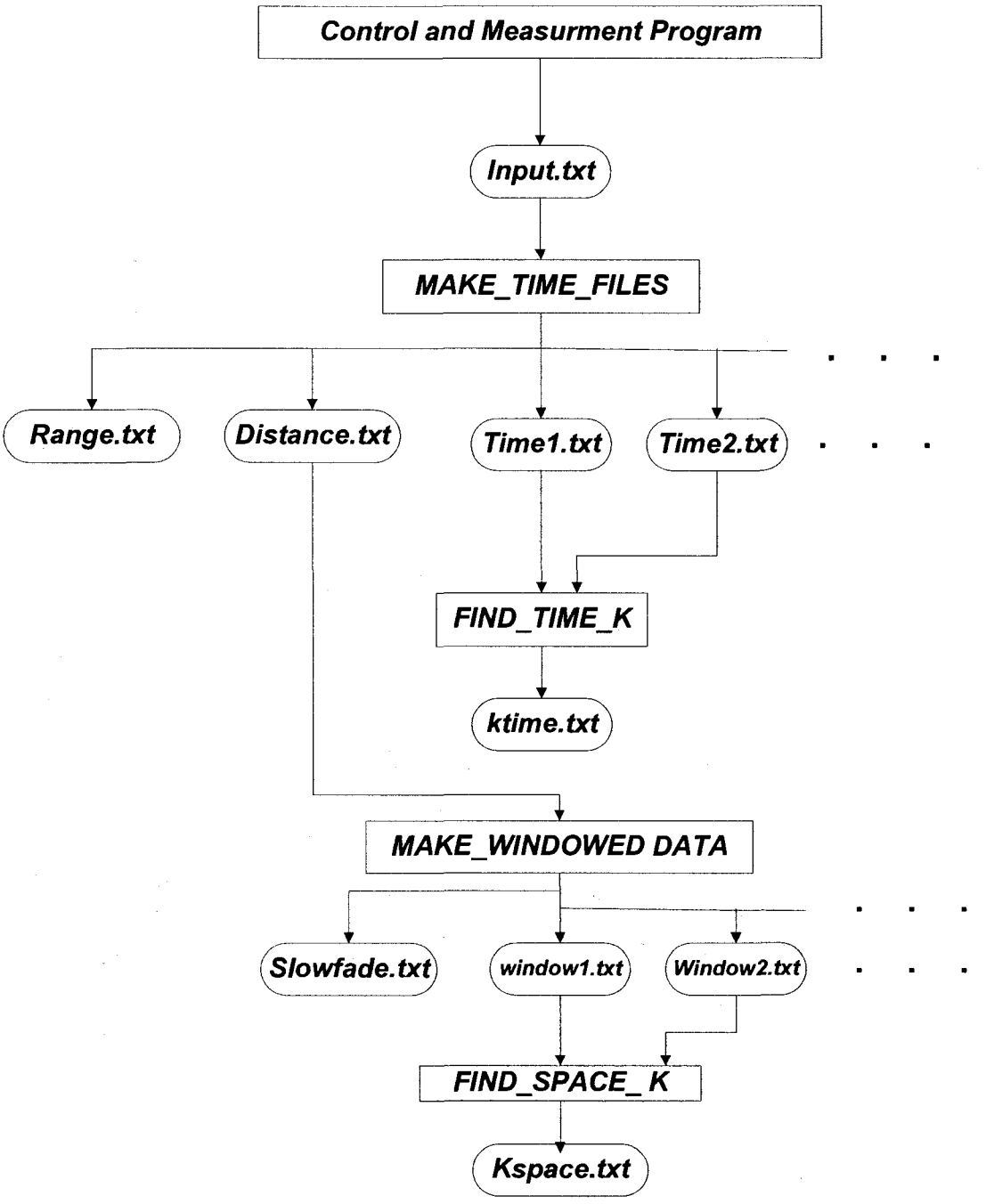

Figure 2.13 Post-processing programs flow chart.

2.7 Post Processing of the Measured Data

The results of the measurements must be analyzed in order to give an interpretation of the measurements campaign. The LabVIEW program report will be named as input.txt to start analyzing its data. In this thesis the Rician-K factor values for the spatial and temporal variation of the received signal power will be calculated from the measured data, according to the methods mentioned in Chapter one. A sample of the text file "input.txt" generated is shown in Appendix C.

Figure 2.13 shows a flow chart of the post processing programs process. It starts with the measurement and control program of the control unit. The output of this program is the "input.txt" which contains the results of the measurement campaign. This text file contains the time varying received power for each Rx, Tx separation.

The "input.txt" file is used as an input for the "MAKE_TIME_FILES" program. This program sorts each Rx, Tx distance reading and puts them in an individual file; each file is called Time1.txt,Time2.txt, ..., till Time(n).txt, where n is the number of distance points being measured. These file formats have a header that shows the distance value for each file, and which indicates that the two-column data format displays distance on the left and the corresponding linear voltage on the right. This program generates a text file called "Distance.txt" with two-column data, the first column on the left displays the distance value and second column on the right is the corresponding average time-varying received voltage. The program also generates a file called "Range.txt" which is

similar to the "Distance.txt" file except that the second column is the maximum divided by minimum of each time(n).txt file instead of average. Since all results are in linear scale and will be plotted later in (dB) format the range file is the division of maximum by minimum which is the equivalent of difference between the maximum and minimum value in (dB).

The next program is "FIND_TIME_K". This program will read each Time1.txt, Time2.txt,...Time(n).txt and calculate the K value using five methods: K_G, K_{24}, K_{12}, K_{CDF}, and K_{MLE}, mentioned in Chapter One. This program uses the "halving interval" method to find the root of the equations of K_{12} and K_{MLE}.

The program "MAKE_WINDOWED_DATA" arranges the "Distance.txt" in another format using a sliding window with a predefined number of measurement points or samples. This sliding window moves along the data starting from the first data point. The next sliding window starts with the second data point and discards the first data point on the left and so on until all of the path is completed. This program generates text files called windows1.txt,windows2.txt,.....windows(n).txt, and generates a file called "large_scale.txt". The file "large_scale.txt" has two-column data. The column on the left is for the middle of the distance corresponding to each window, and the average of the voltage for each window is displayed on the right.

The program "FIND_SPACE_K" calculates the K value using four methods mentioned in Chapter one, K_G, K_{24}, K_{12}, and K_{MLE} that are also used in

"FIND_TIME_K". It calculates the K values for each window and writes them to a text file. Each K value will correspond to the middle point of the distance of the window. The temporal variation of measured data is discussed in the next Chapter.

Chapter 3

Temporal Variation

3.1 Introduction

In this Chapter, temporal variations of the received electric field for two environments are considered: the hallway and the microwave lab. For each environment the time variations of the received signal in volts (dB) for four fixed receiver (Rx), transmitter (Tx) distances are shown. The four methods used to evaluate the Rician-K factor mentioned in Chapter one are explained in detail. Time-varying Rician-K factors for both environments are plotted and explained. This Chapter shows that the time-varying signal is constant, and that the possible movement of people near the Tx and the Rx caused small variations in the time-varying received signal. The time-varying Rician-K factor found using the four methods from the literature presented a good match; K_G / K_{24} are the same and are the best methods to be considered when evaluating the time-varying Rician-K factor in a wireless channel.

3.2 Voltage in dB versus Time

Field strength may vary over time at a fixed distance from the source. Therefore it can be important to understand the behavior of the electric field as a function of both time and distance. In the following Sections, representative distance points between the transmitter and the receiver are chosen to show the behavior of the time-varying received voltage for the two environments, the hallway and the microwave lab. The setup of the measurement system is shown in Figure 3.1. The robot moves in steps of 1.5 cm. At each step-distance, 30 time-varying readings of the received voltage were taken, at a time interval of two seconds. The readings obtained from the spectrum analyzer are in power (dBm) and the plotted graphs are in voltage (dB).

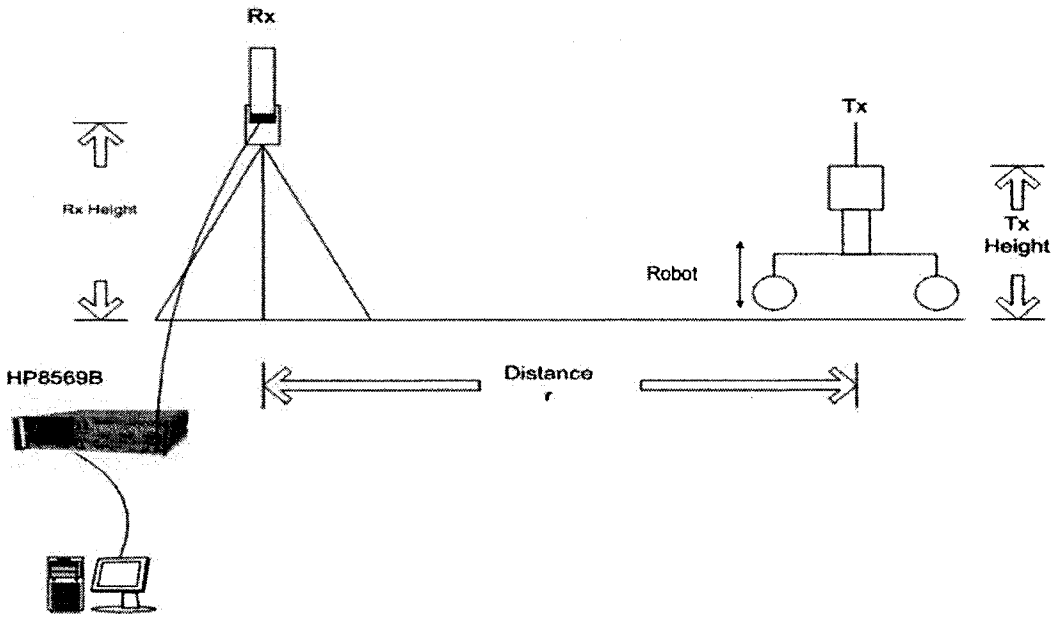

Figure 3.1 General setup of the measurement system.

3.3 Conversion from dBm to Voltage

The spectrum analyzer measures the power delivered to a 50 ohm load, in dBm. This Section describes how to find the voltage across the 50 ohm load, starting with this equation

$$P_{dBm} = 10\log\left(\frac{P}{1\text{mW}}\right). \tag{3.1}$$

where P_{dBm} is the power measured from the spectrum analyzer in dBm and P is the power measured in linear scale. The power reference level is 1 milliwatt. By replacing the linear scale of power with the equivalent voltage, (3.1) can be expressed as

$$P_{dBm} = 20\log\left(\frac{v}{\sqrt{0.001R}}\right), \tag{3.2}$$

where v is the measured voltage in linear scale and R is the resistance. Arranging (3.2) to express the linear voltage in terms of the measured power in dBm and replacing R with a 50 ohm matched load, we obtain

$$v = \sqrt{0.001 \cdot 50}\left[10^{P_{dBm}/20}\right]. \tag{3.3}$$

This equation is used to transform the measured power in dBm from the spectrum analyzer to voltage in linear scale. All results obtained are in linear scale and will be plotted using dB scale. The reference level for voltage in dB is 1 volt RMS.

3.3.1 Hallway

The hallway of the 15^{th} floor of the EV Building at Concordia University was chosen as one measurement setting . Figure 3.2 shows the floor plan of the north-west corner. The readings were taken using the measurement system described in Chapter 2. Figure 3.3 shows the Rx dipole on a tripod near room EV15.185 and the equipment trolley in hallway 15.172. Figure 3.4 shows another view of the measurement system setup in the hallway; it shows the Rx dipole mounted on the tripod near room 15.185, the spectrum analyzer HP8569 B, and the monitor of the desktop PC that is part of the control unit. The transmitted frequency was 2.388 GHz. The height of the transmitter was 107 cm above the floor and the height of the receiver was 103 cm. The Rx antenna was located 60 cm away from the wall of room number 15.185, as shown in Figure 3.2. The measurement path of the robot started at 60 cm from the Rx antenna. The measurement path in the hallway ended 1005 cm from the Rx antenna and was 945 cm long.

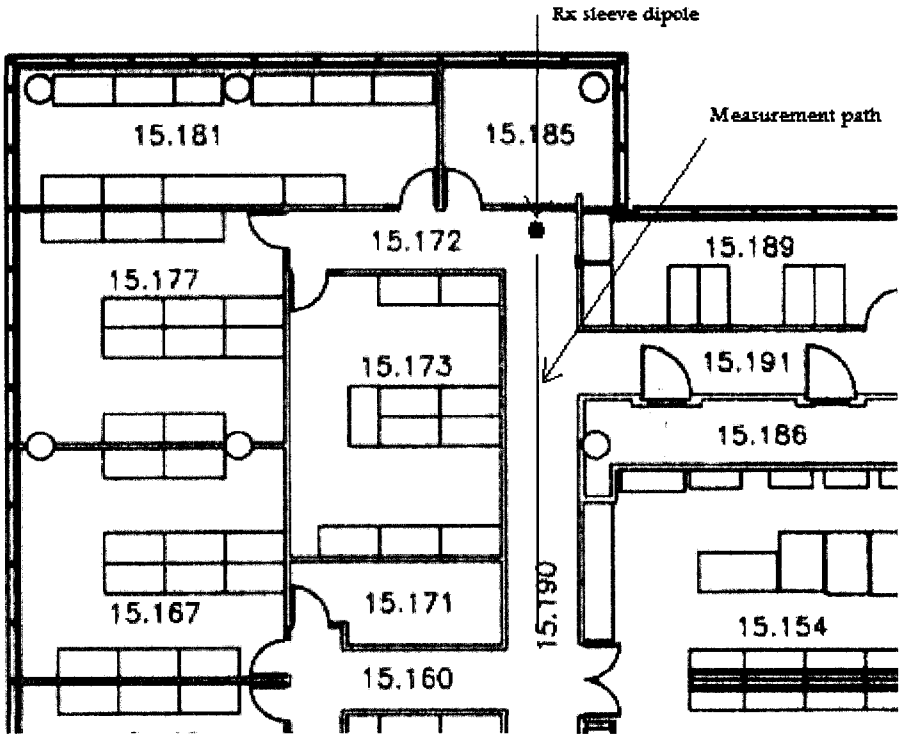

Figure 3.2 North-west corner map of the 15th floor of the EV showing the measurement path along a hallway and the location of the receiving sleeve dipole antenna.

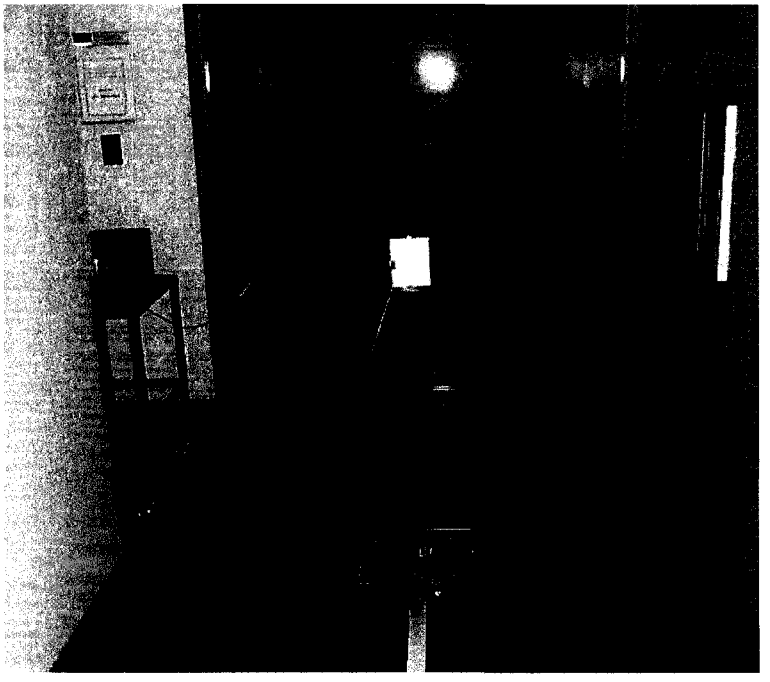

Figure 3.3 Concordia University EV15 hallway measurements setup part 1.

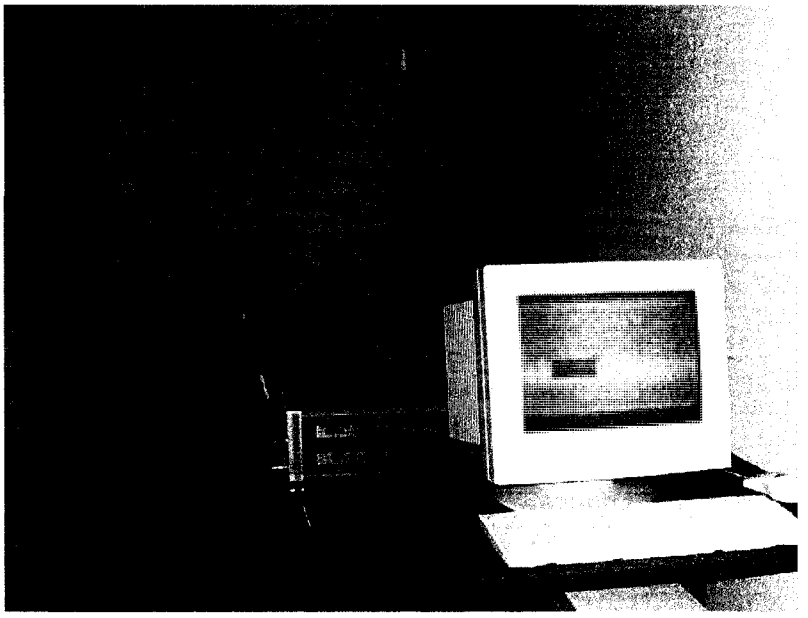

Figure 3.4 Concordia University EV 15 hallway measurements setup part 2.

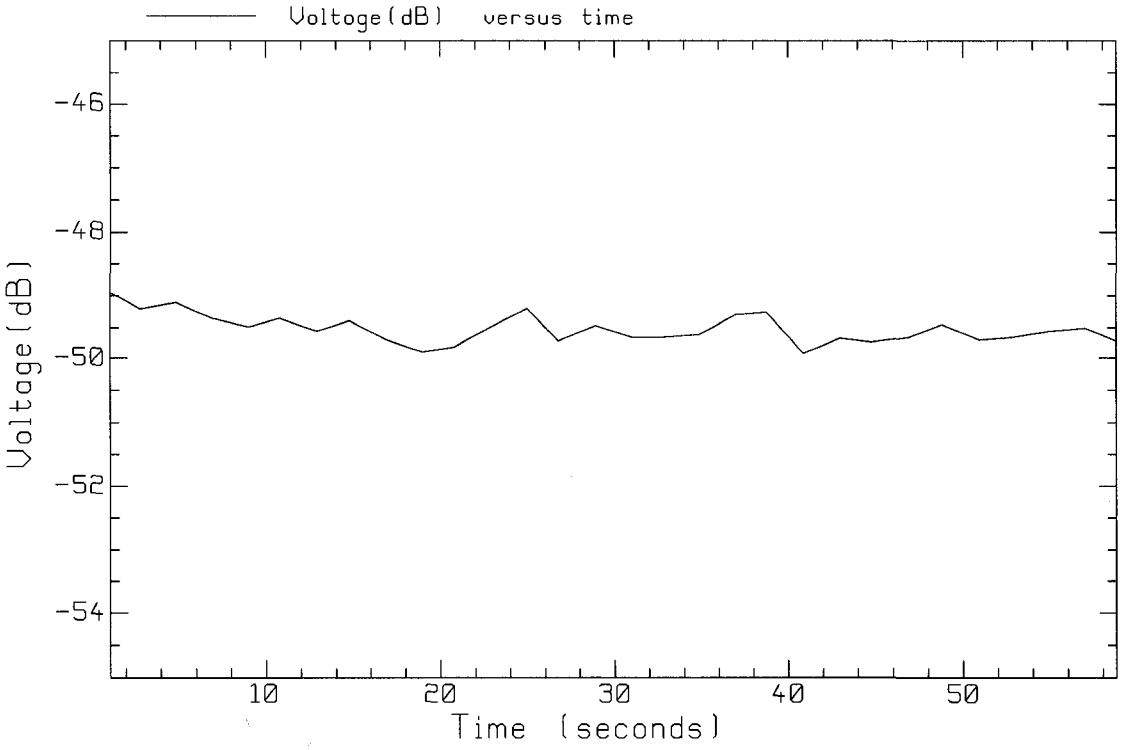

Figure 3.5 EV15 hallway time varying voltage (dB) ,Tx, Rx separation 60 cm.

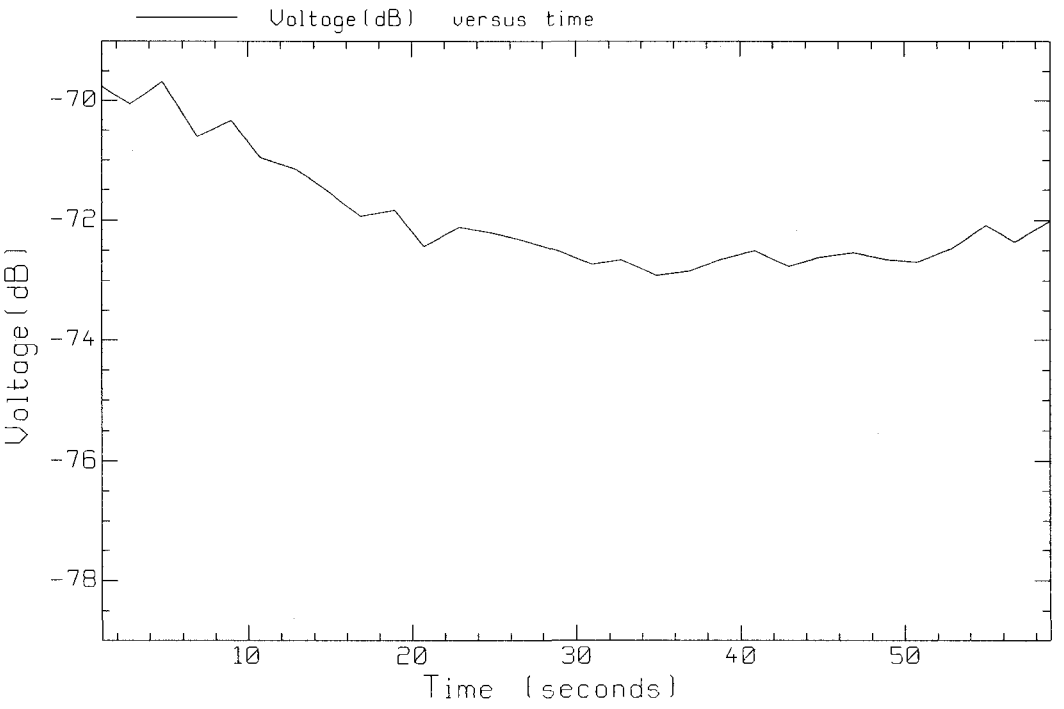

Figure 3.6 EV15 hallway time varying voltage (dB) ,Tx, Rx separation 294 cm.

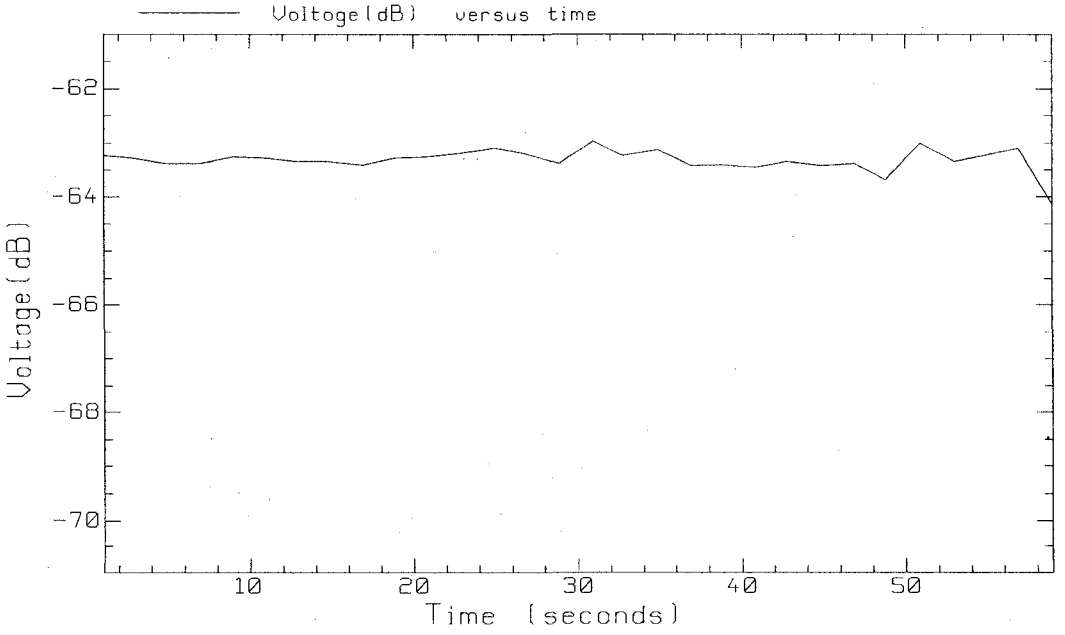

Figure 3.7 EV15 hallway time varying voltage (dB) ,Tx, Rx separation 531cm.

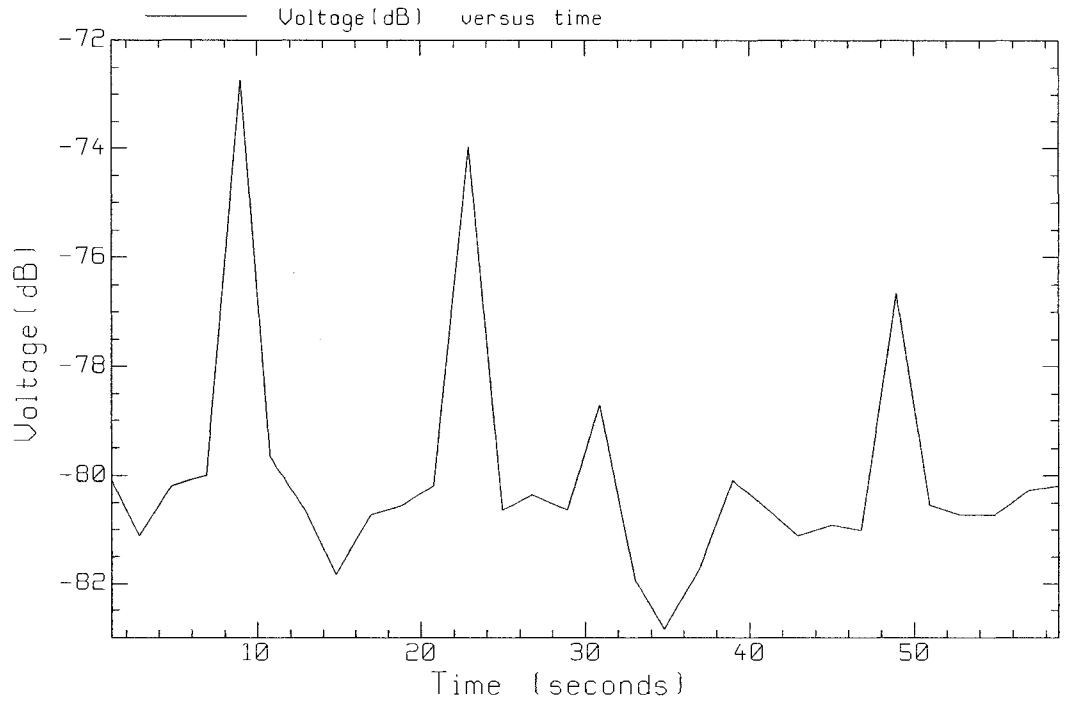

Figure 3.8 EV15 hallway time varying voltage (dB) ,Tx, Rx separation 1005cm.

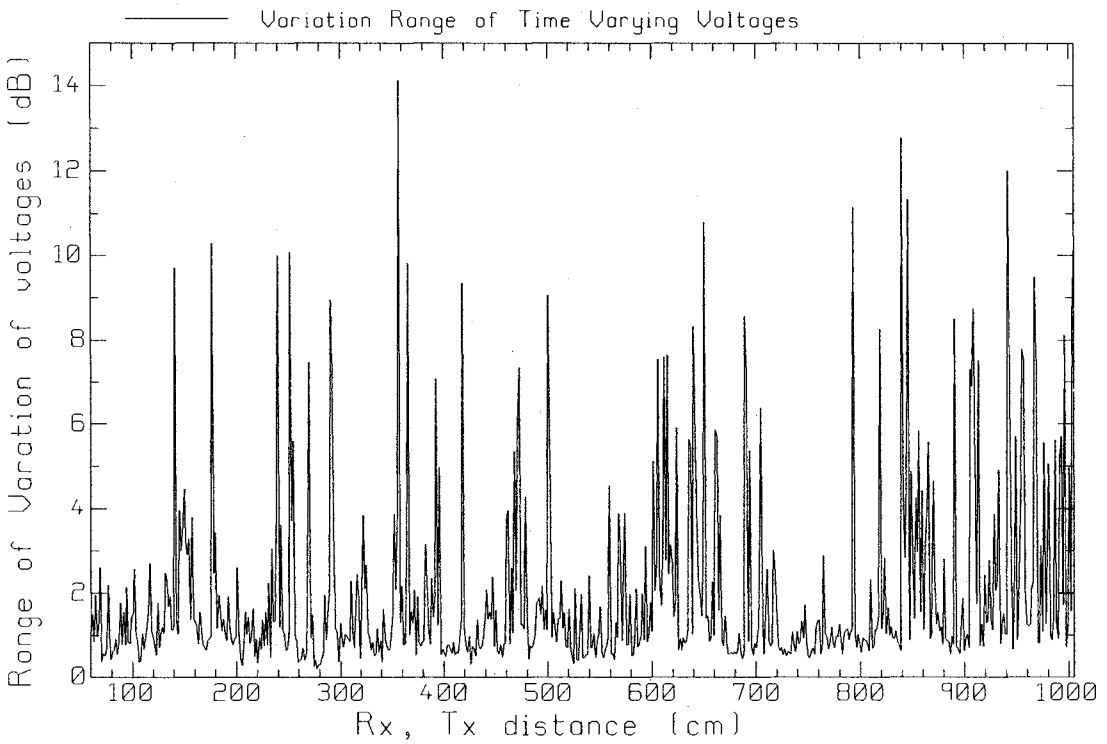

Figure 3.9 EV15 hallway range of voltages versus distance.

Figures 3.5 to 3.8 show the time-varying received voltage at four representative distances between the transmitter and receiver. Figure 3.5 shows the data at distance 60 cm. Figures 3.6 and 3.7 show the data at 294 and 531 cm, respectively, and Figure 3.8 shows the data at the largest separation of 1005 cm. In Figure 3.5, at the 60 cm distance the received voltage varies between -49.0 to -50.0 dB in a range of 1 dB. This range can be considered as rather small and the time-varying received voltage might be approximated as being constant. In Figure 3.6, at separation 294 cm, the variation of the voltage is between -70 and -73 dB in a range of 3dB, which can be viewed as high. The graph shows a declining behavior for the first 30 seconds. From 30 seconds onwards, the voltage is observed as having a constant behavior. Figure 3.7 shows the time variation of the received voltage at a separation of 531 cm. The received voltage varies between - 63.5 and -64 dB in a range of 0.5 dB. This range can be considered to be very small and the time-varying received voltage might be approximated as being constant. The field is almost constant for the first 30 seconds, and then the variation after 50 seconds steadily increases. Figure 3.6 shows the voltage at the longest distance of 1005 cm between the transmitter and the receiver, where the received voltage is highly variable. The voltage varies between approximately -72 to -82 dB in a range of 10 dB, which is quite large. One possible explanation for the different variations in voltage in the previous four graphs could be that the operator and the equipment trolley are located in hallway 15.172 , and since the measurement path is in hallway 15.190, the operator cannot observe what is actually moving near the robot, or if people are moving in nearby rooms. There could also be possible movements of the operator near the transmitter. The degree of variation is influenced by the degree of movement of people [14]. Figure 3.9

shows the range of variation for the time-varying received voltage of each distance point. This Figure shows the nature of the environment during the measurements, which is highly variable. Figure 3.9 shows that the path being measured can be divided into two regions. The first region is from 60 to around 830 cm, and the second region is from 830 cm till the end of the path being measured, or 1005 cm. The first region shows, in general, that almost 80 percent of the variation of the field strength for the distance points is less than 3 dB, and the signal strength value for this region is a high value, as shown in Figures 3.5 to 3.7. The second region shows a higher field strength variation for most distance points, and the signal strength value is low, as shown in Figure 3.8 which has a voltage value around -81 dB and two peaks at -73 and -74 dB.

3.3.2 Room H853 -Microwave Lab

Room H853 is used as a laboratory for a course. This is a room with a significant amount of equipment, much of it is microwave measurement equipment on lab benches as shown in Figures 3.11 and 3.12. The microwave lab was chosen as a second example for Rician-K factor analysis because it is a very different environment than the hallway, and is full of many scattering objects. Figure 3.11 shows the Rx antenna which was located 90 cm away from the bench behind it. The measurement path as shown in Figure 3.11 started 30 cm from the Rx antenna and ends at 450 cm. The length of the measured path was 420 cm. Figure 3.12 shows the operator location with the equipment trolley, the Rx antenna on a tripod is facing the bench. The PC desktop which is part of the control unit is behind the filing cabinet.

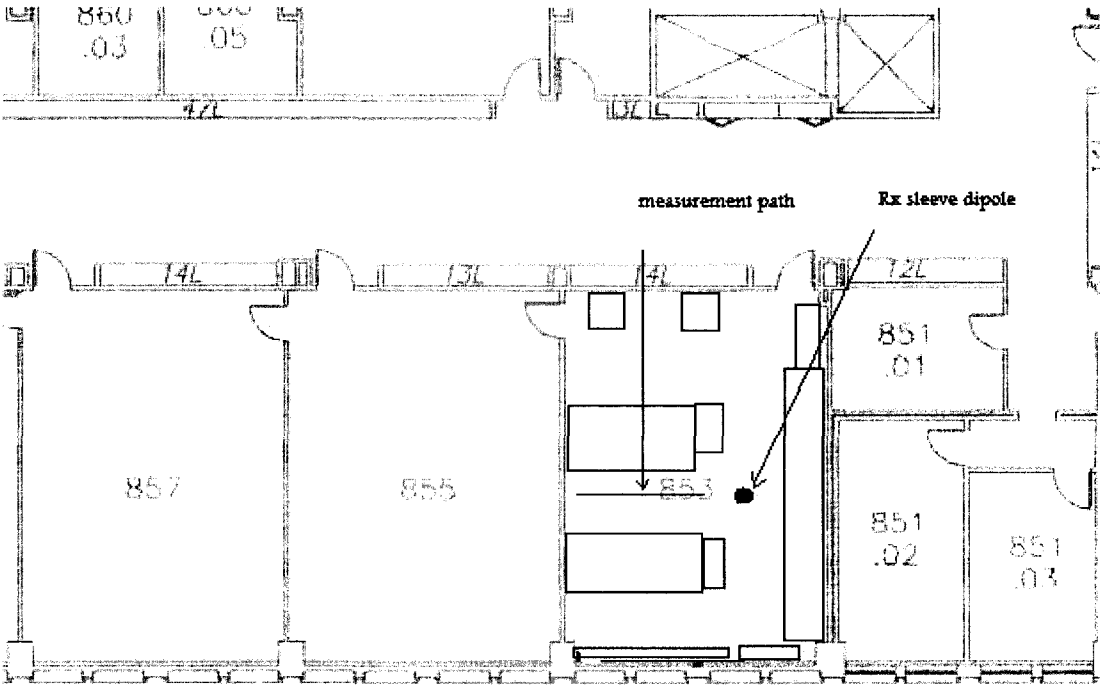

Figure 3.10 Lower right corner map of Concordia University Hall Building 8th floor. The microwave lab is room 853 and the location of the Rx antenna is denoted by a dot, the path location of the moving platform is denoted by a straight line facing it.

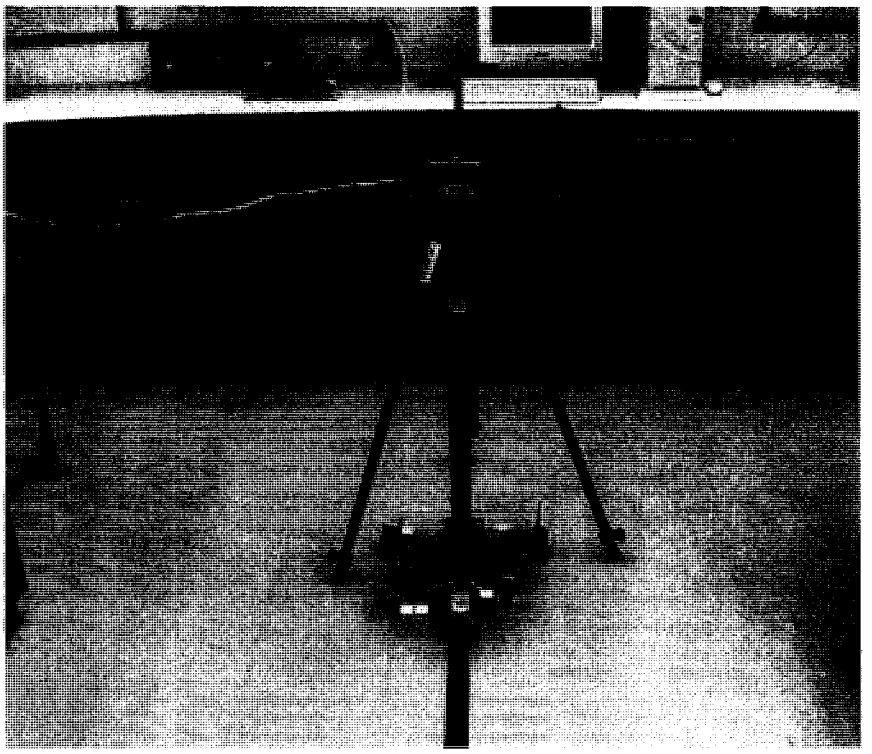

Figure 3.11 Concordia University H853 microwave lab measurement setup part 1.

Figure 3.12: Concordia University H853 microwave lab measurement setup part 2.

Four different distance points of the measured path have been chosen to show the time-varying power of the distance points. Figure 3.13 shows the received voltage at 30 cm. Figures 3.14 and 3.15 show the received voltage at 133.5 cm and 238.5 cm, respectively. Figure 3.16 shows the received voltage at 450 cm, representing the end of the path. In Figure 3.13, the beginning of the measured path at 30 cm separation, the received voltage is variable between -47.8 and -48.2 dB. The range is 0.4 dB. In Figure 3.14, the separation is 133.5 cm the whole received voltage is highly variable, compared to the previous graph. The received voltage varies between -57.0 and -57.5 dB, with a range of 0.5 dB. In Figure 3.15, with a separation of 238.5 cm, the received voltage varies between -61.5 and -62.2 dB. The range is 0.7 dB and the variation is larger than the previous graph. In Figure 3.16 the separation is 450 cm. The received voltage varies between -65.8 and -66.8 dB. The variability is the same as for the previous graph,

Figure 3.15. The range of variation of the time-varying field in the microwave lab is less than in the hallway. There were no people moving in the microwave lab and it is possible that the small variation observed is due to the movement of the operator. Figure 3.17 shows the range of variation for the time-varying received voltage of each distance point.. Figure 3.17 shows two regions, the first from 30 cm till 210 cm, and the second is from 210 cm till the end of the path being measured -- 450 cm. The first region shows that all the distance points have a high field strength with a variation less than 3 dB, as displayed in Figures 3.13 and 3.14. The second region shows less field strength and higher variation values, as can be seen in Figures 3.15 and 3.16.

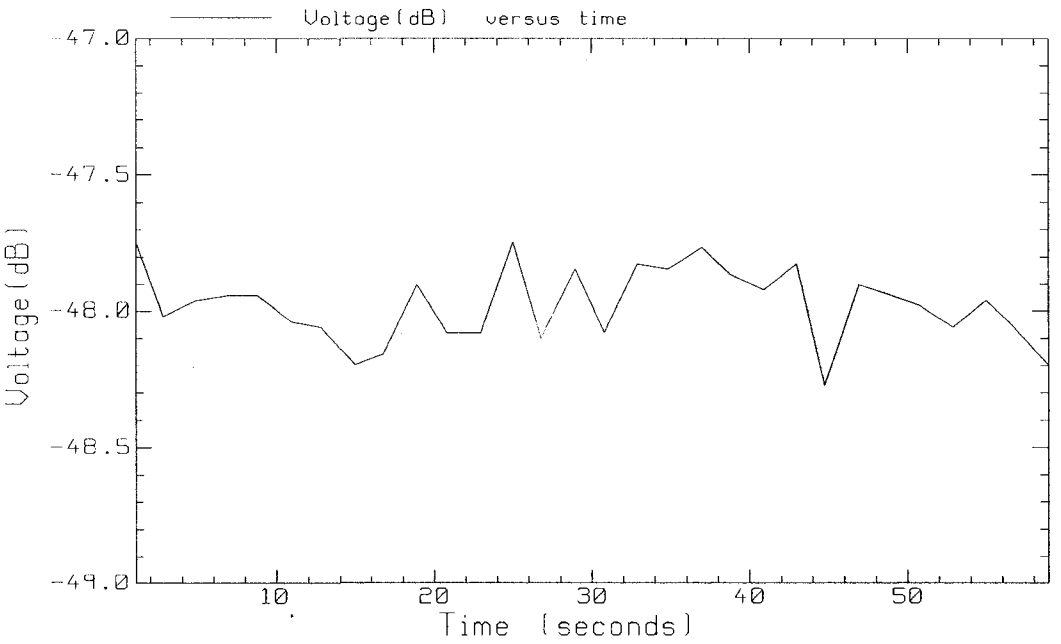

Figure 3.13 Room H853 time-varying voltage (dB) ,Tx, Rx separation 30 cm.

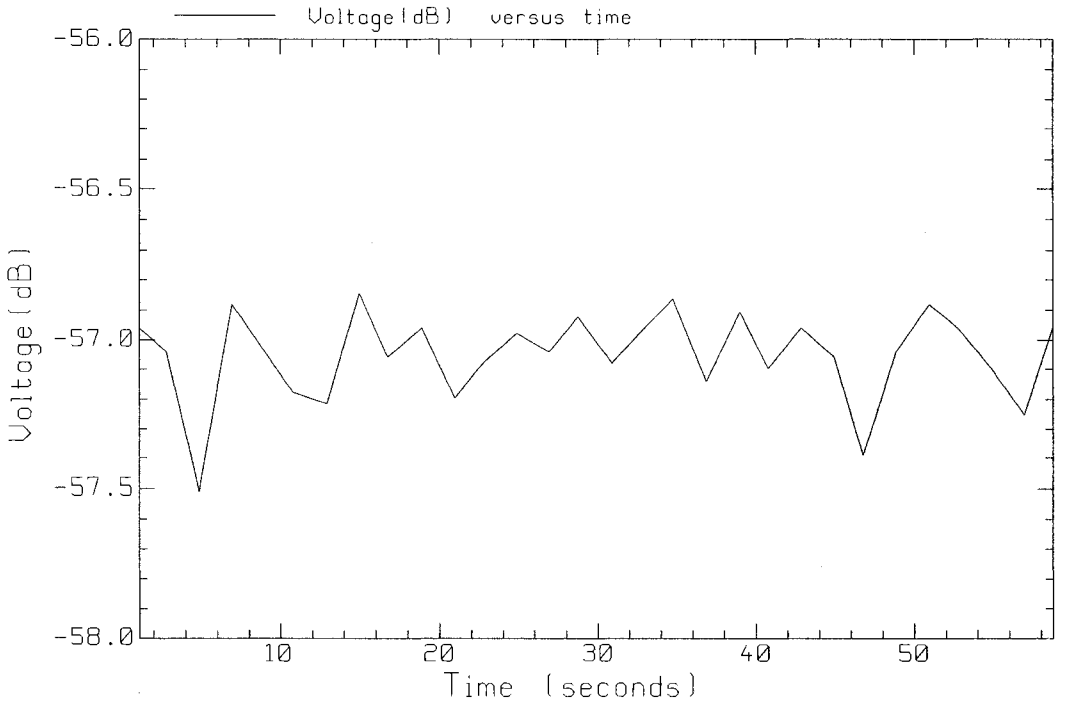

Figure 3.14 Room H853 time-varying voltage (dB) ,Tx, Rx separation 133.5cm.

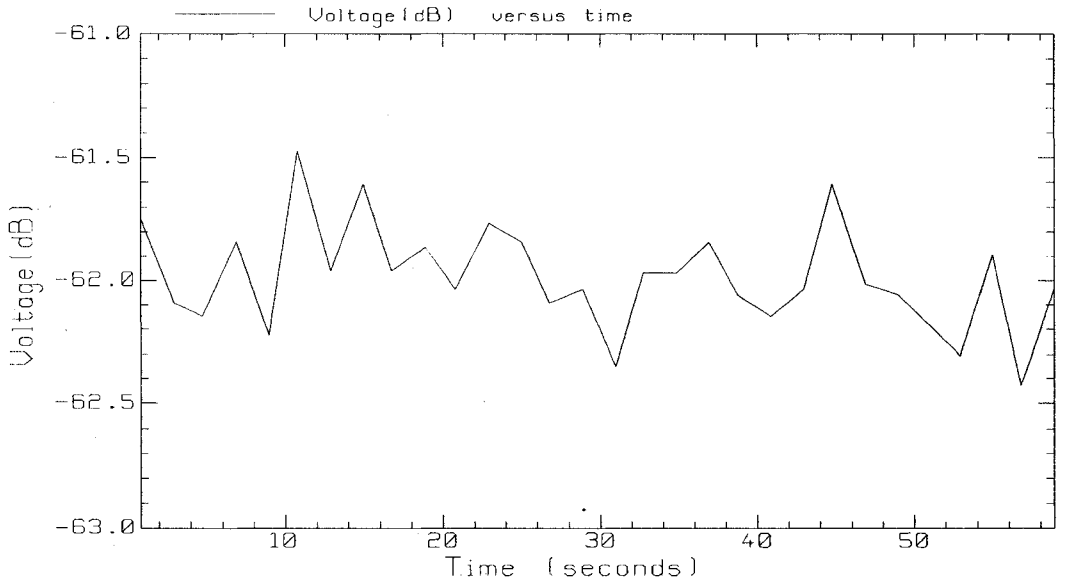

Figure 3.15 : Room H853 time-varying voltage (dB),Tx, Rx separation 238.5cm.

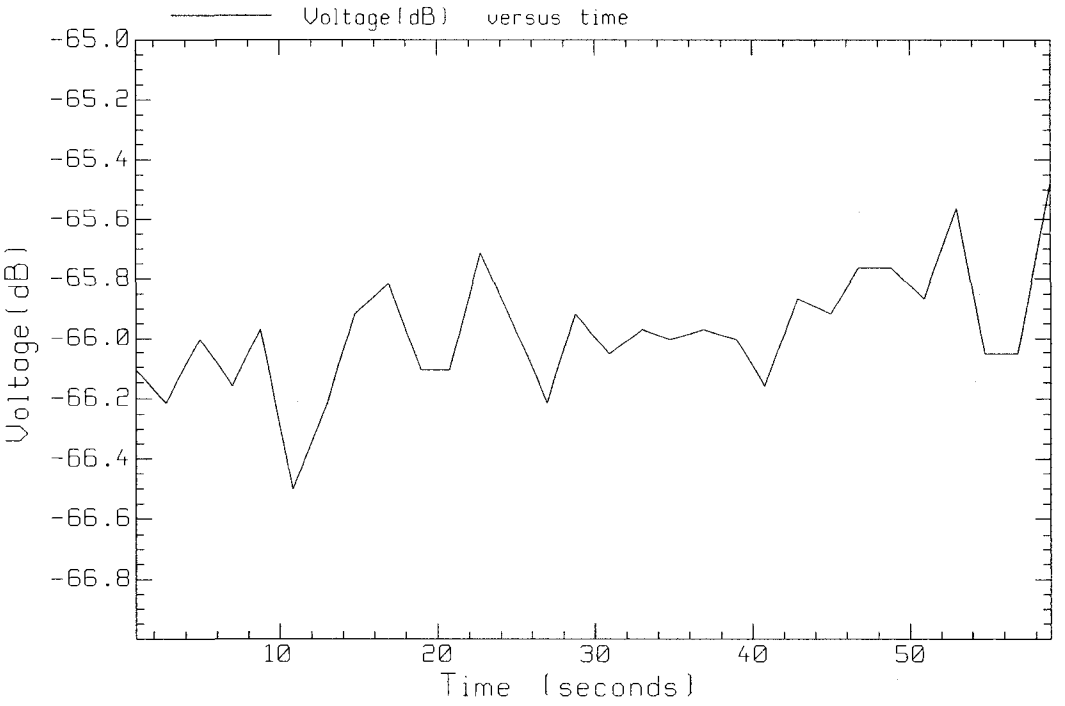

Figure 3.16 Room H853 time-varying voltage (dB) ,Tx, Rx separation 450 cm.

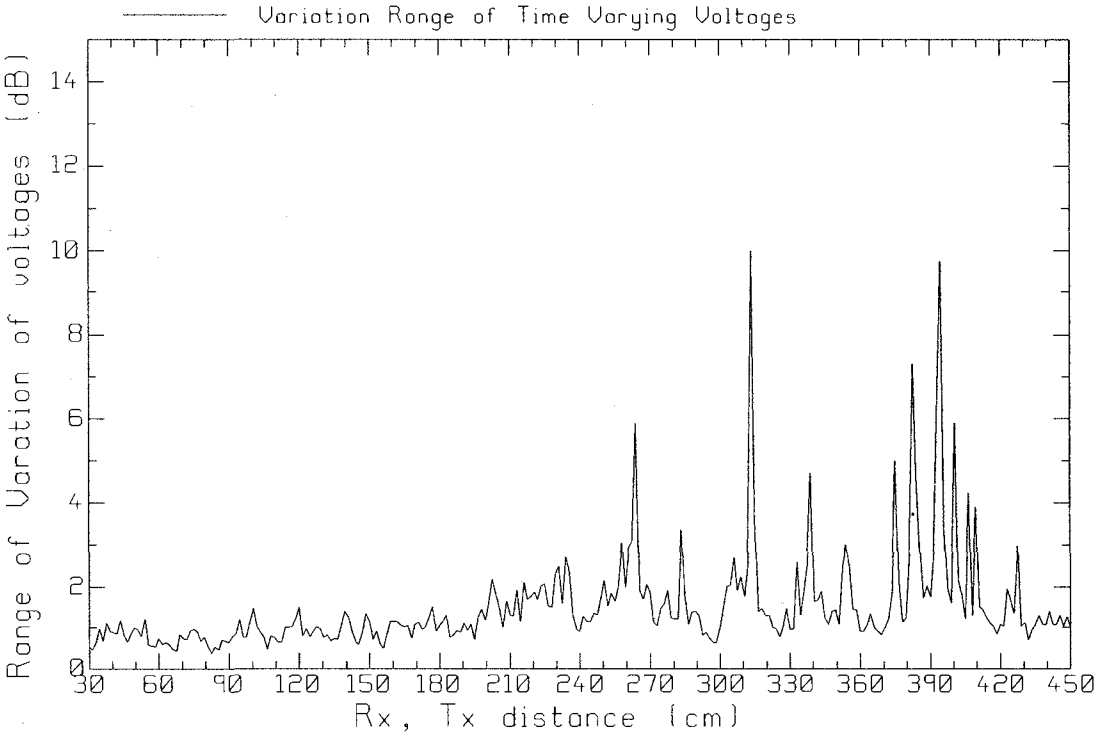

Figure 3.17 Room H853 microwave range of voltages versus distance.

3.4 Methods for Evaluating the Rician-K Factor

In this Section, before presenting the time-varying Rician-K factor results for both the hallway and the microwave lab, detailed explanations will be given for each method used to calculate the Rician- K factor for a set from measured voltage data. These will be organized as the K_G method, the K_{12} and K_{24} methods , and the K_{MLE} method. The same methods with the same formulas will be used to evaluate the space-varying Rician-K factor.

3.4.1 The K_G method

In [19] a method was developed to find the Rician-K factor based on moments standard notation, expressed in terms of moments in the following manner. The k^{th} moment, μ_k is defined as

$$\mu_k = \frac{1}{N}\sum_{l=0}^{N-1} v_l^k \tag{3.4}$$

where v_i is the set of measured voltages measured in a linear scale. Then K_G is calculated in terms of the second and the fourth moment as:

$$K_G = \frac{\left(2\mu_2^2 - \mu_4\right)^{0.5}}{\mu_2 - \left(2\mu_2^2 - \mu_4\right)^{0.5}} \tag{3.5}$$

The "G" subscript is for Greenstein, the first author in [19].

3.4.2 The K_{12} and K_{24} methods

In [20] the Rician-K factor is found from either the first and second moment, K_{12}, or the second and fourth moment, K_{24} with a general formula for estimating the Rician-K factor based on the moments of the received signal voltage $\{v_k\}$ given by

$$f_{n,m}(K) = \frac{(\mu_n)^m}{(\mu_m)^n} \tag{3.6}$$

where $f_{n,m}(K)$ is a function of K used to estimate its value based on its n and m moments, μ_n^m is the n^{th} moment of the received signal voltage raised to the m^{th} power, and μ_m^n is the m^{th} moment of the received signal voltage raised to the n^{th} power.

The paper gives two formulas for the evaluation of K. One is based on the first and second moment, given by

$$f_{1,2}(K_{12}) = \left(\frac{\pi \cdot e^{-K_{12}}}{4(K_{12}+1)} \right) \left[(K_{12}+1) \cdot I_0\left(\frac{K_{12}}{2} \right) + K_{12} \cdot I_1\left(\frac{K_{12}}{2} \right) \right]^2 \tag{3.7}$$

where $f_{1,2}(K_{12})$ is the function of K based on the first and second moment, $I_0(\,)$ is the modified Bessel function of the first kind and zero order, and $I_1(\,)$ is the modified Bessel function of the first kind and first order, and K_{12} is the Rician-K factor found using this method.

Since

$$f_{1,2}(K) = \frac{\mu_1^2}{\mu_2^1} \tag{3.8}$$

where μ_1^2 is the first moment squared of the measured data or the mean square of the measured voltage, and μ_2^1 is the second moment of the measured data or the mean of the measured power.

Combining (3.7) and (3.8), the resultant formula is:

$$\frac{\mu_1^2}{\mu_2^1} = \left(\frac{\pi \cdot e^{-K_{12}}}{4(K_{12}+1)} \right) \left[(K_{12}+1) \cdot I_0\left(\frac{K_{12}}{2} \right) + K_{12} \cdot I_1\left(\frac{K_{12}}{2} \right) \right]^2 \tag{3.9}$$

In (3.9) all quantities are known except K_{12}, which can be found from the first root that satisfies the above equation.

The second formula for K in [20] is based on the second and fourth moment and is given by

$$f_{2,4}(K_{24}) = \frac{(K_{24}+1)^2}{K_{24}^2 + 4K_{24} + 2} \tag{3.10}$$

where $f_{2,4}(K_{24})$ is the function of K based on the second and fourth moment, and K_{24} is the Rician-K factor determined from this method. Since

$$f_{2,4}(K) = \frac{\mu_2^4}{\mu_4^2} \tag{3.11}$$

where μ_2^4 is the second moment of the measured data or the mean of the power being measured raised to the 4^{th} power, and μ_4^2 is the fourth moment of the measured data squared, or the mean of the square of the measured power.

Combining (3.10) and (3.11) gives

$$\frac{\mu_2^4}{\mu_4^2} = \frac{(K_{24}+1)^2}{K_{24}^2 + 4K_{24} + 2}. \tag{3.12}$$

Reorganizing the above equation to determine K_{24} results in

$$K_{24} = \frac{-2\mu_2^2 + \mu_4 - \mu_2\sqrt{2\mu_2^2 - \mu_4}}{\mu_2^2 - \mu_4}. \tag{3.13}$$

Hence K_{24} is readily evaluated. K_{24} and K_G can be proved to be identical by performing some algebraic manipulations on the K_G formula, resulting in the formula for K_{24}. The proof is given in Appendix D. Since K_G and K_{24} are identical, in calculating the values of the Rician-K factor the symbols of both methods will be merged and denoted by K_G / K_{24} and thus be referred to as one method.

3.4.3 The K_{MLE} method

Reference [20] presents a formula for evaluating the Rician-K factor using the Method of Least square Estimators (MLE). The Rician-K factor found by this method is called K_{MLE}, determined by

$$1+\mu_2 = \frac{1}{1+K_{MLE}} + \frac{1+2K_{MLE}}{N\sqrt{K_{MLE}(K_{MLE}+1)}} \sum_{k=1}^{N} v_k \frac{I_1\left(2v_k\sqrt{K_{MLE}^2+K_{MLE}}\right)}{I_0\left(2v_k\sqrt{K_{MLE}^2+K_{MLE}}\right)}. \qquad (3.14)$$

Examining (3.14) it can be seen that the arguments of $I_0(\ )$ and $I_1(\ )$ should be unitless. Also, the units of $1+\mu_2$ are inconsistent because the units of $\mu_2 = \frac{1}{N}\sum v_k^2$ are in volts. Another problem with (3.11) is that the Rician-K factor is unitless while $\sum v_k$ has "volts" units, which means that the various terms in the equation do not have the same units. In [22], a formula is given for finding the Rician-K factor which overcomes the problems of (3.14) by replacing each v_i with a normalized variable $y_i = \frac{v_i}{\sqrt{\mu_2}}$. So $1+\mu_2 = 1+\frac{1}{N}\sum v_k^2$ is replaced by $1+\frac{1}{N}\sum y_i^2$ where $y_i = \frac{v_i}{\sqrt{\mu_2}}$. The term $1+\frac{1}{N}\sum y_i^2$ can be simplified to $1+\frac{1}{N}\sum y_i^2 = 1+\frac{1}{N}\sum \frac{v_k^2}{\mu_2}$, which equals

$1+\frac{1}{\mu_2}\frac{1}{N}\sum v_k^2 = 2$. And each v_i argument of $I_0(\ )$ and $I_1(\ )$ is replaced by $\frac{v_i}{\sqrt{\mu_2}}$. So (3.14) becomes

$$2 = \frac{1}{1+K_{MLE}} + \frac{1+2K_{MLE}}{N\sqrt{K_{MLE}(K_{MLE}+1)}} \sum_{k=1}^{N} \frac{v_k}{\sqrt{\mu_2}} \frac{I_1\left(2\frac{v_k}{\sqrt{\mu_2}}\sqrt{K_{MLE}^2+K_{MLE}}\right)}{I_0\left(2\frac{v_k}{\sqrt{\mu_2}}\sqrt{K_{MLE}^2+K_{MLE}}\right)} \qquad (3.15)$$

where v is the measured received voltage, N is the number of samples of measurements, $I_0(\ )$ is the modified Bessel function of the first kind and zero order, and $I_1(\ )$ is the modified Bessel function of the first kind and first order. This formula is unitless and is straightforward to evaluate.

The K_{12} and K_{MLE} formulas have been found by searching for a zero crossing of (3.15) and then using interval halving to refine the zero crossing for a precise result for K_{MLE} and K_{12}.

3.5 Time Variation of the Rician-K Factor

The time-varying Rician-K factor was evaluated for each time varying received voltage at each Rx, Tx distance separation, for both the hallway and the microwave lab.

3.5.1 Hallway

The time-varying Rician-K factor values were calculated using the methods given in Section 3.4. The results are shown in Figure 3.18. These results are explained, based on each method, in this sub-Section. The Rician-K factor found by the K_G / K_{24} method reaches as high as 81 dB and as low as -9 dB. The Rician-K factor found by the K_{12} method is clipped at 62 dB, because the method used to find the roots of (3.9) is unable to find a value larger than 62 dB or about 1200. The Rician-K factor value found by the K_{MLE} method is also clipped, at 74 dB, because the method used to find the roots of (3.15) is unable to find values larger than 74 dB or about 5000. These high values for the Rician-K factor suggest deterministic field behavior. In Figure 3.5 the field is nearly constant and this gives rise to a high Rician-K factor value of 74 dB from the K_{MLE} method. In Figure 3.8 the field is highly variable and this gives rise to a small Rician-K factor value around 0 dB using the K_G / K_{24} method. All three methods gave a good match below the "clipping value" 62 dB . The K_G / K_{24} is the best method used.

3.5.2 Room H853 -Microwave Lab

The time-varying Rician-K factor values were calculated using the methods of Section 3.4. The results are shown in Figure 3.19. The results are explained based on each method. Rician-K factor values found from the K_G / K_{24} method reach as high as 70 dB and as low as 20 dB. The Rician-K factor found from the K_{12} method is clipped at 62 dB. In Figure 3.13 the field is nearly constant and this gives rise to a high Rician-K factor value of 74 dB from the K_{MLE} method. In Figure 3.17 the field is highly variable at 310 cm, which gives rise to small Rician-K factor values around 20 dB using the K_{12} method. For values less than the "clipping" value of 62 dB the three curves correlate quite well in Figure 3.19. As in the hallway, all three methods generate K values that lie very nearly on the same curve. In conclusion, the K_G / K_{24} method is the best, since it is easier to evaluate, has no clipping and agrees with other measurements.

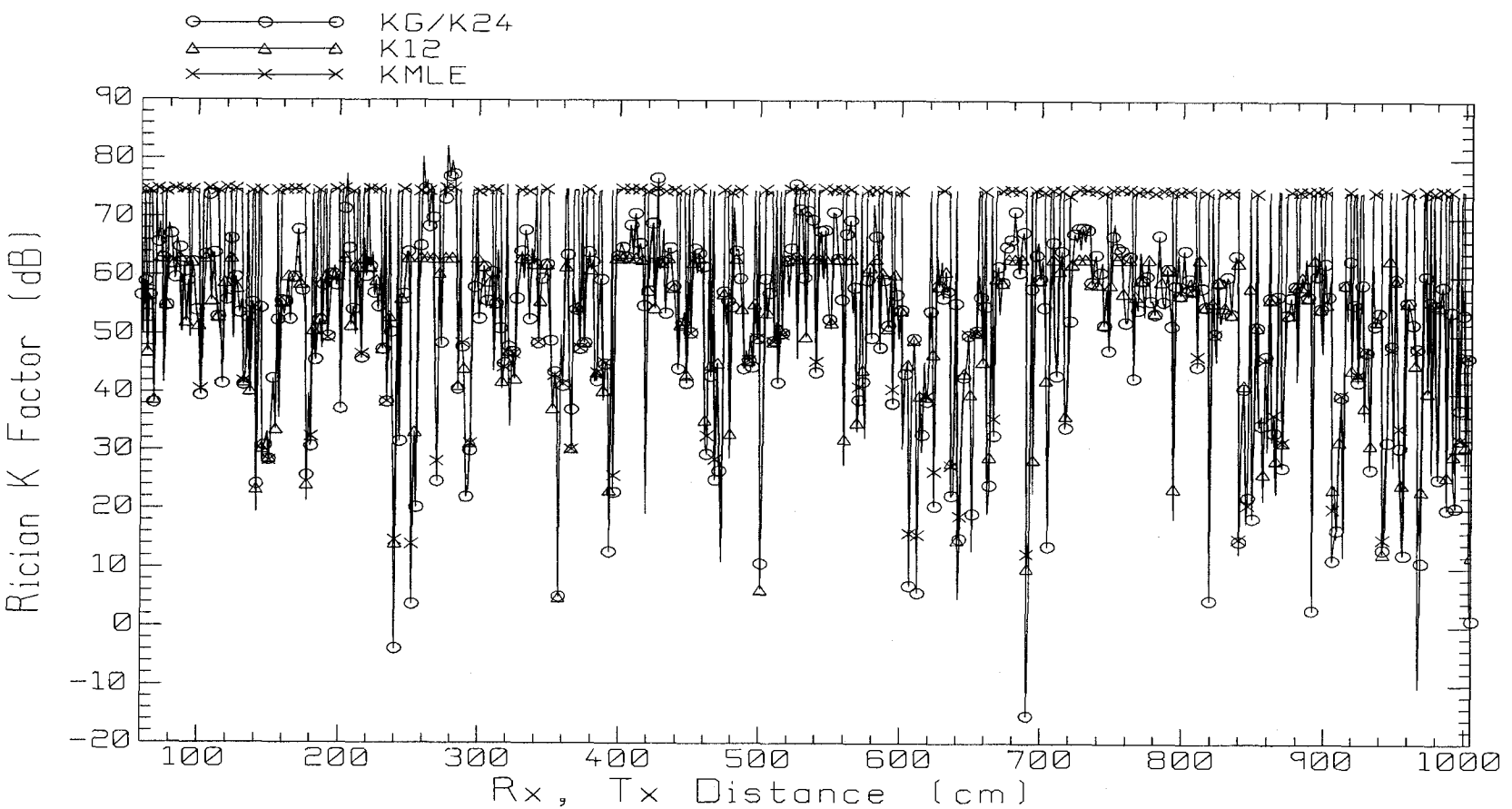

Figure 3.18 Time-varying Rician- K factor values for the hallway.

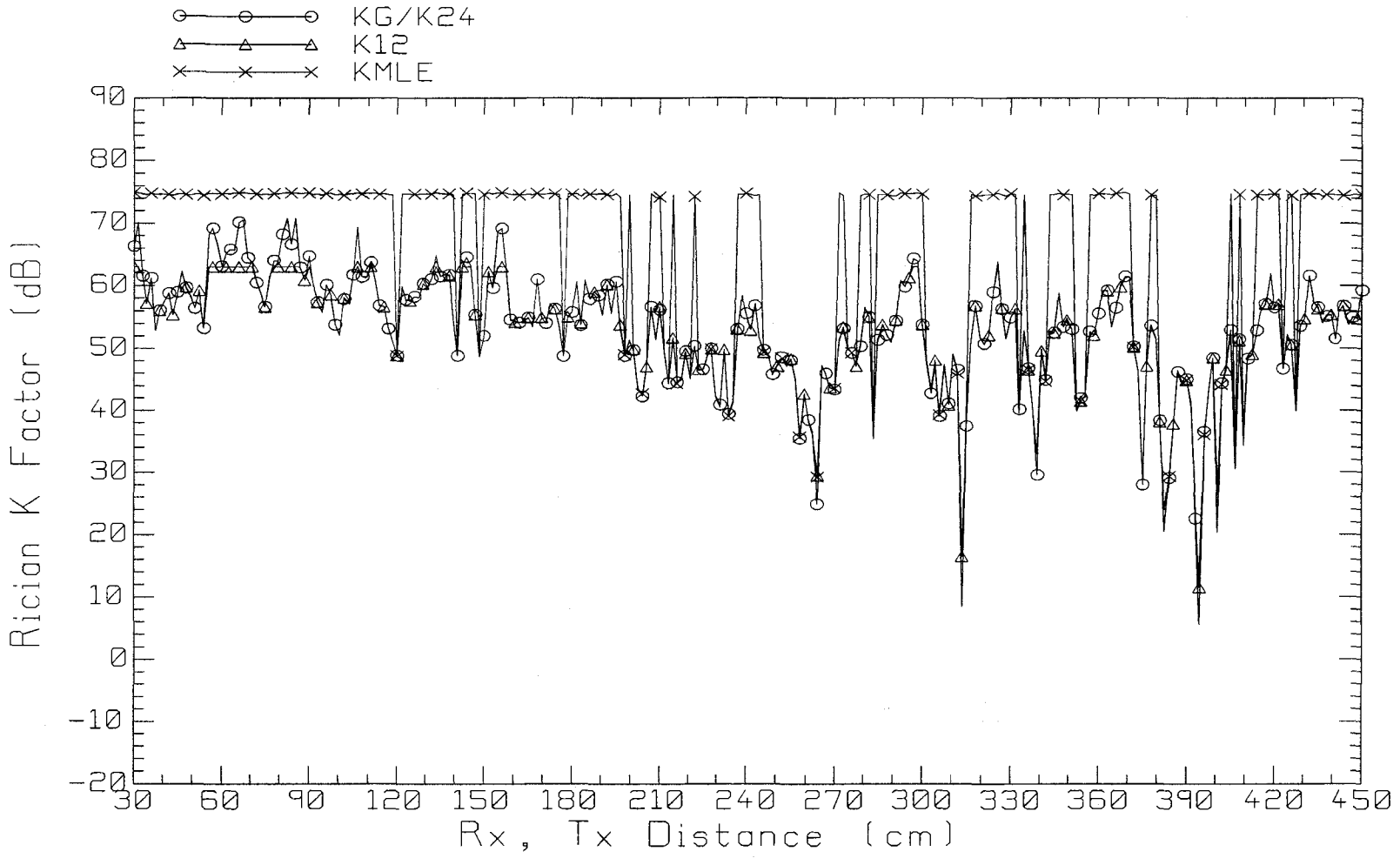

Figure 3.19 Time-varying Rician K Factor values for the microwave Lab.

3.6 Conclusions

In the hallway Figures 3.5 to 3.8 and the microwave lab Figures 3.13 to 3.16, the received voltage is nearly constant over time. In [25] it was noted that in a hospital, fields were constant over time. The voltage variation that was observed was due to the possible movements of people nearby. In [14] it was demonstrated that the time variation of the field occurs, for measurement purposes, when people movement near the receiver antenna is induced. These types of measurements are not reproducible because the signal strength behavior is time-dependent. Measurement of the field strength at a fixed location and at various times of the day, in [29], showed that the random measured field is not reproducible. The range of variation of the received voltage at each distance point was larger in the hallway than in the microwave lab. The hallway is a busy environment, with more people moving in the vicinity, compared to the microwave lab.

Figures 3.18 and 3.19 show the Rician-K factor for the hallway and the microwave lab, respectively. High Rician-K factor values are interpreted as nearly deterministic field behavior, whereas low values indicate a field with randomly-varying behavior. In the hallway, there are many individual points where K values are lower than 30 dB, whereas in the microwave lab, K is between 40 and 60 dB and few points fall below 30 dB. The three methods used to calculate the Rician-K factor showed a good match for values smaller than the clipping level of 64 dB for K_{MLE}. Since the K_G / K_{24} formula is the simplest, it is recommended for evaluation of the Rician-K factor.

Chapter 4

Spatial Variation

4.1 Averaged Temporal Voltage in dB versus Distance

The measurement campaign for the hallway in the EV15th floor and for the microwave lab, room H853, considered both time and space variation of the received signal. At each distance point 30 time samples were taken. In this Chapter, the average value of the 30 samples is taken at each point, and the average voltage is plotted versus distance to study the space variation of the field. The method deployed here is similar to that used by Loredo in [30] , using a Rician model to represent the spatial variation of the field. Loredo used the Rician-K factor to estimate the spatial variation by taking different local area windows along the path and estimating the Rician-K factor value for each window.

4.1.1 Hallway

The space variation of the received signal for the hallway is plotted in Figure 4.1. For small distances between the transmitter and the receiver, up to 250 cm, the average value of the curve in Figure 4.1 decreases with distance, similar to free space behavior. In this range of distances the direct field is much greater than the reflected field component and it is dominant. For distances greater than 250 cm, the field strength

decreases more slowly than the inverse distance and shows multipath fading. There are nulls which repeat every 100, 400, 500 and 600 cm. According to [38], multipath fading is due to reflected rays that go in and out of phase with the dominant ray, and this behavior is clearly observable in Figure 4.1.

4.1.2 Room H853 - Microwave Lab

The 30 time samples taken at each distance post are averaged, and this average voltage for the path measured in the microwave lab is shown in Figure 4.2. The average value of the received voltage decreases as the distance in free space increases from 30 cm to 225 cm along the measured path. Deep nulls occur at 300 cm and 390 cm. From 225 cm to 390 cm the voltage variation has a range of around 29 dB. The received voltage varied around 15 dB, with a maximum at -60 dB and a deep null at -89 dB. From 390 to 450 cm the voltage has a range of 12 dB with a maximum of -67 dB and a minimum of -89 dB .

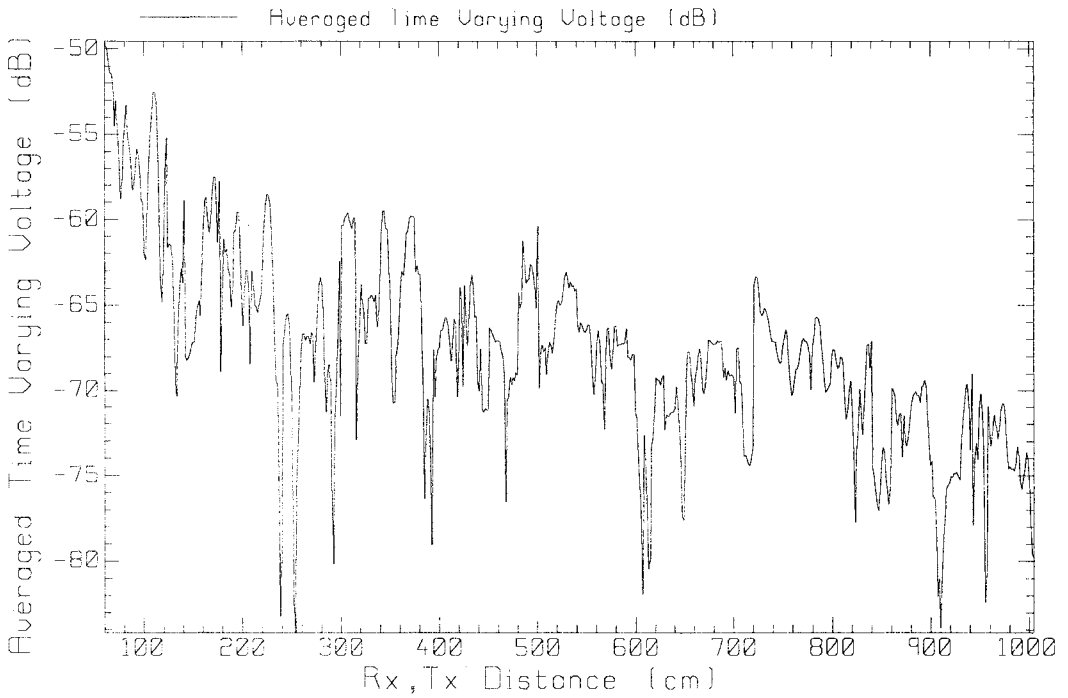

Figure 4.1Time- averaged voltage versus distance for the hallway.

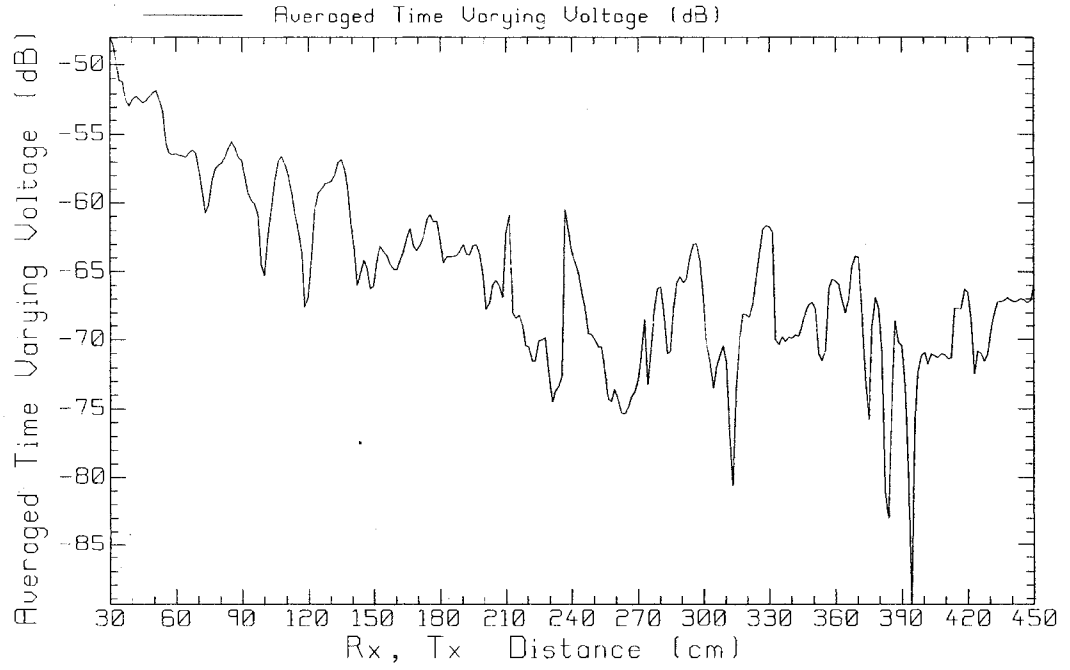

Figure 4.2 Time- averaged voltage versus distance for the microwave lab.

4.2 Large-Scale Fading

Large-scale fading or slow fading for the signal strength is found by averaging all the voltage values in a window of width W centered at some distance r along the path. The window slides along the path as r increases, and the average value within the window is graphed as a function of r. In the next Section, slow fading is shown for window sizes of W = 51.5, 101.5 and 151.5 cm, comparing to 4.8 and 12 λ at 2.388 GHz.

4.2.1 Hallway

In the hallway, the field strength was measured at 631 points 1.5 cm apart. Figures 4.3, 4.4 and 4.5 show the large scale fading with window sizes of 4λ, 8λ and 12 λ, respectively. Figure 4.3 shows that the 4λ window size effectively eliminates the fast fading and displays the average value of the received voltage as a function of distance. Close to the antenna at distances from 85.5 to 141.0 cm, the average received voltage decreases as the inverse of distance. That is, at 85.5 cm the voltage is -54.74 dB, and at twice the distance, or 171.0 cm, it is -61.88 dB, for a difference of 7.14 dB. The ratio of space-free behavior at twice the distance gives a voltage level difference of 6 dB. The observed value of 7.14 dB for twice the distance is a good approximation. Figure 4.4 with an 8λ window further suppressed the spatial variation. Figure 4.5 with a 12 λ window shows the field is straight for 150 to 200 cm, constant from 200 to 400 cm and slightly variable from 400 to 1000 cm.

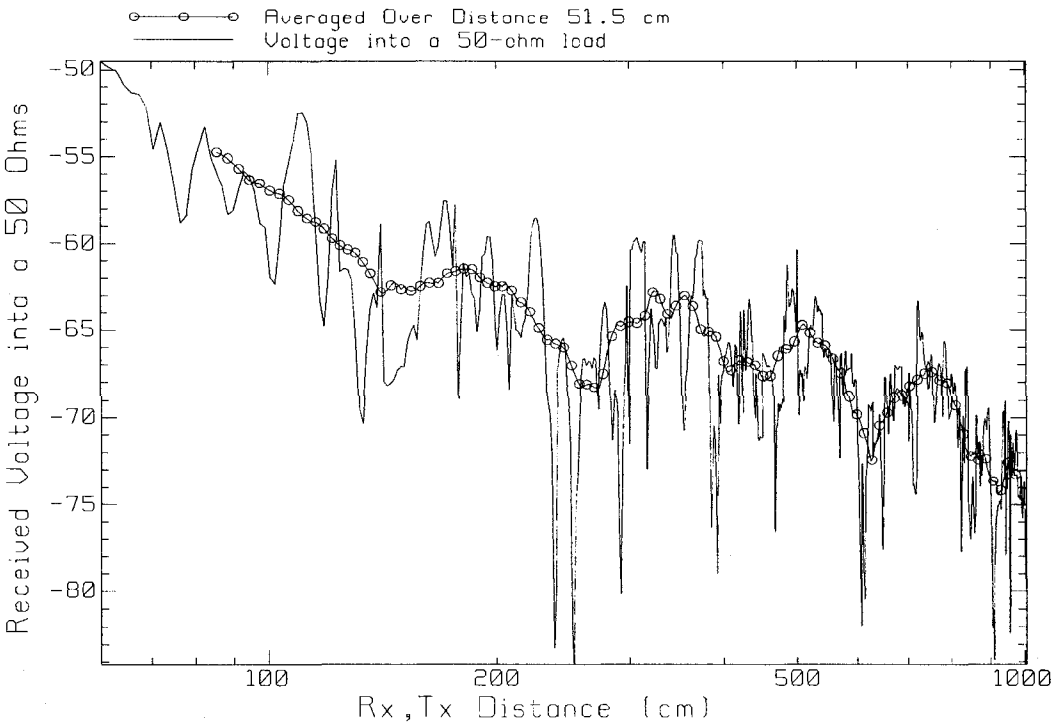

Figure 4.3Comparison between the point-by-point measured voltage and the voltage averaged over a 51.5 cm (4λ) window for the hallway.

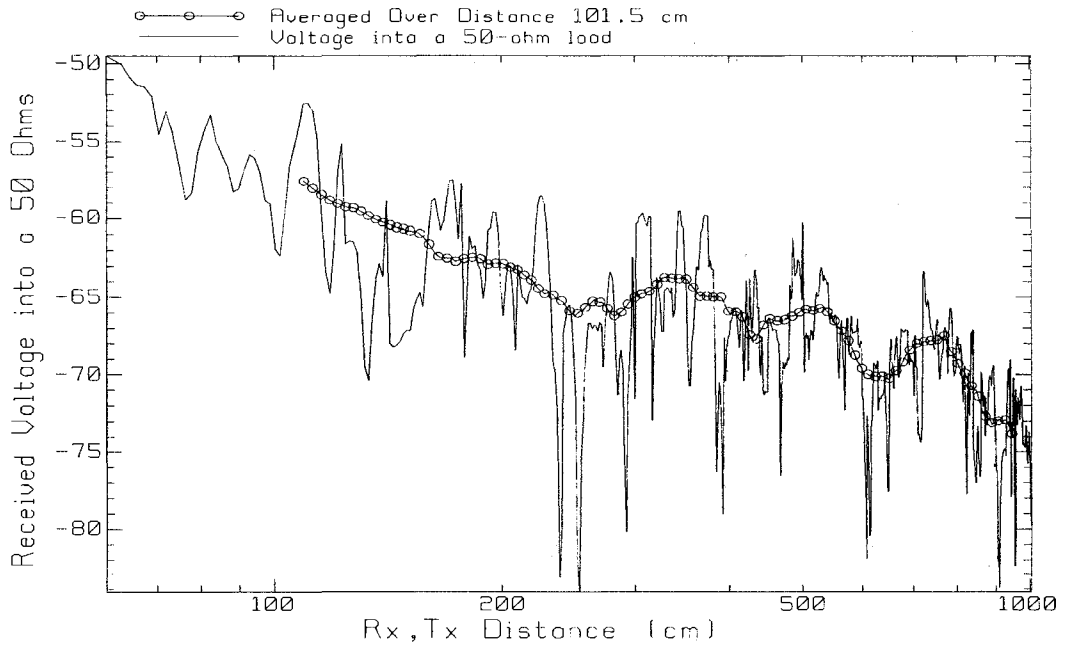

Figure 4.4 Comparison between the point-by-point measured voltage and the voltage averaged over a 101.5 cm (8λ) window for the hallway.

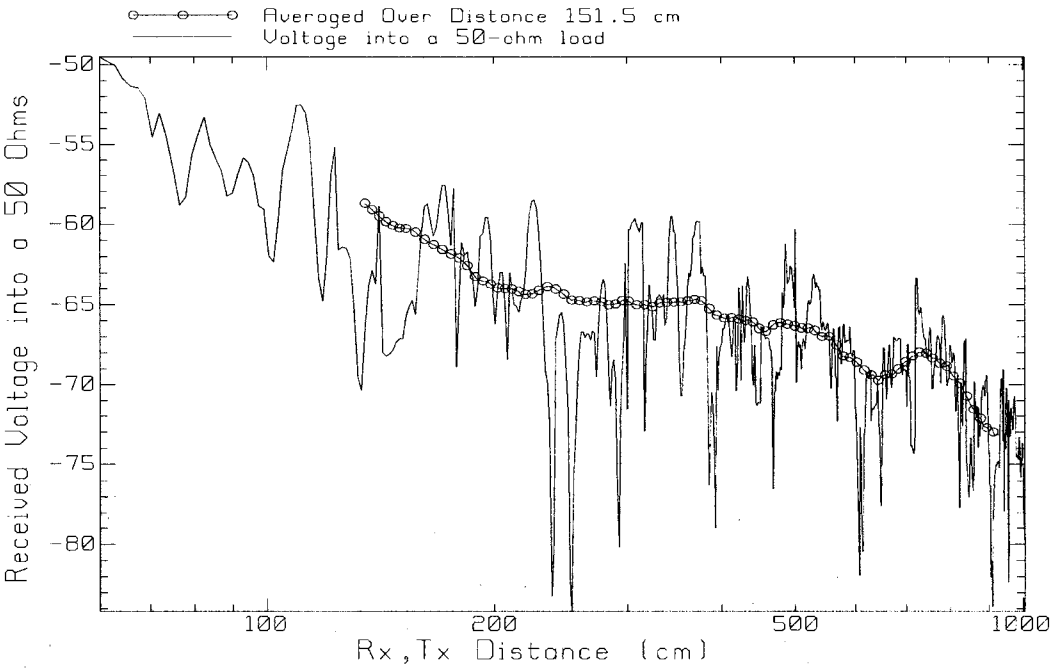

Figure 4.5 Comparison between the point-by-point measured voltage and the voltage averaged over a 151.5 cm (12λ) window for the hallway.

4.2.2 Room H853 -- Microwave Lab

In the microwave lab, the field strength was measured at 281 points 1.5 cm apart. Figures 4.6, 4.7 and 4.8 show the large scale fading for the microwave lab, with window sizes 4, 8 and 12 λ, respectively. The received voltage is less variable with distance in the microwave lab than in the hallway, that is, it shows less small-scale variation. The window size is not as significant as in the hallway, as can be observed by the very similar curves for each window size. In other words, changing the size of the averaging window does not have as much effect as in the hallway. At closer distances the averaged voltage acts as free space. To verify this, two samples are taken: the second distance twice that of

the first, to see if their corresponding averaged voltage value difference is 6 dB. In Figure 4.6 at distance 55.5 cm the averaged voltage value is -54.02 dB, while at 111.0 cm the averaged voltage value is -59.26 . The difference between the two averaged voltage values is 5.25 dB which is considered a good approximation for free space.

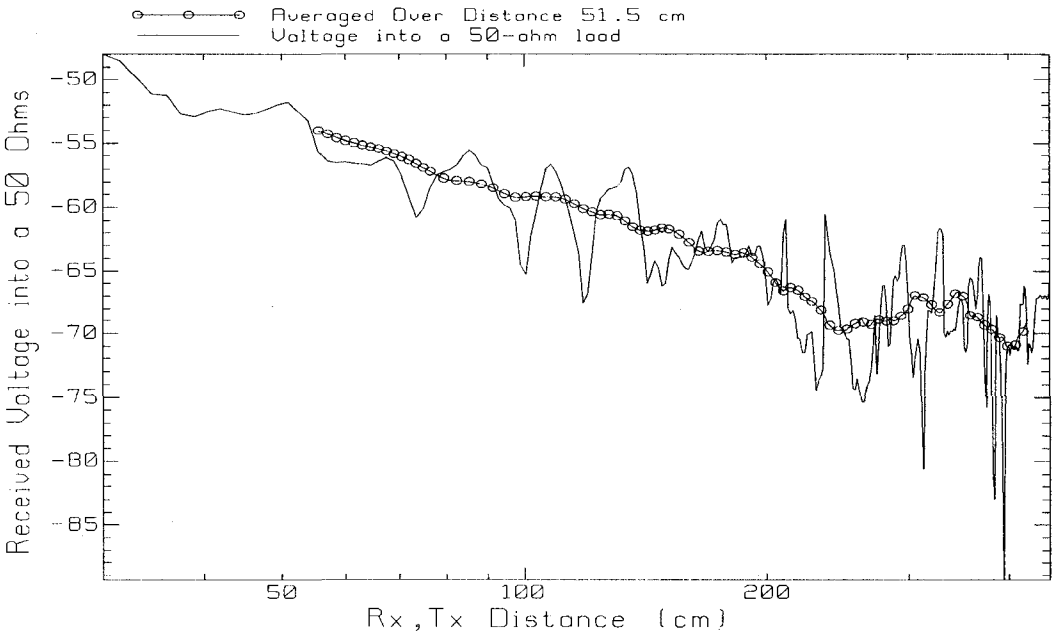

Figure 4.6 Comparison between the point-by-point measured voltage and the voltage averaged over a 51.5 cm (4λ) window for the microwave lab.

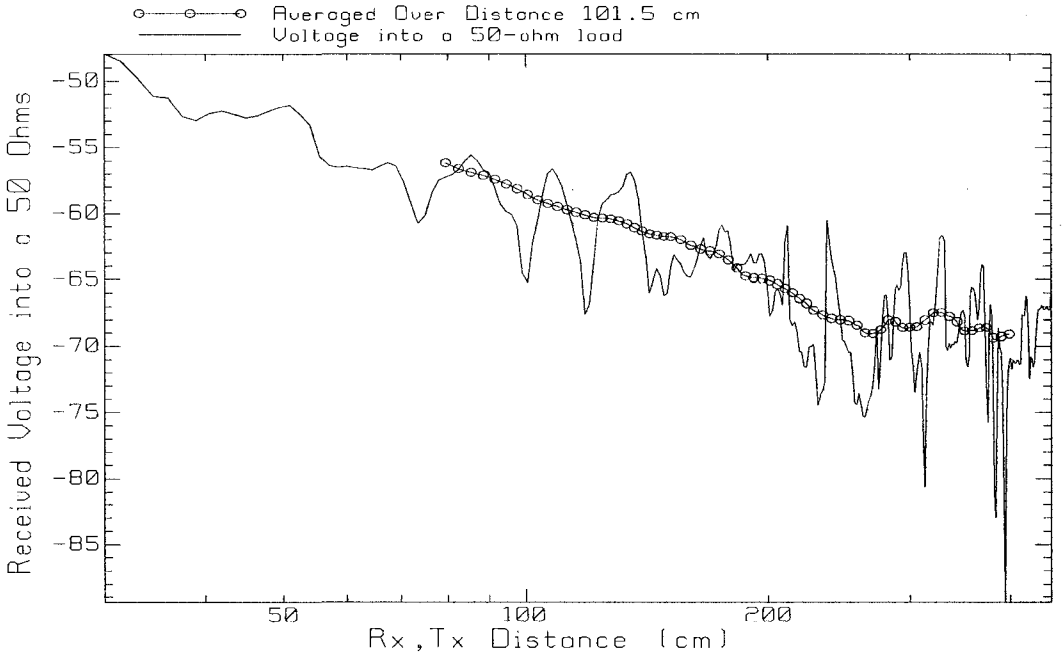

Figure 4.7 Comparison between the point-by-point measured voltage and the voltage averaged over a 101.5 cm (8λ) window for the microwave lab.

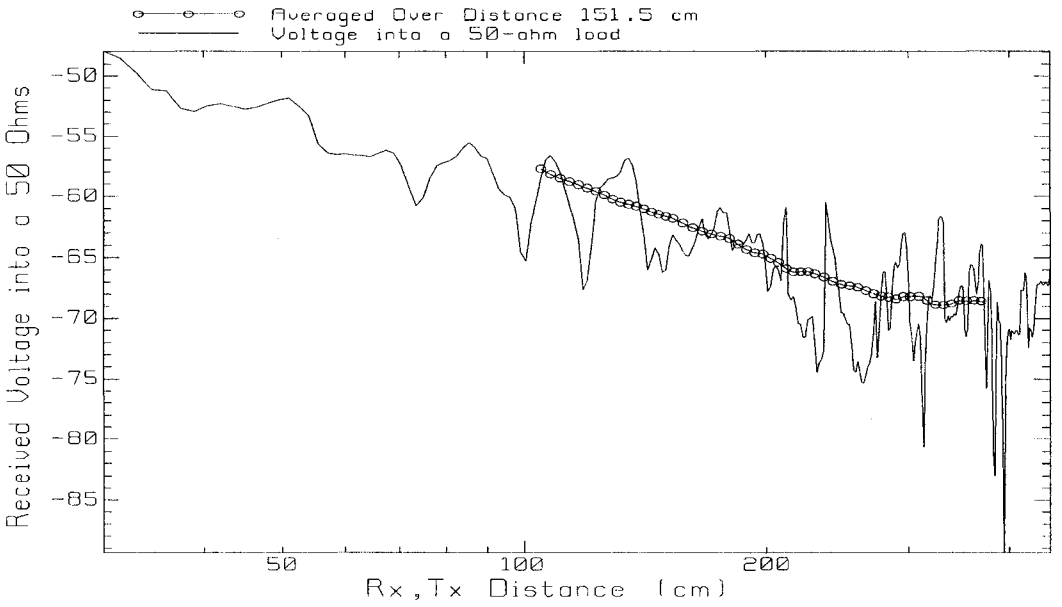

Figure 4.8 Comparison between the point-by-point measured voltage and the voltage averaged over a 151.5 cm (12λ) window for the microwave lab.

4.3 Spatial Variation of the Rician-K Factor

For a given distance between the transmitter and the receiver, all the data points within a window of width W were taken, extending from (r- W/2) to (r+W/2). This set of "windowed" data points are then used to calculate the Rician-K factor using the methods of Chapter 3 to evaluate $K_G / K_{24}, K_{MLE}$ and K_{12}. Three sizes for the sliding window will be considered, W = 51.5 cm, 101.5 cm and 151.5 cm, which correspond to approximately 4, 8 and 12 λ. The results are given in the following Sections.

4.3.1 Hallway

Figures 4.9, 4.10 and 4.11 show the space-varying Rician-K factor as a function of distance in the hallway for sliding windows of sizes 4λ, 8λ and $12\ \lambda$ respectively. In Figure 4.9 the curve for K_G / K_{24} (circles) has missing data from 120 to 130 cm and again from 230 to 280 cm, where the K_G formula of (3.5) leads to the square root of a negative number. Figures 4.10 and 4.11 also have distance ranges where no value of K_G could be found. In Figure 4.9, for K_{12} (triangles), in some distance ranges such as 110 to 140 cm, 220 to 240 cm and 280 to 320 cm, the root-finding algorithm used to solve (3.9) clips at about 18 dB. There are similar distance ranges in Figure 4.10 and 4.11. The K_{MLE} formula (3.14) (crosses) always gives a solution.

In Figures 4.9, 4.10 and 4.11 two distance ranges are observed. The first range is from 90 cm to 400 cm in Figure 4.9, 110 cm to 400 cm in Figure 4.10, and 130 cm to 400 cm in Figure 4.11. Methods for finding the Rician-K factor do not agree well in the first range. However, for the second range, from 400 to 980 cm in Figure 4.9, 400 to 945 cm in Figure 4.10, and 400 to 925 cm in Figure 4.11, the values found by the three methods correlate well in Figures 4.9 and 4.10. In Figure 4.11 the curve for the K_{MLE} is almost constant and does not have the large maxima and minima observed with other methods.

For the hallway measurement, the K_{MLE} formula is the best tool for evaluating the Rician-K factor because it found values for every distance between the transmitter and the receiver. For a window of 4λ, K_{MLE} (crosses) is about 12 dB and shows peaks and nulls for distances between 90 and 980 cm. For a size 8λ window, K_{MLE} is much more nearly constant and for a 12λ window, K_{MLE} is almost constant. Therefore, for a large window size the Rician-K factor is about the same everywhere in the hallway.

4.3.2 Room H853-Microwave Lab

Figures 4.12, 4.13 and 4.14 show the space-varying Rician-K factor for the microwave lab. The size of the sliding window is 4λ,8λ and 12 λ, respectively. For the K_G / K_{24} method (circles) data is missing between 220 and 260 cm and between 320 and 330 cm in Figure 4.12. In Figure 4.13, K_G / K_{24} has missing data at 80 cm and between 255 and 280 cm. In Figure 4.14, K_G / K_{24} has missing data at 100 cm, between 190 and 210 cm and around 280 cm. This missing data occurs because (3.5) leads to the square root of a negative number, as was the case in the hallway. The K_{12} method (triangles) is clipped at 18 dB by the algorithm used to find the root for (3.9), observable in the ranges between 220 and 260 cm, 320 and 330 cm and between 370 and 390 cm in Figure 4.12. In Figure 4.13 this same clipping can be seen between 210 and 240 cm, 250 and 300 cm and between 320 and 360 cm. In Figure 4.14 it is between 108 and 120 cm, 180 and 210 cm, 230 and 250 cm, 260 and 270 cm, 280 and 290 cm, and between 320

and 340 cm. The K_{MLE} method, however, finds the Rician-K value for all of the distances between the transmitter and the receiver.

In Figure 4.12 K_{MLE} values vary with distance, with a large maximum at 165 cm, and a minimum between 220 and 250 cm. K_{MLE} is almost constant between 260 and 420 cm. In Figure 4.13, with an 8λ window, K_{MLE} is approximately constant along the path. Figure 4.14 show that with a 12λ window K_{MLE} is very nearly constant, especially from 210 to 360 cm.

The correlation among the three methods for calculating the Rician-K factor is as follows. The graphs in Figures 4.12, 4.13 and 4.14 all show two regions. The first region is from 60 cm until 230 cm in Figure 4.12, 80 to 230 cm in Figure 4.13 and from 100 to 230 cm in Figure 4.14 The second region is from 230 cm until the end of the path. In Figure 4.12 the three curves K_G / K_{24}, K_{12} and K_{MLE} correlate well in the first region. In Figure 4.13 the three curves correlate less in the first region. In Figure 4.14 there is no correlation between the curves in the first region. In the second region in Figure 4.12 K_G / K_{24} and K_{12} correlate recursively but do not agree with K_{MLE}. In Figure 4.13, the K_{12} method fails over the second region and K_G / K_{24} does not agree with K_{MLE}. In Figure 4.14 there is little agreement among the three methods in the second region. As in the hallway, the K_{MLE} method is the best method to use to find the space-varying Rician-K factor since it estimates all values of K along the path.

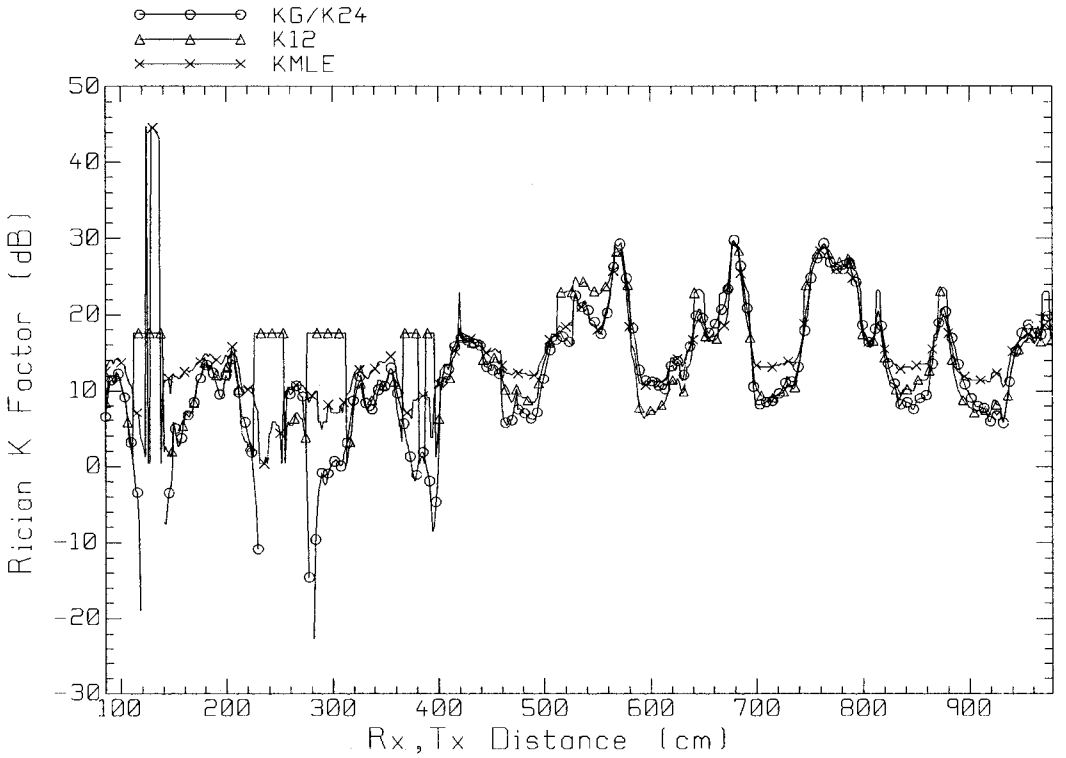

Figure 4.9 Space-varying K values for the hallway, sliding window size approx. 4λ.

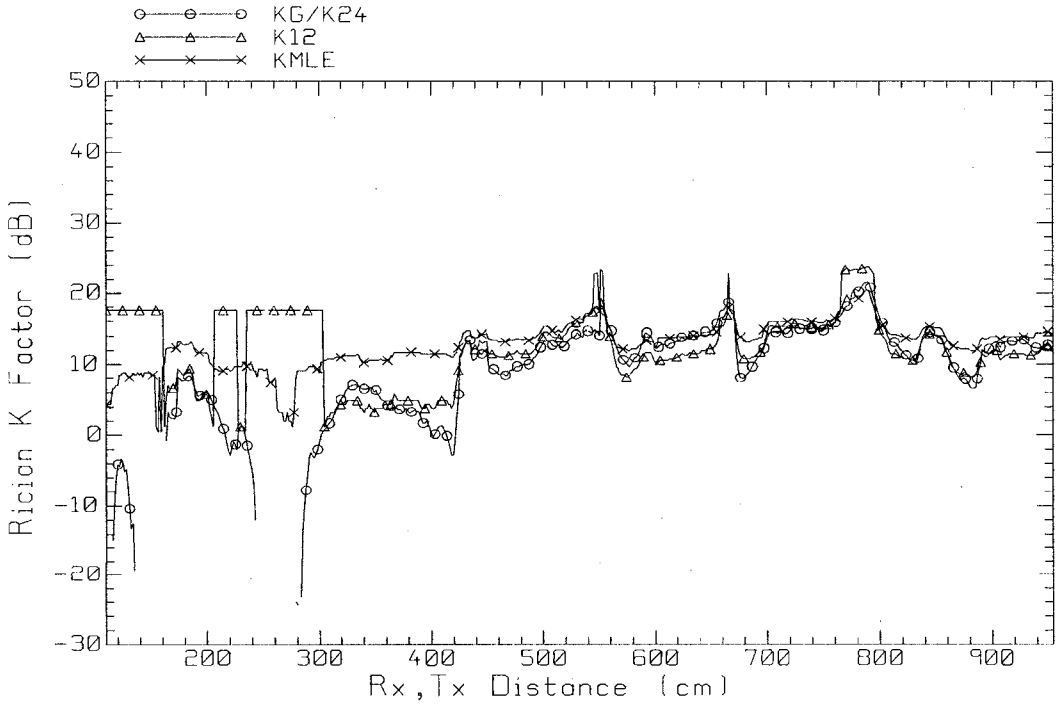

Figure 4.10 Space-varying K values for the hallway, sliding window size approx. 8λ.

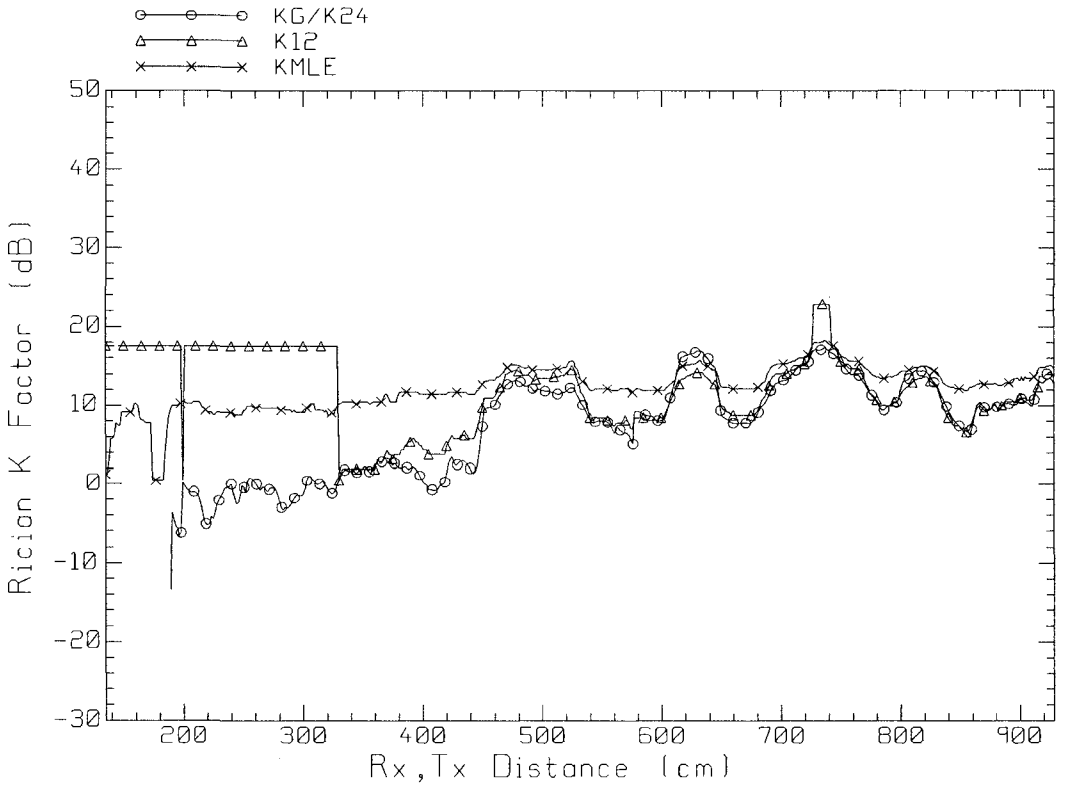

Figure 4.11 Space-varying K values for the hallway, sliding window size approx.12 λ.

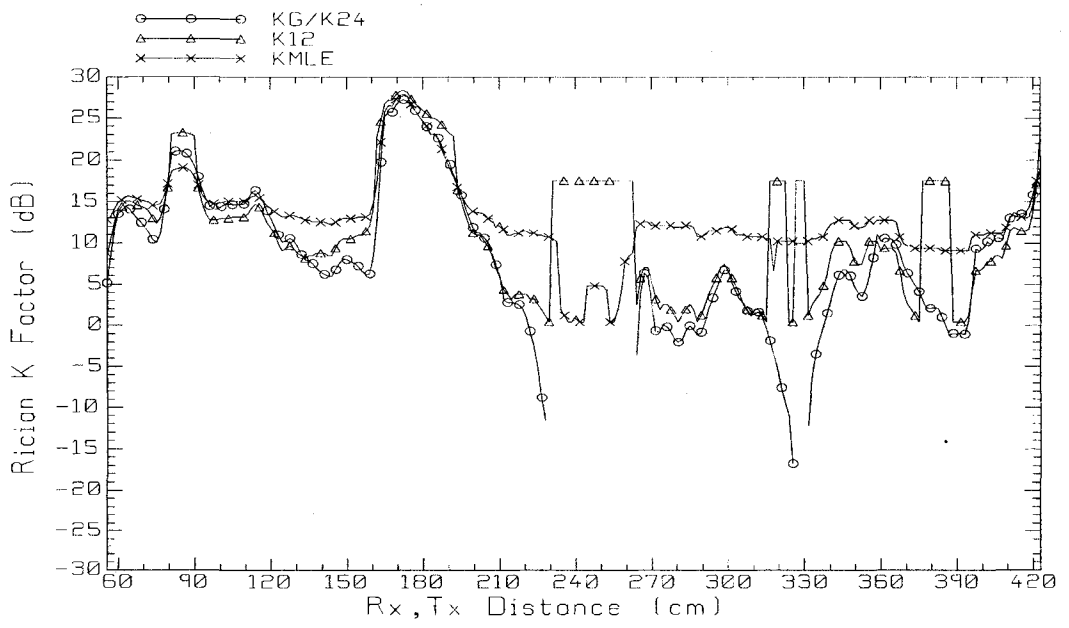

Figure 4.12 Space-varying K values for the microwave lab, sliding window size approximately 4 λ.

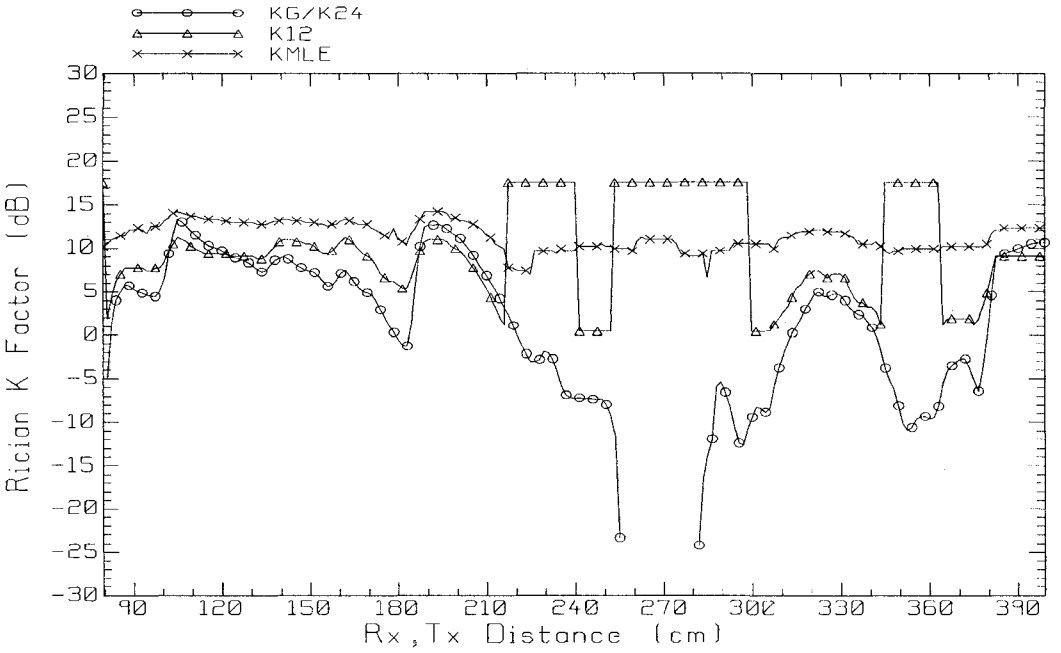

Figure 4.13 Space-varying K values for the microwave lab, sliding window size approximately 8λ.

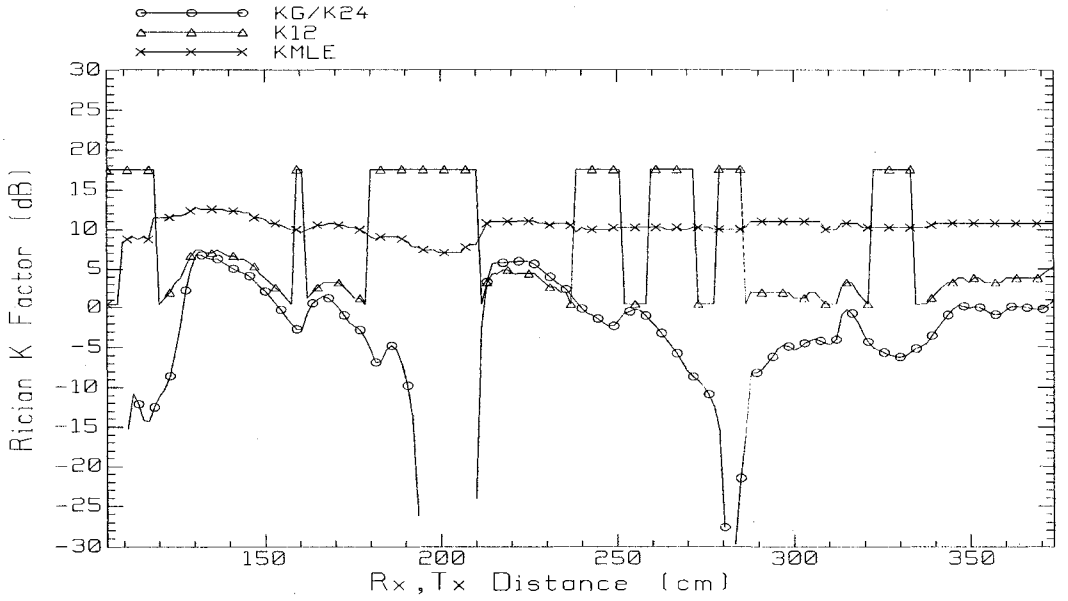

Figure 4.14 Space-varying K values for the microwave lab, sliding window size approximately 12λ.

4.4 Conclusions

Large-scale fading is sensitive to the number of points being averaged and to the variation of the received voltage. For the hallway, it is obvious in Figures 4.3 to 4.6 that as the size of the window is increased, large-scale fading tends to be less variable. However, for the microwave lab, increasing the size of the window did not lead to a significant change in the shape of the curve, as can be seen in Figures 4.6 to 4.8. The space-varying Rician–K factor is best evaluated using the K_{MLE} method, since this method estimated all values for K for all of the windows. With a large average window of 12λ, the Rician-K factor estimated by the K_{MLE} method is approximately constant with distance along the path for both the hallway and the microwave lab, and in both cases has a value of about 12 dB. In [30] the range for the space varying Rician-K factor had 3.45 as the maximum value, but in this thesis the maximum value found for the Rician-K factor is 45 dB for the hallway using the K_{MLE} method and 27 dB for the microwave lab using the three methods mentioned in literature. The results for the Rician-K factor obtained are significantly different than in [30].

Chapter 5

Geometrical Optics Simulation

5.1 Modeling

In this Chapter, ray tracing will be used to simulate the hallway and microwave lab using the GO_3D program [3]. The received electric field strength will be calculated for a transmitter with frequency and output power similar to the one used for the measurements with the site survey system. Note that in the ray-tracing simulation the transmitter and receiver are interchanged, compared to how they were used in taking measurements. The transmitter here is at a fixed location and the receiver is moving along the measurement path. By reciprocity, the received field strength should be the same.

Also, in the simulation, the transmitting antenna is a half-wave dipole radiating 10 mW. The received field strength will be converted to received voltage as explained in Section 5.2.

5.1.1 Hallway

Figure 5.1 shows the floor plan of the northwest corner of the 15^{th} floor of the EV building modeled for analysis of the GO_3D program. The location of the sleeve dipole and the position of the path corresponds precisely to the measurement scenario.

The following dimensions are shown in Figure 5.1. The location of the Tx antenna is in the center of the hallway 60 cm from the wall behind it. The measurement path initial distance is 60 cm for the Tx dipole. The path length is 945m. The received signal values were calculated every 1.5 cm along the path. The Tx is placed 103 cm above the ground and the Rx is displaced 107 cm above the ground. Transmitting frequency is 2.388 GHz and the output power is 10 mW.

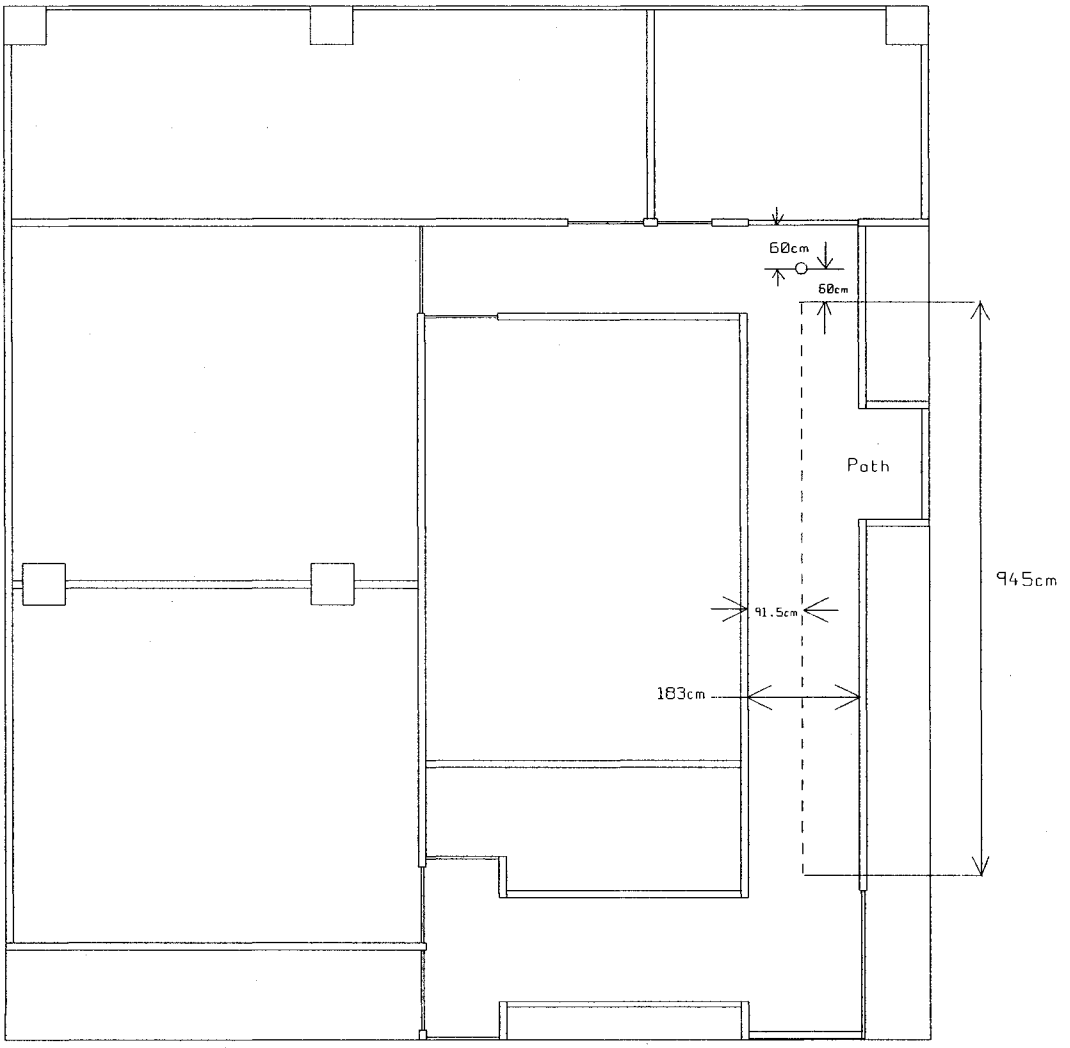

Figure 5.1 GO_3D simulated version of the northwest corner of the 15th floor in Concordia's EV building showing the Tx location and the path for the received electric field [39].

5.1.2 Room H853 Microwave Lab

Figure 5.2 shows a simulated version of the microwave laboratory with representation of some equipment, showing all of the dimensions of the measurement setup. The transmitting dipole is 90 cm from the nearby lab bench, labeled in the Figure "wood table". The path starts 30 cm from the dipole and has a length of 450 cm. The path is in the middle of the space between the two benches. The Tx is 103 cm above the ground and the Rx is 107 cm above the ground. The transmitting frequency is 2.388 GHz and the output power is 10 mW.

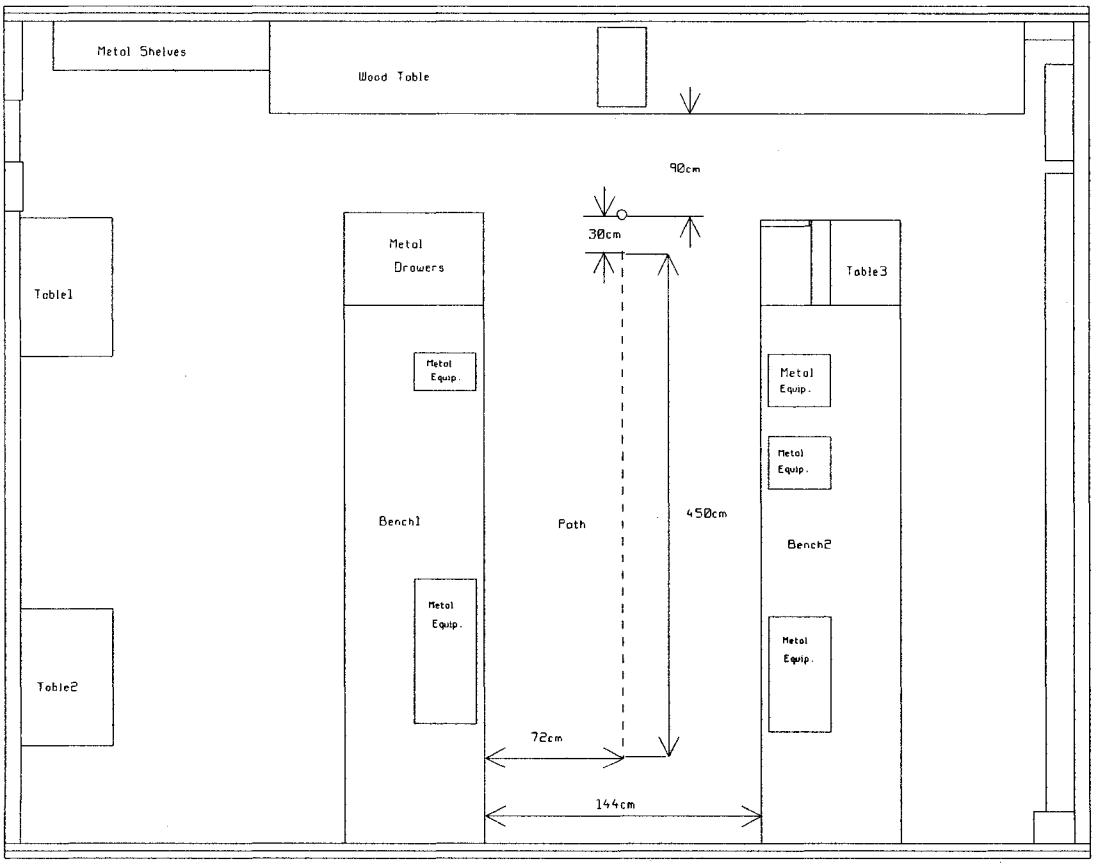

Figure 5.2 GO_3D simulated version of the microwave lab showing the Tx location and the path for the received electric field.

5.2 Voltage in dB versus Position

The GO_3D program calculates the amplitude of E_x, E_y, and E_z at every point along the path. These are combined to get the "total" electric field amplitude E_t using

$$E_t = \sqrt{|E_x|^2 + |E_y|^2 + |E_z|^2} \,. \tag{5.1}$$

The total electric field values are transformed into received voltage across a 50-ohm load in dB for comparison with measured received voltage values. The following formulas were used to make the transformation. The amplitude of the total electric field strength computed by GO_3D is converted to an RMS value using

$$E_{rms} = \frac{E_{ampl}}{\sqrt{2}} \tag{5.2}$$

where E_{ampl} is the amplitude of the total electric field strength computed by GO_3D, and E_{rms} is the RMS value of the total electric field strength.

The RMS value of the electrical field strength is transformed to dB using

$$E_{dB} = 20\log_{10} E_{rms} \tag{5.3}$$

where E_{dB} is the electric field strength in dB, relative to 1 V/m field strength.

To transform the electrical field strength in V/m to voltage in dB, a parameter known as the Antenna Factor (1/m) must be found for the Rx antenna. This is found using [25]

$$AF_{dB} = 20\log_{10}(f) - G_{dBi} - 149.8 \tag{5.4a}$$

where the frequency f is in Hz, or equivalently

$$AF_{dB} = 20\log_{10}(f_{MHz}) - G_{dBi} - 29.8 \tag{5.4b}$$

where the frequency f_{MHz} is in MHz and is 2388 MHz in this thesis. In these equations, AF_{dB} is the antenna factor in dB, and G_{dBi} is the gain of the receiving antenna, which is 1.83 dB, obtained from the specification sheet of the sleeve dipole used in the measurements.

From the antenna factor in dB and the electric field strength in dB, the voltage received in dB can be found from

$$V_{dB} = E_{dB} - AF_{dB} \tag{5.5}$$

where V_{dB} is the voltage received in dB.

The voltage received in dB is transformed to linear scale by the following:

$$V = 10^{\frac{V_{dB}}{20}} \tag{5.5}$$

where V is the voltage in linear scale.

Thus, the GO_3D program reports E_{ampl}, which is converted to E_{dB} using eqs. (5.2) and (5.3). Then E_{dB} is converted to voltage V_{dB} using (5.4) after the antenna factor is found from (5.3).

5.2.1 Comparison of Measurement and Simulation Results

When comparing measured results with the simulated data from GO_3D, it must be noticed that the output power of the transmitter in the simulation is assumed to be 10 mW. For the measurement results this was not the case because the actual power radiated is not known. The output power of the circuit in the transmitting unit was measured to be 10 mW into a matched load. But the input impedance of the monopole on the transmitter unit is not known, so the actual radiated power is not known [24]. The measured voltage needs to be calibrated to be the same voltage level as the simulated data. This has been done by multiplying the measured data on a linear scale by the linear ratio of the average value of the simulated voltage to the average value of the measured voltage.

5.2.1.1 Hallway

Figure 5.3 shows the simulated and calibrated measured voltage for the hallway. The fast fading of the simulated voltage does not match the measured voltage very well. Also, [40] shows that the accuracy of the results of a ray-tracing simulation are greatly enhanced if the electrical parameters of the wall materials are measured directly. But in the ray-tracing model used in this thesis the electrical parameters were found from the literature and it is not known if they are a good representation of the actual walls in the hallway.

Another possible reason for the considerable difference between the measured data and the simulation in Figure 5.3 is the construction of the walls in the 15^{th} floor hallway. The ray-tracing model represents the walls as constructed of uniform layers of materials. But the actual wall construction is gyproc sheets about 1 cm in thickness, supported by vertical metal studs with approximately 16 cm spacing. The wall construction is poorly modeled by a uniform layered structure. Instead the metal studs may behave as a secondary source, and this cannot be modeled in the GO_3D program.

5.2.1.2 Room H853 microwave lab

Figure 5.4 shows the simulated and calibrated measured data for the microwave lab. The data shows a good match between the simulated and calibrated measured data from 30 cm to 140 cm, and a reasonable match up to 240 cm. A possible reason for the good match is the detailed representation of the microwave lab in the GO_3D program. There is a marked difference in the region between 240 and 330 cm. Eventually, at about 400 cm, the walls in the microwave lab behave as uniform layered structures.

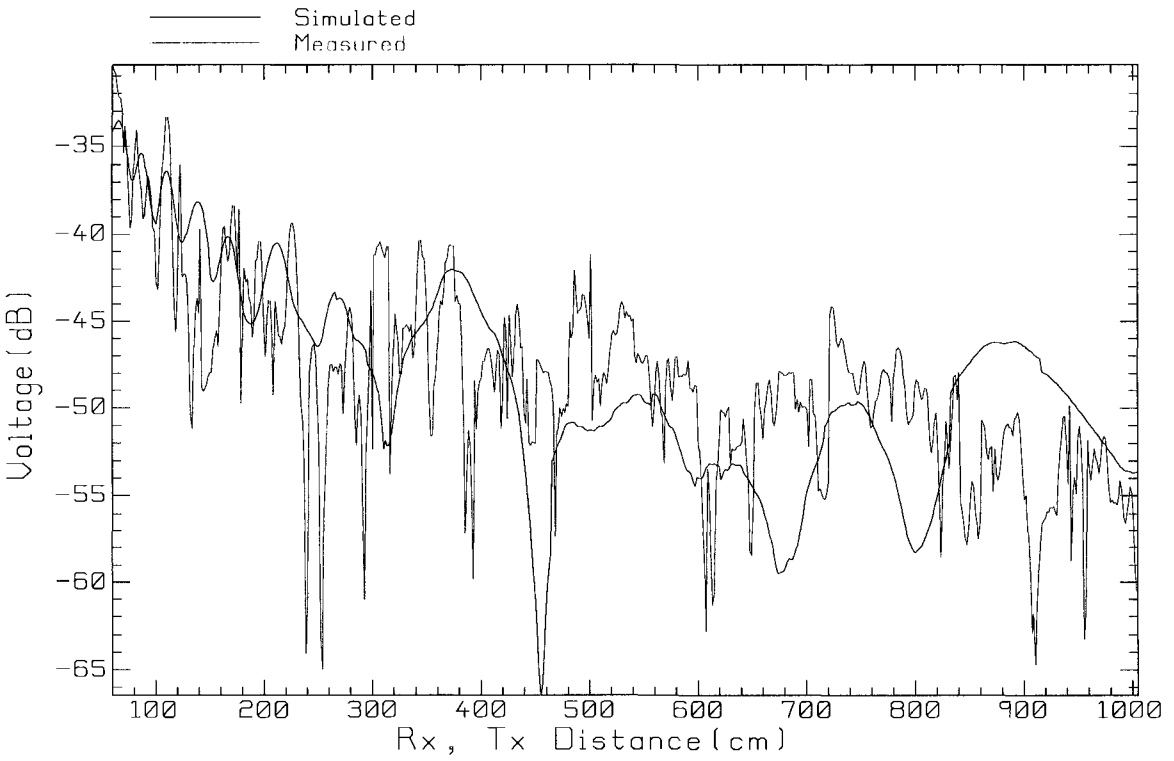

Figure 5.3 Simulated and calibrated measured results of voltage in (dB) versus distance for the hallway.

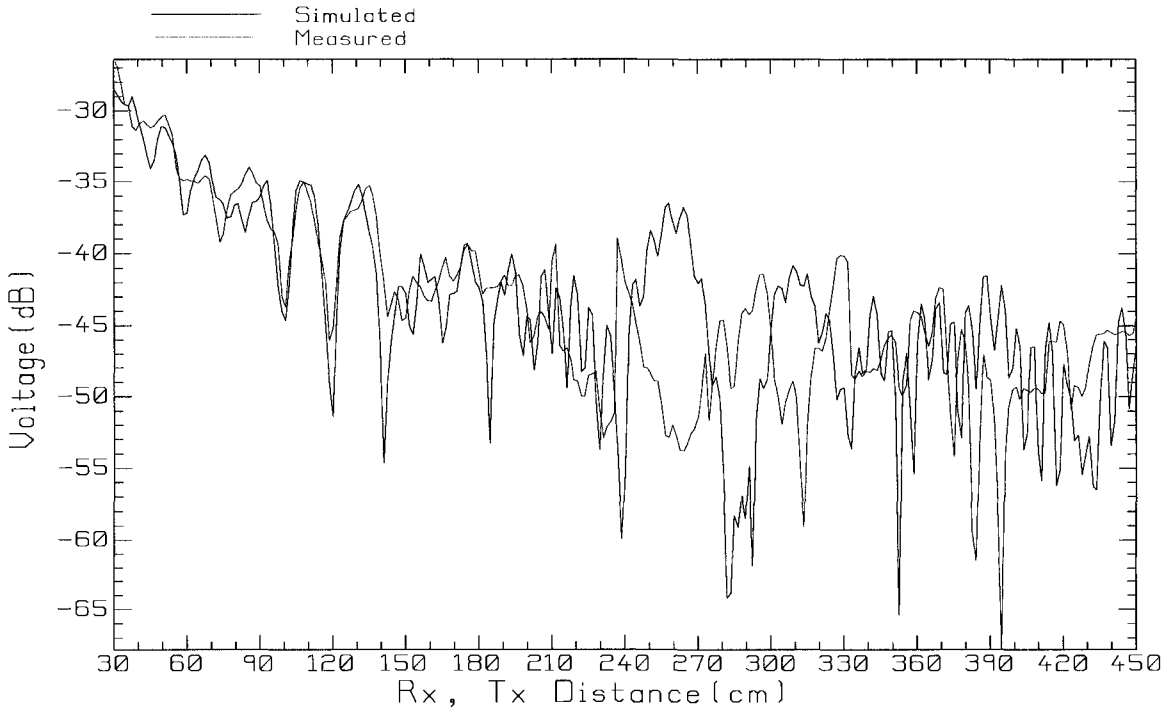

Figure 5.4 Simulated and calibrated measured results of voltage in (dB) versus distance for the microwave lab.

5.3 Path loss Index "n"

The path loss index is a parameter used to describe the variation of the large-scale variation of the received voltage over distance. The path loss index n is calculated from measured data in the following manner [24]. The power law model on a logarithmic scale is

$$V_{dB} = 20.\log\left[\frac{V_o}{r^n}\right]. \tag{5.6}$$

Rearranging results in

$$V_{dB} = 20\log V_0 - n.20\log r_i. \tag{5.7}$$

(5.7) is the equation for a straight line

$$y_i = b + mx_i \tag{5.8}$$

where $y_i = V_{dB_i}, b = 20\log V_0 = V_{dB0}$, $b = -n$ and $x_i = 20\log r_i$.

Using the method of least square error which assumes that the square of the sum of the difference between the measured value of data and the straight line is to be minimized. Q is presumed to be the difference between the measured data V_{dB_i} and the straight line $y_i = b + mx_i$. If m is the number of points of measurements, then Q is given by

$$Q = \sum_{i=1}^{m} \left(V_{dBi} - \left(V_{dB0} - n20\log r_i\right)\right)^2 \tag{5.9}$$

To find the values of V_{dB0} and n that make Q minimum, take the partial derivative of Q with respect to V_{dB0} and set it equal to zero, and take the partial derivative of Q with respect to n and set it equal to zero. This results in two linear equations with two unknown quantities; V_{dB0} and n. Solving the two linear equations for V_{dB0} and n in terms of the other quantities results in

$$n = \frac{\sum_{i=1}^{m} V_{dBi} \sum_{i=1}^{m} 20\log(r_i) - m\sum_{i=1}^{m} V_{dBi} 20\log(r_i)}{m\sum_{i=1}^{m} (20\log(r_i))^2 - \left(\sum_{i=1}^{m} 20\log(r_i)\right)^2} \tag{5.10}$$

and

$$V_{dB0} = \frac{\sum_{i=1}^{m} V_{dBi} + n\sum_{i=1}^{m} 20\log(r_i)}{m}. \tag{5.11}$$

The full derivation for (5.10) and for (5.11) is in Appendix E.

5.3.1 Comparing Measurement and Simulated "n" Values

This Section compares the path loss index n of the measured and simulated voltages. It gives an indication of whether the received signal declines with distance in the same manner for measured and simulated data. In other words, this gives an insight into how much the simulation and measured data agree based on the path loss index n.

5.3.1.1 Hallway

Figure 5.5 shows the simulated and uncalibrated measured received voltage graphs for the hallway. The path loss index n is 0.7503 for simulated data and 0.6847 for measured data. The measured and simulated data did give a good agreement, based on the path loss index n. Although the detailed variation or fast fading differ considerably, the path loss index is quite similar.

5.3.1.2 Room H853 Microwave Lab

Figure 5.6 shows the simulated and uncalibrated measured received voltage graphs for the microwave lab. The path loss index n is 0.8676 for simulated data and 0.9187 for measured data. Based on the similarity of the n values, we can conclude that the measured and simulated data give good agreement and that the simulation model is a reasonably good model. It is of interest that the path loss index n is much higher in the microwave lab, at about 0.9 than in the hallway at about 0.7.

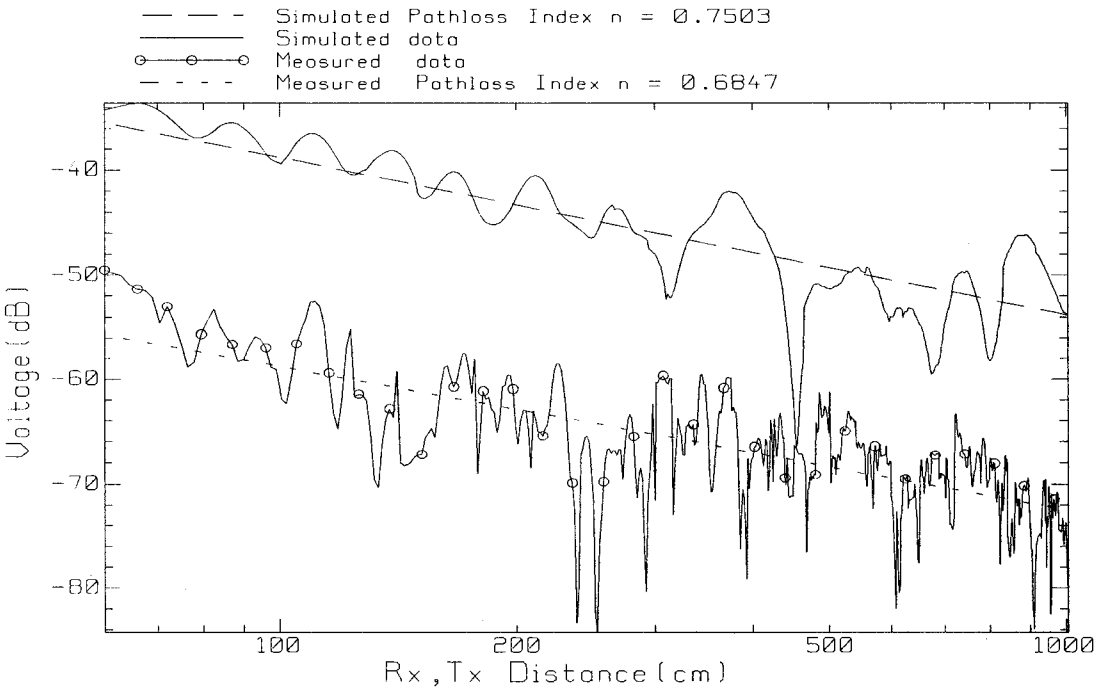

Figure 5.5 Simulated and measured results of voltage in (dB) versus distance for the hallway showing path loss index n.

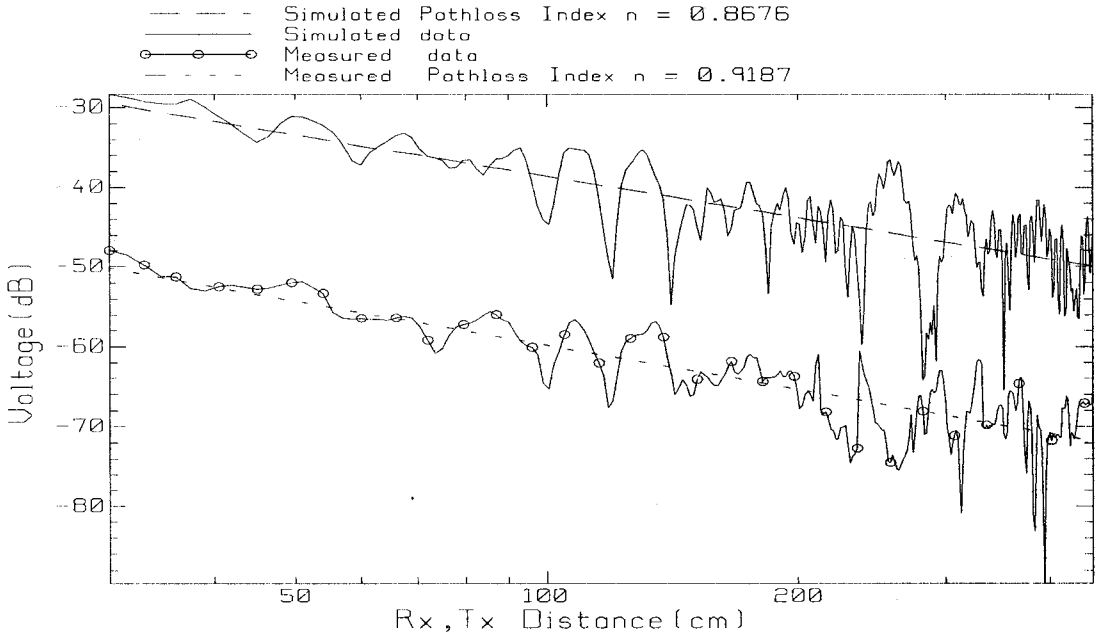

Figure 5.6 Simulated and measured results of voltage in (dB) versus distance for the microwave lab showing path loss index n.

5.4 Large-Scale Fading

The large scale fading for measured and simulated results is compared in this Section. As in Chapter 4, the sliding window concept is used and three window sizes are considered. The window sizes used was 4λ, 8λ and 12λ. The next sub Sections present the large scale fading for measured and simulated data for the hallway and the microwave lab, along with supporting Figures.

5.4.1 Hallway

Figures 5.7 to 5.9 show large-scale fading for measured and simulated data of the hallway for window sizes 4λ, 8λ and 12λ, respectively. In Figure 5.7, with window size 4λ, at closer distances between the transmitter and the receiver, or the free space behavior, there is clearly a good match between measured and simulated data.. At distances from 300 cm till the end of the path being measured, or 1000 cm, there is a marked difference between measured and simulated data. In Figure 5.8, with window size 8λ, the free space region matching is even better than in Figure 5.7. At distances after the free space region or from 300 cm until the end of the path, there is a similar difference between measured and simulated data. The data in Figure 5.9, with window size 12λ, is similar to that of Figure 5.8 but the free space region matching is even better. All three Figures share in common the free space behavior with good matching between the measured and simulated data, and a second region with very little matching. This is also obvious in the small-scale fading.

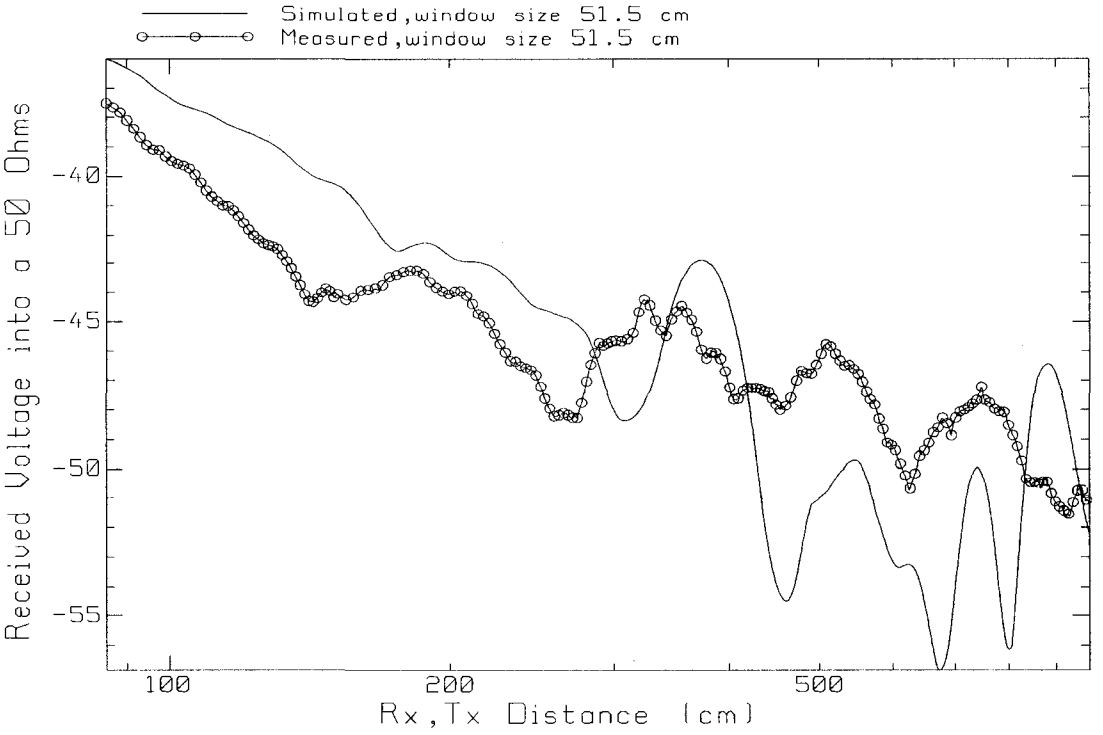

Figure 5.7 Large-scale fading (measured and simulated) for the hallway, window size around 4λ.

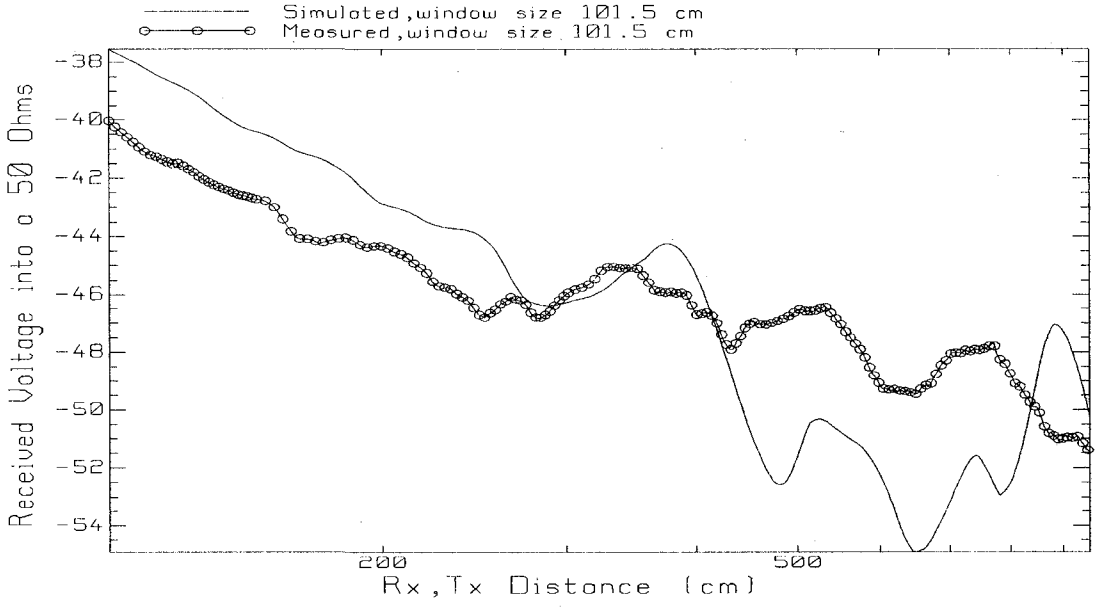

Figure 5.8 Large-scale fading (measured and simulated) for the hallway, window size around 8λ.

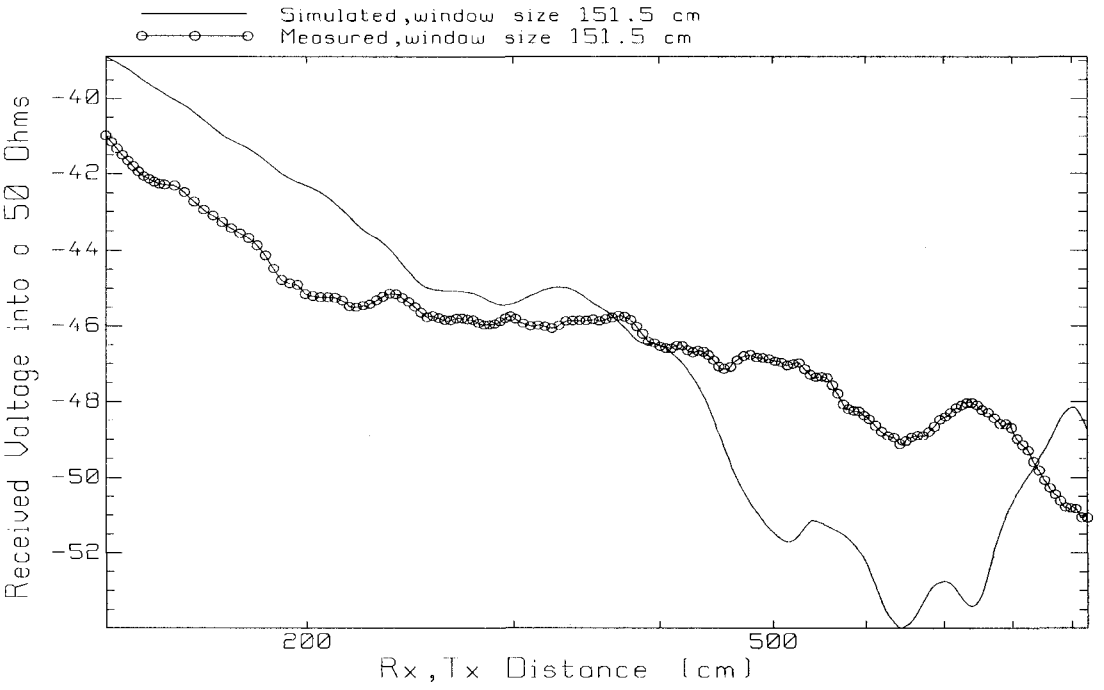

Figure 5.9 Large-scale fading (measured and simulated) for the hallway, window size around 12λ.

5.4.2 Room H853- Microwave Lab

Figures 5.10 to 5.12 show the large scale fading for the simulated and scaled measured data of the microwave lab, for window sizes 4λ, 8λ and 12λ, respectively. In Figure 5.10, for window size 4λ, at closer distances between the transmitter and the receiver there is a very good match between measured and simulated data. From 250 cm until the end of the path there is a notable difference between measured and simulated data. In Figure 5.11, for window size 8λ, the results are very similar to those in Figure 5.10. In Figure 5.12, for window size 12λ, there is a good match between the measured and the simulated data until 300 cm. From 300 cm until the end of the path matching is less. The large scale fading matching for measured and simulated data for the microwave lab is similar to the small scale fading matching.

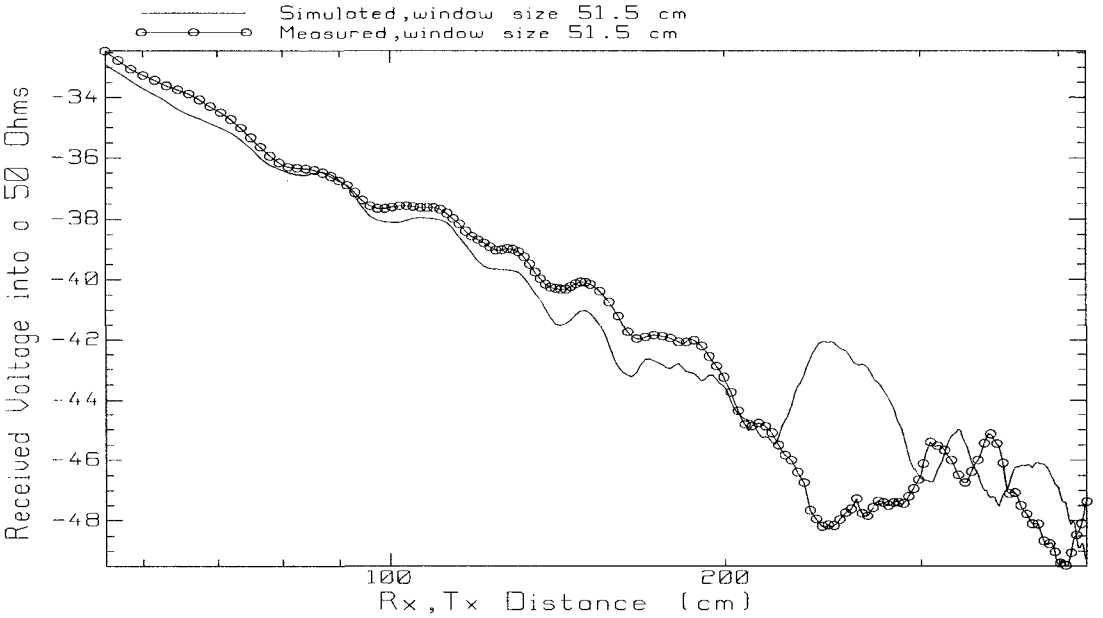

Figure 5.10 Large-scale fading (measured and simulated) for room H853, window size around 4λ.

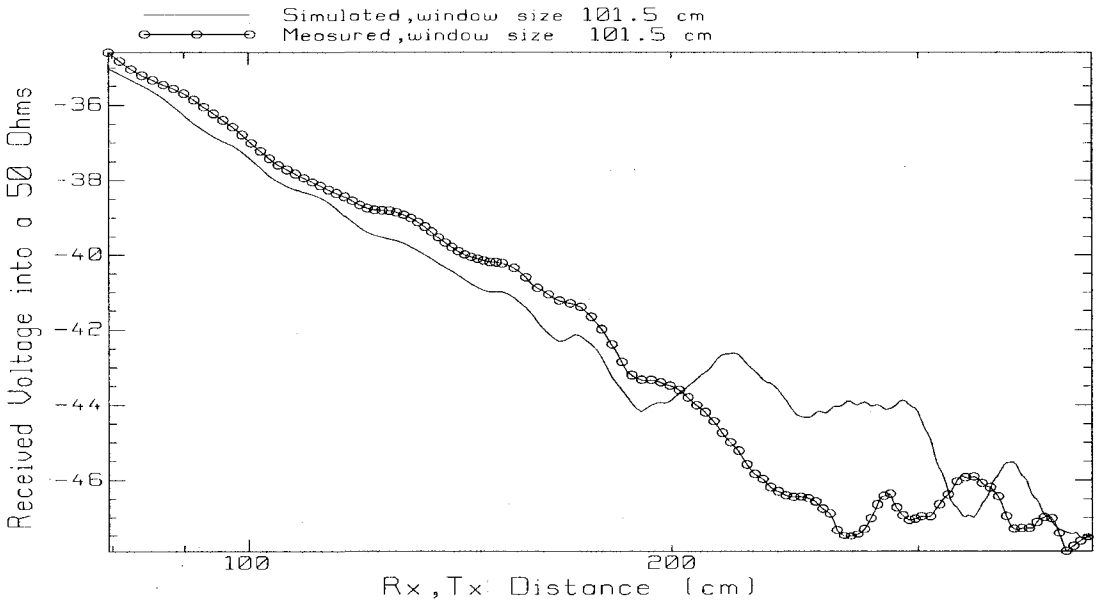

Figure 5.11 Large-scale fading (measured and simulated) for room H853, window size around 8λ.

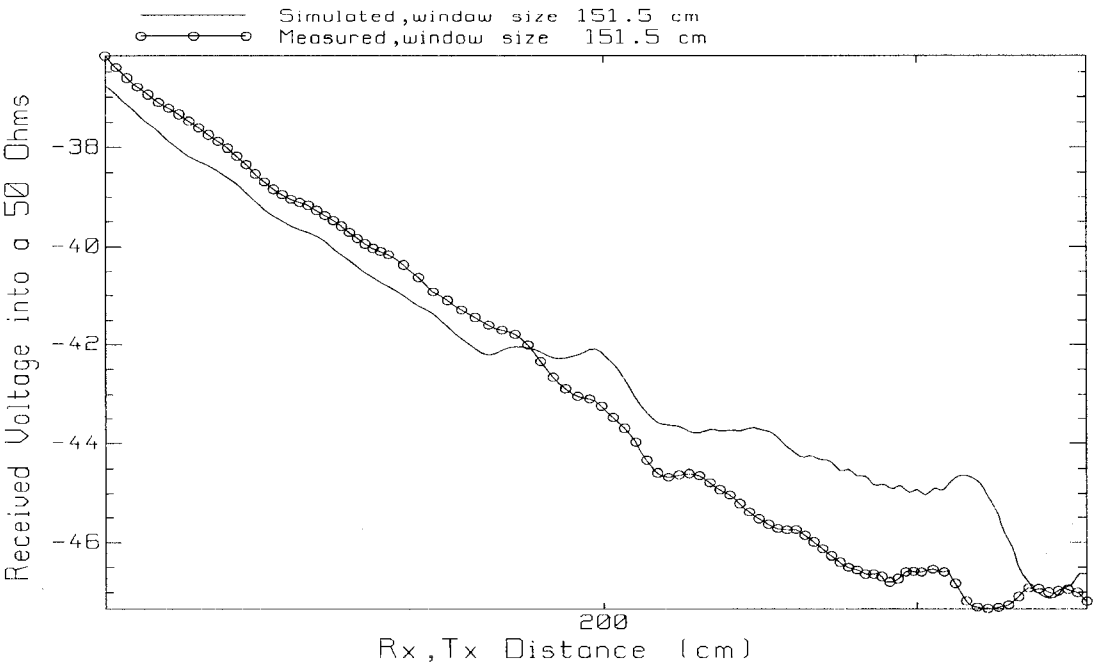

Figure 5.12 Large-scale fading (measured and simulated) for room H853, window size around 12λ.

5.5 Spatial Variation for the Rician-K Factor

In this Section, the space-varying Rician–K factor for the simulated data is estimated using the three methods mentioned in Chapter 3, which are K_G / K_{24}, K_{12} and K_{MLE}. The window sizes are 4, 8, and 12λ. Subsequently, the best method to evaluate the Rician-K factor is determined and then compared with its equivalent found from the measured data.

5.5.1 Hallway

Figures 5.13 to 5.15 show the space-varying Rician-K factor for the hallway. The window sizes are 4, 8, and 12 λ, respectively. In Figure 5.13 the values of the three methods K_G / K_{24} (circles), K_{12} (triangles) and K_{MLE} (crosses) correlate well except between 430 cm and 480 cm for K_{12} (triangles), where values for the algorithm used to search for the root of (3.9) are clipped at around 18 dB. Between 800 and 820 cm there are missing values in the K_G / K_{24} curve. These values are the square root of a negative number in (3.4). The Rician-K factor is highly variable with a maxima at about 500 cm and a minima at about 450 cm. In Figure 5.14 the correlation between the three methods is better than in Figure 5.13 but with two clippings: at 400 to 440 cm and from 800 to 840 cm. The Rician-K factor is less variable than in Figure 5.13 with a maxima at 900 cm. In Figure 5.15 the Rician-K factor is nearly constant at around 12 dB. There are regions from 320 to 460 cm where the Rician-K factor is clipped by the algorithm used to find the root for (3.9) with the K_{12} method and missing data for the K_G / K_{24} method between 440 and 460 cm where (3.4) gives root squares of a negative number. The correlation between the three methods is much less here than in the other two Figures. The K_{MLE} method appears to be the best to find the Rician-K factor for space-varying simulated data since it found all the Rician-K factor values along the distance. For the simulated data, all three methods agree very well.

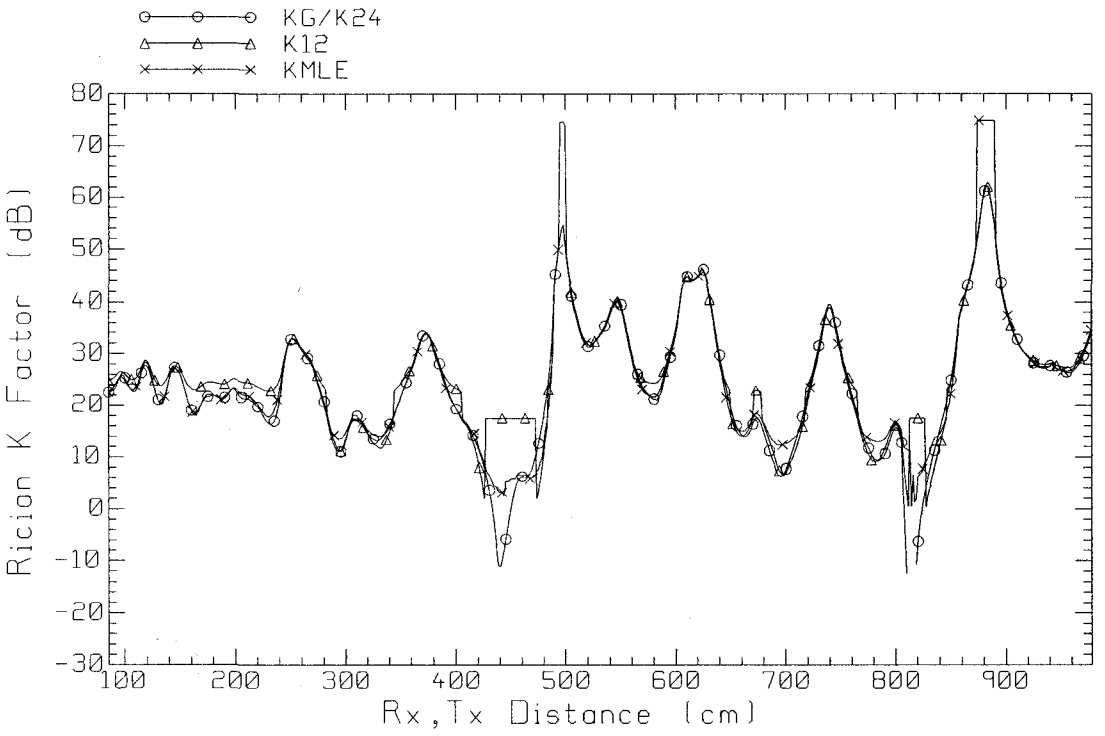

Figure 5.13 Space-varying K for the hallway, window size around 4 λ.

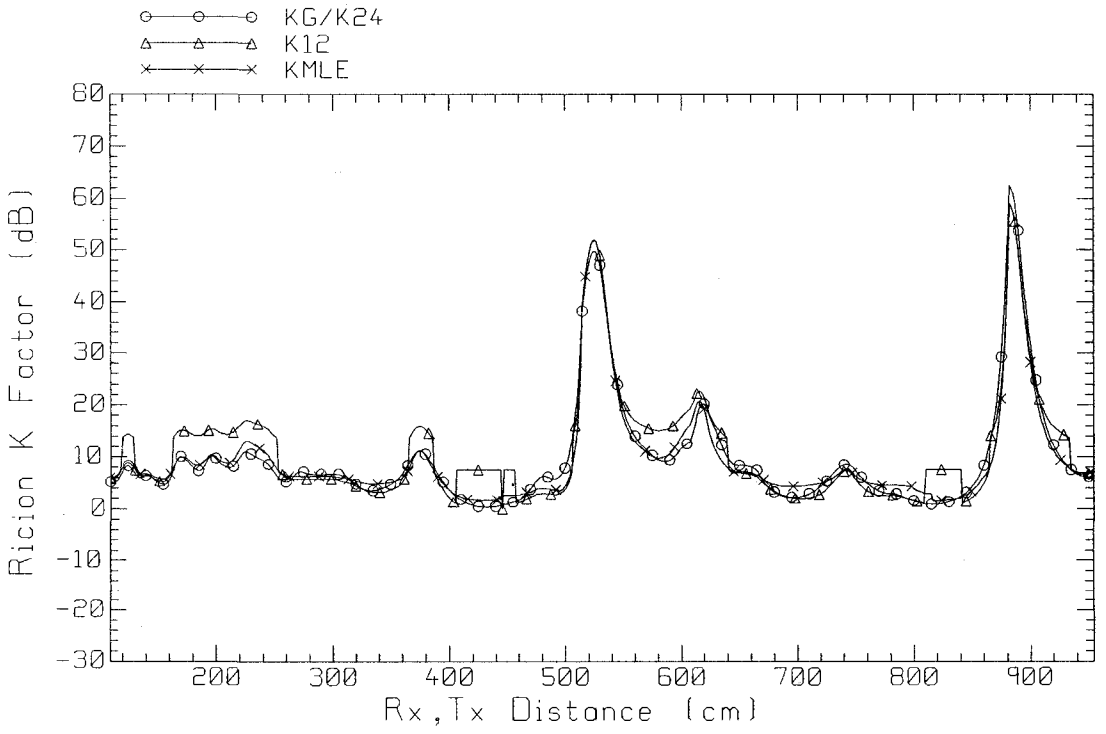

Figure 5.14 Space-varying K for the hallway, window size around 8 λ.

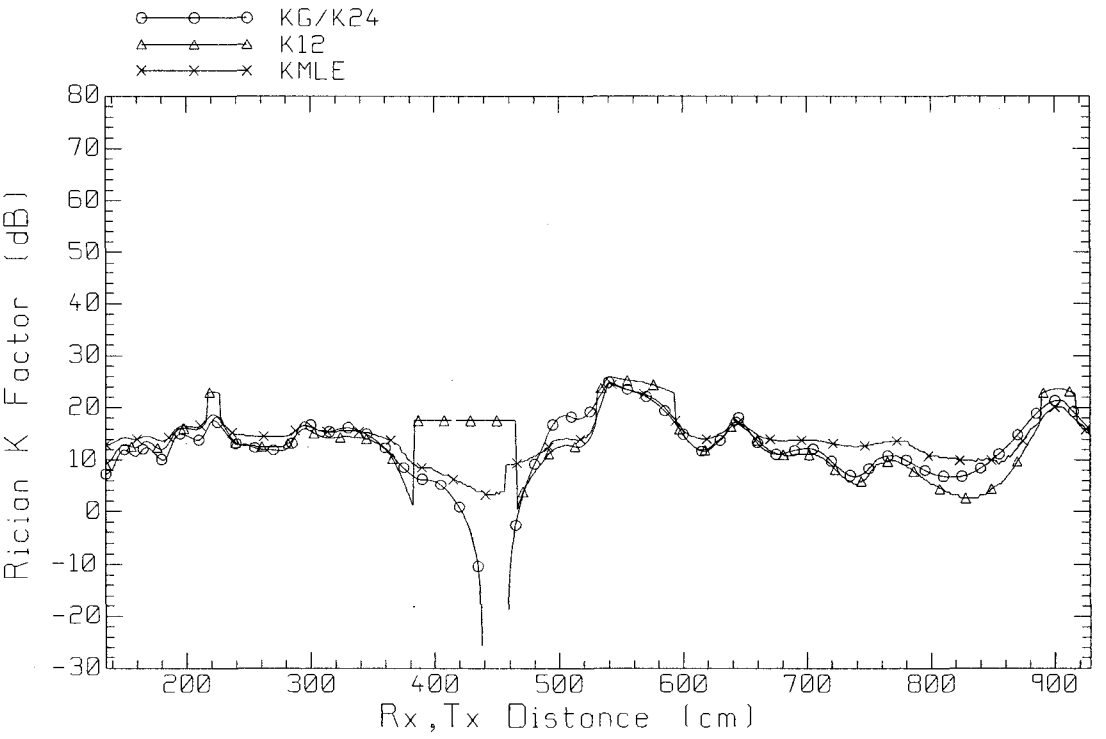

Figure 5.15 Space-varying K for the hallway, window size around 12λ.

5.5.2 Room H853-Microwave Lab

Figures 5.16 to 5.18 show the space-varying Rician-K factor for the microwave lab. The window sizes are 4, 8, and 12λ, respectively. In Figure 5.16 the three methods' values are not correlated at all except in the regions between 160 and 210 cm and 320 to 390 cm. Clipped values are found for the K_{12} method at regions between 120 and 150 cm, 230 to 320 cm, and 310 to 410 cm. Missing data are found for the K_G / K_{24} method because (3.4) gives the root square of a negative number at certain distances. Here, that range is from 270 cm to 290 cm. The Rician-K factor is highly variable with a maximum

at 280 cm and a minimum at 230 cm. In Figure 5.17, correlation between the three methods is even less than in Figure 5.16, aligning only at the region between 345 cm and 400 cm where the values for two methods, K_G / K_{24} and K_{12} correlate. The K_{12} method is clipped at 135 cm, from 140 to 150 cm and from 230 to 330 cm. The K_G / K_{24} method has missing data (root square values for a negative number) in the region from 240 to 320 cm. In Figure 5.18 the Rician-K factor is clipped at 8 dB using the K_{12} method for almost all the distance path. The Rician-K factor has missing data for the K_G / K_{24} method (root square values for a negative number) in the regions 100 to 110 cm, 160 to 180 cm and 260 to 340 cm. The Rician-K factor found using the K_{MLE} method is constant along the path being measured, and it has a value of about 2 dB. The K_{MLE} method is clipped at 0 dB from 250 to 310 cm. Observing Figures 5.13 to 5.17, it is clear that the K_{MLE} method is the best method to find the Rician-K factor. In the next Section, comparison between the space-varying Rician-K factor for measurements and for simulation is presented for the K_{MLE} method since it is the best method in both cases.

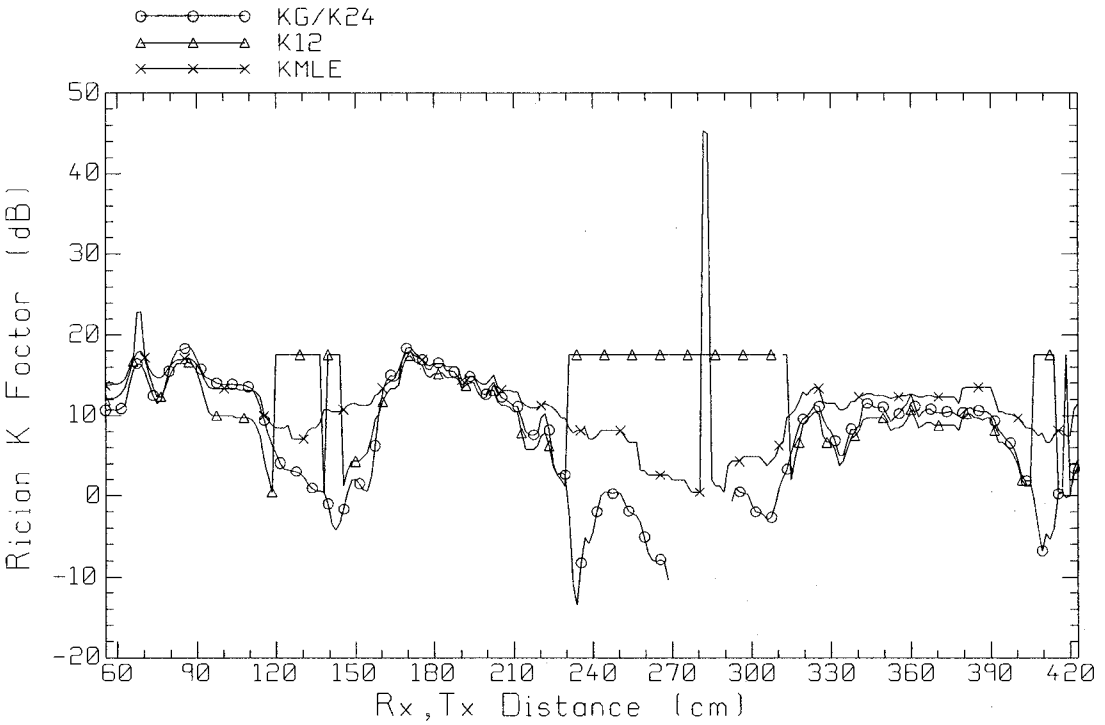

Figure 5.16 Space-varying K for room H853, window size around 4 λ.

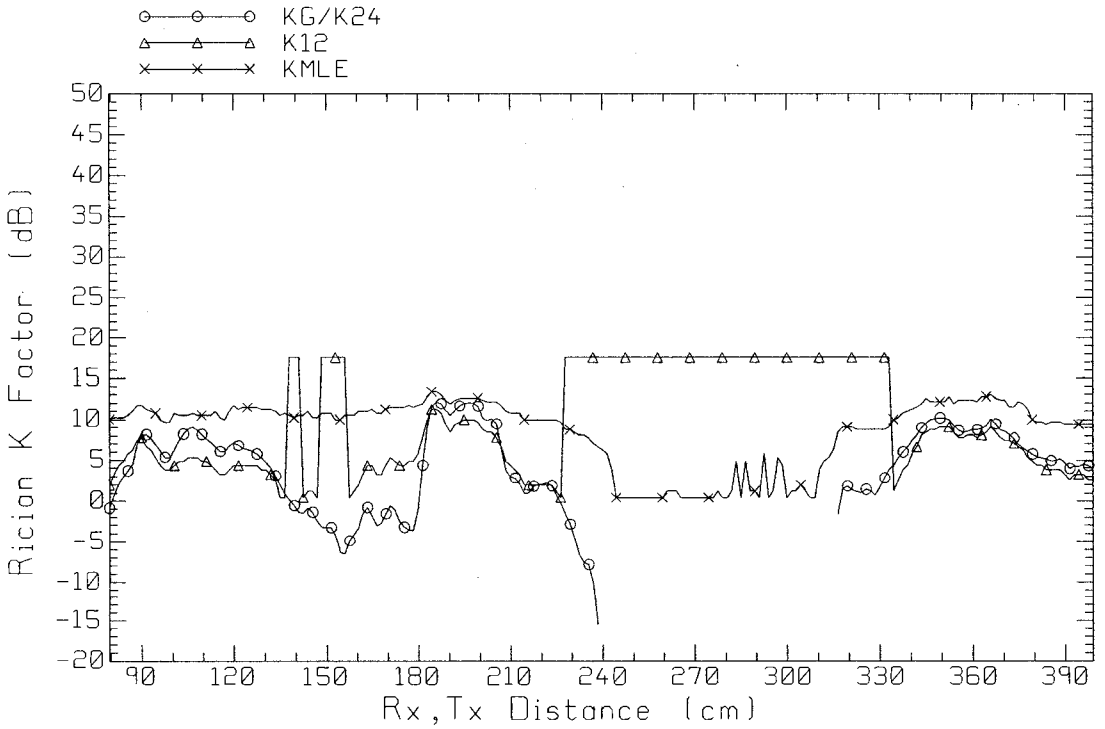

Figure 5.17 Space-varying K for room H853, window size around 8 λ.

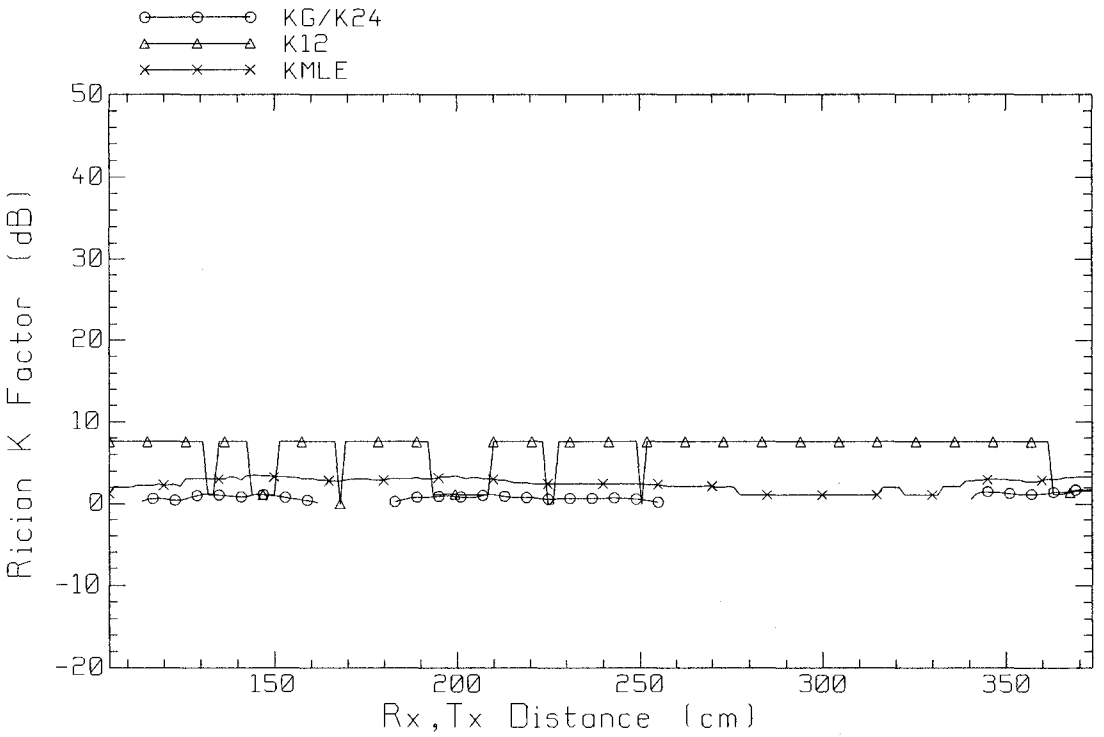

Figure 5.18 Space-varying K for room H853, window size around 12λ.

5.6 Comparison of Simulated and Measured K_{MLE}

The space-varying Rician-K factor for the hallway and microwave lab simulated data was evaluated using the three methods: K_G / K_{24}, K_{12} and K_{MLE}. The best method to use for evaluating the space-varying Rician-K factor from simulated data is the K_{MLE} method since it evaluates K for all distances along the path being measured. Since this is the case for measured data also, K_{MLE} curves for measured and simulated data can be compared. Figures 5.19 to 5.24 show the comparison between the K_{MLE} curves for the measured and simulated data, in the hallway and in the microwave lab for three window sizes 4, 8 and 12λ.

5.6.1 Hallway

Figures 5.19, 5.20 and 5.21 show the space-varying Rician-K factor for measured and simulated data for the hallway, estimated using the K_{MLE} method and at three different windows sizes: 4, 8 and 12λ.

In Figure 5.19, for a window size of 4λ there is no correlation between the K_{MLE} -generated Rician-K factor from measured and simulated data. The average K_{MLE} values from measured data is 14.85 dB, and 24.74 dB from simulated data. The average value for K_{MLE} from simulations in dB is about twice that from measurements. For Figure 5.20, with an 8λ window size, the correlation is better than in 5.19. The average value for K_{MLE} from measured data is 12.83 dB, and from simulated data, 16.93 dB. Figure 5.21 with window size 12λ shows a correlation better than that of Figure 5.20. The average value for K_{MLE} from measured data is 12.23 dB, and for simulated data, 13.98 dB. The three graphs show that at the 12λ window size the K_{MLE} average value from simulations is within 2.2 dB of the measurements, which is a reasonable match. The average values produced for the above graphs are found from the linear scale of the data and then taking the db value of each. Also, with a large window size, K_{MLE} is approximately constant along the path, especially for the measured data.

5.6.2 Room H853-Microwave Lab

Figures 5.22, 5.23 and 5.24 show the space-varying Rician-K factor for measured and simulated data for the microwave lab estimated using the K_{MLE} method and at different windows sizes: 4, 8 and 12λ. In Figure 5.22, with window size 4λ, the K_{MLE} curves found from measured and simulated data are somewhat correlated except in the region from 230 cm to 320 cm. The average K_{MLE} from measured data is 12.84 dB, and from simulated data K_{MLE} is 11.07 dB, which are almost identical. In Figure 5.23, with window size 8λ, K_{MLE} curves have almost identical behavior, with average values of 11.39 dB for measurements and 8.60 dB for simulations. Figure 5.24 with window size 12λ shows that the behavior is almost constant, and K_{MLE} has an average value of 10.15 dB for measured data and 7.026 dB for simulated data. Note that especially for the larger window size, K_{MLE} is nearly constant with position along the path. The simulated data has ranges of distance where the K_{MLE} algorithm returns to near-zero values in dB which corresponds to small values in a linear scale. There is significant variation in the signal of Figure 5.4 from 240 cm to 320 cm. This results in a small value for the Rician-K factor and thus justifies the small values obtained.

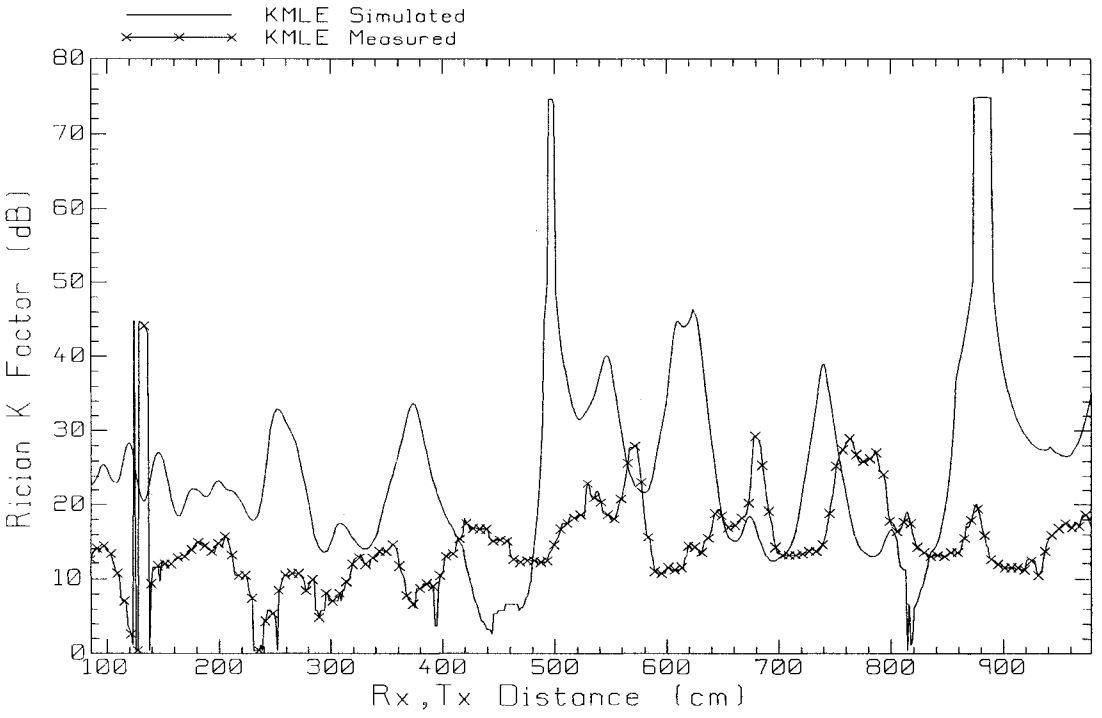

Figure 5.19 Space-varying K comparison for the hallway, window size around 4 λ.

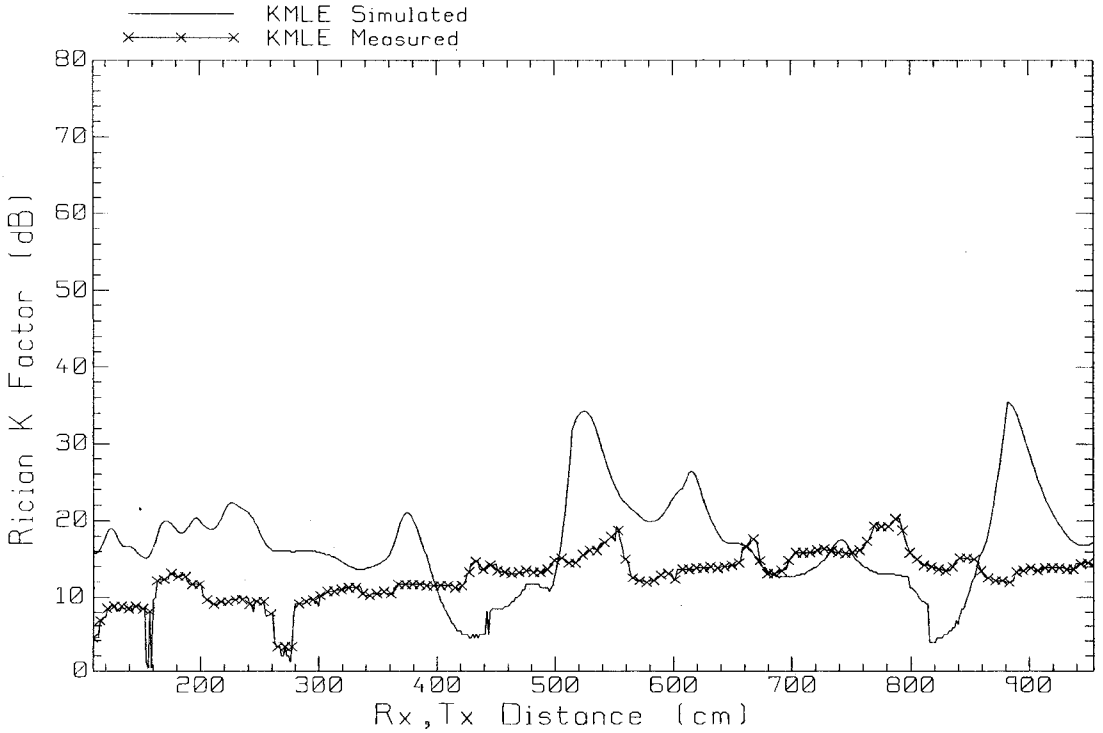

Figure 5.20 Space-varying K comparison for the hallway, window size around 8 λ.

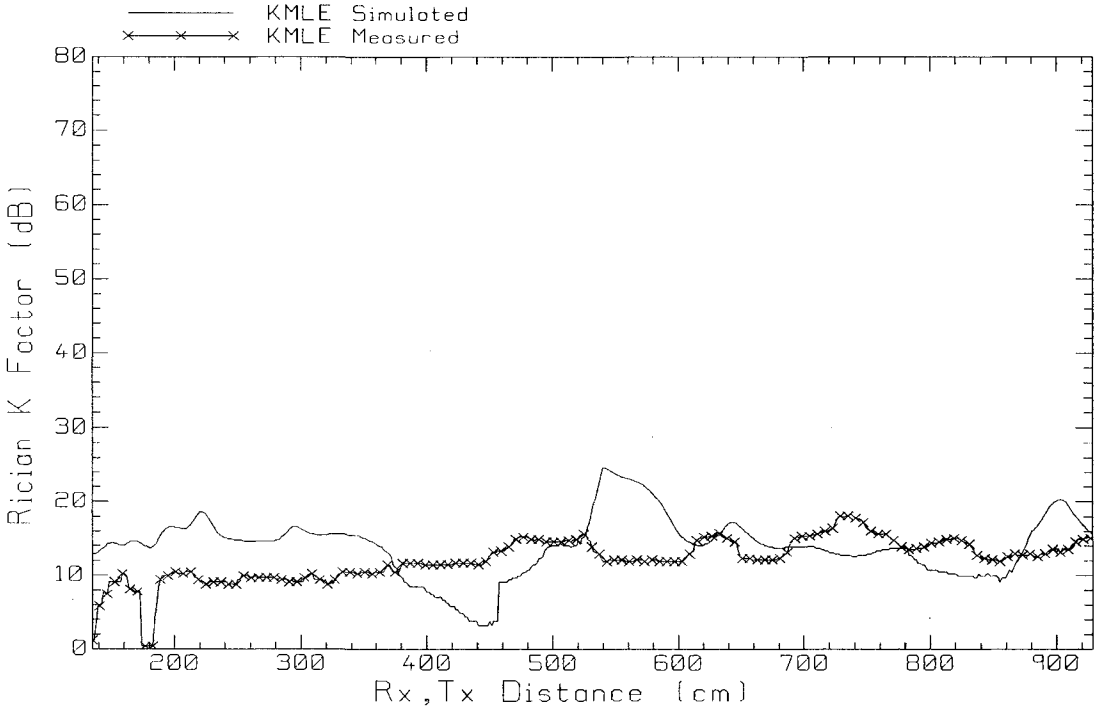

Figure 5.21 Space-varying K comparison for the hallway, window size around 12 λ.

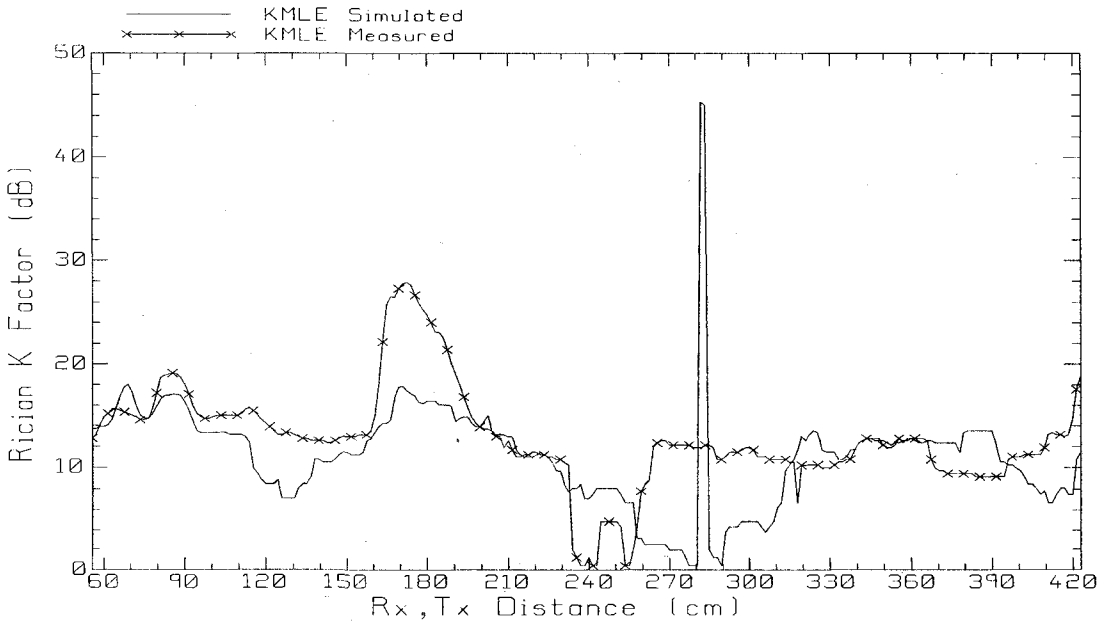

Figure 5.22 Space-varying K comparison for room H853, window size around 4 λ.

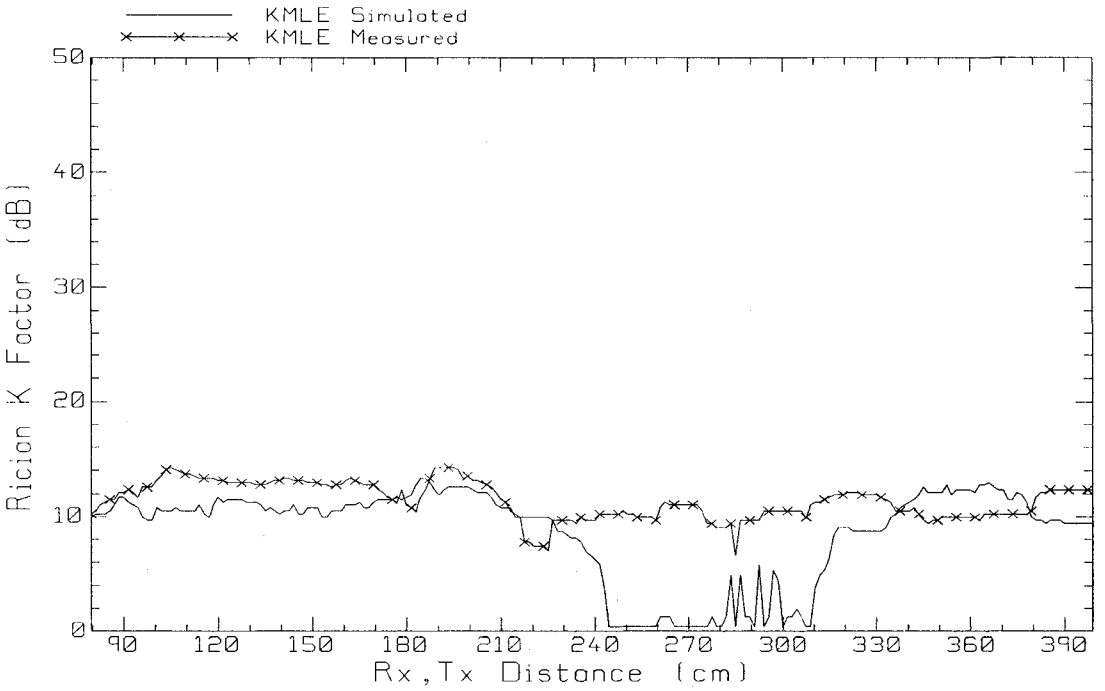

Figure 5.23 Space-varying K comparison for room H853, window size around 8 λ.

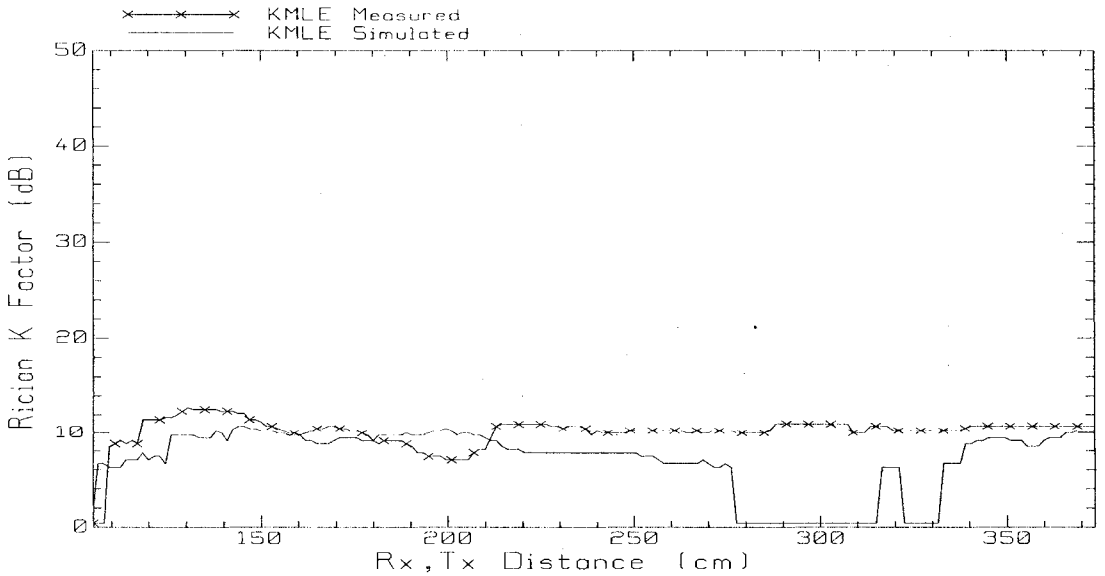

Figure 5.24 Space-varying K comparison for room H853, window size around 12 λ.

5.7 Conclusions

The following is observed when comparing results obtained from measured and simulated data. The measured small-scale fading for the hallway does not match the simulations as shown in Figure 5.3. The ray-tracing model representing the hallway walls is a uniform layered structure, which is probably not a reasonable model. The hallway walls are constructed from vertical metal studs spaced 16 cm each, covered with gyproc panels about 1 cm thick. The metal studs should be modeled with the uniform-layer representation. They act as secondary sources. In the microwave lab the matching between measured and simulated small-scale fading results as shown in Figure 5.4 is better due to proper representation of the microwave lab environment. One reason for the differences between measured and simulated small-scale fading results for both the hallway and the microwave lab might be that the ceiling in the simulation is modeled as perfectly smooth and as reflecting the signal specularly. The reality is that above the hanging ceiling, there are pipes, ducts, electrical conducts and so forth which scatter the signal rather than reflect it specularly, and this is not modeled in the simulations. Some researchers "calibrate" the wall model chosen, the electrical parameters of the wall matched so that the calculated slow fading matches the measured slow fading for some paths. Then the "calibrated" model is used to calculate the calculate the slow fading and path loss for many other paths. After calibration the match between simulation and measurements is greatly enhanced. Large-scale fading in the hallway was a poor match between the measured and simulated data, but was a reasonable match in the microwave lab. When comparing measured and simulated data based on the path loss index n for the

hallway and microwave lab, there is good agreement for the path loss index generated from measured and simulated data. The path loss index is higher in the hallway than in the microwave lab. Reference [24] shows that the path loss index is dependant on the location of the path being measured, and reference [12] shows that the path loss index is directly proportional to the height of the transmitter. Hence, if the measurements had been done at a different height and a different spacing, a different value of the path loss index n would have been found. The K_{MLE} method is the best to find the space-varying Rician-K factor. Measured and simulated curves for the K_{MLE} method using three window sizes have been compared for the hallway and the microwave lab. The comparison showed that the Rician-K factor becomes independent of position with large window sizes. The situation of large-scale fading and representation using the log-normal distribution [7][35] has not been investigated in the thesis.

Chapter 6

Conclusions and Future Work

6.1 Highlights

A site-survey measurement system has been built and is described in Chapter 2. It has the advantage of being automated so that only one operator is needed to operate the system and to monitor the measurement campaign. The spectrum analyzer and the moving platform are controlled in sequence by one control unit (the pc unit) using LabVIEW programming. Space and time power variation measurements for two different geometrical environments, an empty hallway and a heavily-equipped microwave lab room, were performed using the site survey system.

In Chapter 3, time variation of the received signal for four representative distance points in the hallway and for the microwave lab were shown. Three methods from the literature were used to find the Rician-K factor for time-varying received voltages. Figure 3.18 for the hallway and Figure 3.19 for the microwave lab show that the K_G / K_{24} method is the best means to find K since it is able to find a value for K at every point along the distance path being measured. In Figure 3.9 for the hallway and Figure 3.20 for the microwave lab, and the corresponding Rician-K factor Figures for the hallway and the microwave lab, small time variations of the received signal correspond to a high value of

K, corresponding to an almost deterministic voltage. But higher time variations of the received field corresponded to smaller values of K.

Space variations for the hallway and the microwave lab are found in Chapter 4 by taking the average value of the time-varying voltage at each distance point along the path being measured, as shown in Figure 4.1 for the hallway and Figure 4.2 for the microwave lab. Large-scale fading for the hallway and the microwave lab is investigated using three averaging windows of sizes 4, 8 and 12 λ, shown in Figures 4.3 to 4.5 for the hallway and Figures 4.6 to 4.8 for the microwave lab. The space-varying Rician-K factor is found using the same three methods that were used to find the time-varying Rician-K factor. Three different window sizes, of 4, 8 and 12 λ, are considered. as shown in Figures 4.9 to 4.11 for the hallway and Figures 4.12 to 4.14 for the microwave lab. The best method for estimating the Rician-K factor for space variation is the K_{MLE} method.

In Chapter 5, small-scale fading for the calculated simulated voltages versus distance for the hallway and the microwave lab is compared with the corresponding calibrated and measured space-varying voltages versus distance, shown in Figure 5.3 for the hallway and in Figure 5.4 for the microwave lab. The comparison shows that there is poor agreement for the small-scale fading in the hallway and better agreement in the microwave lab. The large-scale fading for the calibrated measured and simulated voltages for the hallway and the microwave lab was found using three window sizes of 4, 8 and 12 λ, shown in Figures 5.7 to 5.9 for the hallway and Figures 5.10 to 5.12 for the microwave lab. There is better agreement in the microwave lab between measured and

simulated large-scale fading than in the hallway. The space-varying Rician-K factor for the simulated data is estimated using the same methods for the measured data shown in Figures 5.13 to 5.15 for the hallway and Figures 5.16 to 5.18 for the microwave. The K_{MLE} method is the best method used to estimate the Rician-K factor for the space variations. The K_{MLE} curves for space-varying measured and simulated data are compared in Figures 5.19 to 5.21 for the hallway and Figure 5.22 to 5.24 for the microwave lab. In these Figures it is clear that as the window size increases, the Rician-K factor becomes constant with distance.

6.2 Contributions of the Work

The contributions of the thesis are described in the following Sections.

6.2.1 Site-Survey System

The robot used in the site survey system was designed and built by the author. The robot is a substantial improvement over the one in [24] in terms of wireless control and automated measurements. In [24] the fixed antenna on the tripod is the transmitter and the moving robot carries a receiver antenna. A cable is used between the robot and the spectrum analyzer. As the robot moves the cable trails behind it. The site survey system in this thesis eliminates the trailing cable. Also in [24] the robot was moved manually by one distance step, and the power received by the spectrum analyzer was recoded by the operator on paper. Hence to measure the power at 600 locations, the

system in [24] required the operator to move the robot manually 600 times and to write down the measured received power 600 times. These problems have been overcome by the site-survey system described in Chapter 2. The robot carries a battery-operated transmitter and no trailing cable is needed. Commands to move the robot are sent over a 900 MHz wireless channel, rather than manually. The receiver is fixed on a tripod connected by a short cable to the spectrum analyzer. The wireless command channel at 900 MHz does not interfere with the wireless channel for measurements, which is at the ISM band frequency of 2.4 GHz. The 900 MHz channel and its corresponding harmonics, second harmonic 1.8 GHz and third harmonic 2.7 GHz, do not lie within the band of the measurement wireless channel. The power received by the spectrum analyzer is recorded automatically at each point by the controlling program and written to a text file, which will be saved on the computer. The site survey system described in Chapter 2 has total automation, with no need for manual intervention even for long distances being measured. The drawbacks in this site-survey system are that the robot does not follow corners and sometimes it gets stuck between the grooves in-between the floor tiles. The battery life-time needs to be improved. It would be better to use one source for the whole system to power the mobile platform, instead of three different sets of batteries.

6.2.2 Time-Varying Measurements and Rician-K Factor

The Rician-K factor for the time-varying voltages is better estimated using the K_G / K_{24} method. High values of the time-varying Rician-K factor correspond to small time variations of the received voltage. Low values of the Rician-K factor correspond to

received voltage values that show some variation over time. The varying values of voltages received over time are likely due to movements of people in the vicinity of the measurement environment. Hallway results in Figure 3.9 show more varying voltage values received compared to the microwave lab in Figure 3.17.

6.2.3 Space -Varying Measurements and Rician-K Factor

The investigation of the space variation using the measured data showed that the Rician-K factor values are much smaller than those for time variation, and that the K_{MLE} method is the better method to use to estimate the value of space-varying Rician-K factor. It was found that for a large window size, 12λ, shown in Figure 4.11 for the hallway and in Figure 4.14 for the microwave lab, the K_{MLE} estimate of the Rician-K factor is approximately constant all along the path.

6.2.4 Simulations

The measured and simulated results were compared to see if the ray-tracing model is a good representation of the real environments. The comparison was based on small-scale fading, path loss index n, large-scale fading and the K_{MLE} curves for both measured and simulated data. The small-scale fading in the hallway agreed poorly between the measurements and simulations. The agreement was much better in the microwave lab. The layered model for the wall is a poor representation of the gyproc and

metal studs construction of the hallway walls. The large-scale fading was compared on the basis of path loss index n, and there was good agreement for both the hallway and the microwave lab. The microwave lab gave a higher value for n. The large-scale fading for both measured and simulated data gave a good match in the free space region. For the Rician-K factor estimated by the K_{MLE} method, it was found that as the size of the window increases, K_{MLE} becomes more constant along the path. This is shown in Figure 5.21 for the hallway and in Figure 5.24 for the microwave lab, both for window size 12λ.

6.2.5 Validation of The Methods For Evaluating the Rician-K Factor

Figure 3.19 shows that the three methods used to estimate the value of the Rician-K factor give the same values of K at many points, for example from 250 to 270 cm, and also from 380 to 400 cm. This indicates that the algorithms used to evaluate K_G / K_{24}, K_{12} and K_{MLE} are correctly implemented. However, when the data leads to large values of K_{12} and K_{MLE}, the root-finding algorithm is not adequate and the large values are clipped. A better root-finding algorithm should be found, capable of calculating large values. Also Figure 5.23 shows that the K_{MLE} method returns a zero value from 245 to 310 cm distance, which is clearly incorrect. The algorithm should be improved to overcome this shortcoming.

6.2.6 The Three Methods For Evaluating The Rician-K Factor

In this section, the advantages and disadvantages of the three methods used in this thesis to estimate the value of the Rician-K factor are discussed. The advantages for the three methods are as follows. K_G / K_{24} is evaluated with a simple, closed-form formula. For the nearly-constant temporal data in Chapter 3, the formula always gives a value for this high-K case. Conversely, for the rapidly-varying fast fading presented in Chapter 4, the K_{MLE} method always gives a value for this low-K case. The values obtained with the K_{12} method match the K_G / K_{24} values well, but K_{12} is much harder to evaluate. The K_{12} method has the advantage that it obtains values over some ranges of distance where the K_G / K_{24} method fails in Figs. 4.9 and 4.10. The disadvantages for the three methods are as follows. The K_G / K_{24} formula sometimes leads to the square root of a negative number for spatial variations, and so the formula fails. The K_{MLE} method poorly matches the other methods for high K values, and the implementation used here suffers from clipping. The K_{MLE} method requires root-finding and is hard to implement. The implementation in this thesis led to both clipping and zero values for some of the spatial data. Also, K_{MLE} agreed poorly with the K_G / K_{24} and K_{12} methods for spatial data. The disadvantage of the K_{12} method is that it is also difficult to evaluate because it requires a root-finding algorithm. K_{12} agrees reasonably well with K_G / K_{24} for spatial data in Figs. 4.9 and 4.10.

6.3 Recommendations for Future Work

Future work would include more extensive measurements and investigation of the Rician-K factor for different scenarios. This could be done by additional measurements for the same environment but with different setups, such as varying the height of the transmitter and the receiver, and using different frequencies and different polarizations. Investigating different numerical root finding methods might lead to better results for K_{MLE}. Some investigation should be done on how to properly model the walls in the GO_3D program in order for a particular environment to be simulated. This is an essential issue to ensure that the simulated data matches the measured data and that the ray-tracing based GO_3D program can be used as an alternative to measurements for a quick investigation of the wireless channels of certain indoor environments.

References

[1] Dobkin D. M., " RF Engineering for Wireless Networks Hardware, Antennas, and Propagation," Elsevier Publishing, Amsterdam, 2005, ISBN 0750678739 .

[2] Sarkar T. K., Ji Z., Kim K., Medouri A., Salazar- Palma M., "A Survey of Various Propagation Models for Mobile Communication," IEEE Antennas and Propagation Magazine, Vol. 45, No. 3, pp. 51- 82, June 2003.

[3] Trueman C.W., "Three Dimensional Geometrical Optics Code for Indoor Propagation," Applied Computational Electromagnetics Society Journal, Vol.17, No.2, pp. 134- 144, July 2002.

[4] Trueman C.W., "User's Guide for Program GO_3D, Version 1K," Concordia University, November 16 1998.

[5] Rappaport T.S., "Wireless Communications Principles and Practice," Prentice Hall Publishing, Upper Saddle River, New Jersey, USA, 1996, ISBN:0-13-375536-3.

[6] Anderson J. B., Rappaport T.S., Yoshida S. "Propagation Measurements and Models for Wireless Communications Channels," IEEE Communications Magazine, Vol. 33, No. 1, pp.42-49, January 1995.

[7] Hashemi H. "The Indoor Radio Propagation Channel," Proc. of the IEEE, Vol. 81, No.7, pp. 943-968, July 1993.

[8] Hall M.P.M., Barclay L.W. and Hewitt M.T., "Propagation of Radio waves," The Institute of Electrical Engineers, London, UK, 1996, ISBN 0 85296 819.

[9] Sklar B., "Rayleigh Fading Channels in Mobile Digital Communication Systems," IEEE Communications Magazine, Vol. 35, No. 9, pp. 136-146, September 1997.

[10] Chryssomallis M., "Simulation of Mobile Fading Channel," IEEE Antenna's and Propagation Magazine, Vol. 44, No.6, pp. 172-183, December 2002.

[11] Pozar D. M., "Microwave and RF Design of Wireless Systems," John Wiley and Sons Inc., New York, Chichester, Weinbeim, Brisbane, Toronto, Singapore, 2001, ISBN: 0-471-32282-2.

[12] Muneer W., Abdallah I., Davis D. and Trueman, C.W. "A Novel Automated Site Survey System," ANTEM/URSI conference, pp. 147-150, Montreal , Quebec , July 17-19 , 2006.

[13] Lee W.C.Y., "Mobile Communications Engineering Theory and Applications 2nd Edition," McGraw Hill Publishing, USA, 1998, ISBN: 0-07-037103-2.

[14] Hashemi H., "A Study of Temporal and Spatial Variations of the Indoor Radio Propagation Channel," 5th IEEE International Symposium on Personal Indoor and Mobile Radio Communications, The Hague, The Netherlands, Vol.1, pp. 127-134, September 18-22 , 1994.

[15] Vasconcelos P. and Correia L. M., "Fading Characterization of the Mobile Radio Channel at the Millimetere Waveband," IEEE Vehicular Technology Conference 47 Th, Vol. 2, pp. 999-1003 , May 4-7, 1997.

[16] Wijik F. V., Kegel A., Prasad R., "Assessment of a Pico – Cellular System Using Propagation Measurements at 1.9 GHz for Indoor Wireless Communications," IEEE Transactions of Vehicular Technology, Vol. 44, No.1, pp. 155-162, February 1995.

[17] Yacoub M.D., "Fading Distributions and Co-Channel Interference in Wireless Systems," IEEE Antennas and Propagation Magazine , Vol.42, No.1, pp. 150-159, February 2000.

[18] Abdi A., Tepedelenlioglu C. and Giannakis G., "On the Estimation of the K parameter for the Rice Fading Distribution," IEEE Communications Letters, Vol. 5, No.3, pp. 92-94 , March 2001.

[19] Greenstein L.J. , Michelson D.G. and Erceg V., " Moment – Method estimation of the Rician K – Factor," IEEE Communications Letters, Vol. 3, No. 6, pp. 175-176 , June 1999.

[20] Tepedelenlioglu C., Abdi A., Giannakis G.B. and Kaveh M., "Performance Analysis of Moment Based Estimators for the K parameter of the Rice Fading Distribution," IEEE Acoustics, Speech and Signal Processing Conference, Vol. 4, pp. 2521-2524 ,2001.

[21] Tepedelenlioglu C., Abdi A. and Giannakis G., "The Ricean K factor : estimation and performance Analysis," IEEE Transactions On Wireless Communications , Vol. 2 , No. 4 , pp. 799-810 , July 2003.

[22] Talukdar K., Lawing W., "Estimation of the parameters of the Rice distribution," Acoustical Society of Canada, Vol. 89, No. 3, pp. 1193-1996, March 1991 .

[23] Ailes L., Keitz M.D., McCulley S.Y., Seidel S.Y., Deisenroth M., Rappaport T.S., "Development of an Automated Guided Vehicle For Indoor Propagation Measurements," Vehicular Technology Conference, 1990 IEEE 40th, pp. 119-123, Orlando, Florida, May 6-9,1990.

[24] Davis D., "Indoor Radio-Wave Behavior at 850 and 1900 MHz with Electromagnetic Compatibility Applications in Hospitals: An Experimental, Theoretical, Statistical and Morphological Characterization," PhD Thesis, McGill University, Montreal, Quebec, Canada, October 2003.

[25] Krishnamoorthy S., "Interference Measurements and Throughput Analysis for 2.4GHz Wireless Devices in Hospital Environments," Master of Science Thesis, Blacksburg, Virginia, USA, April 2003.

[26] LabVIEW, Version 8, National Instruments Cooperation, Austin, TX, USA.

[27] National Instruments Corporation, "LabVIEW Basics I and II," Course Manual.

[28] Aragon A. and Saunders S., "Autonomous Positioning System For Indoor Propagation Measurements," IEEE Vehicular Technology Conference 49 Th., Amsterdam, pp. 785-789 , September 19-2, 1999.

[29] Biggs M., Henley A., Clarkson T. "Occupancy analysis of the 2.4 GHz ISM band," IEE Proc.-Commun., Vol. 151, No.5, pp. 481-488, October 2004 .

[30] Loredo S., Valle L., Torres R., "Accuracy Analysis of GO/UTD Radio-Channel Modeling in Indoor Scenarios at 1.8 and 2.5 GHz," IEEE Antennas and Propagation Magazine, Vol. 43, No. 5, pp. 37-51, October 2001.

[31] Lukama L.C., Edwards D.J., "Analysis of Wideband Indoor Propagation Measurements at 2.4 GHz," Twelfth International Conference of Antenna and Propagation 2003 (ICAP 2003), Vol.2, No. 491, pp. 509-512, 31 March -3 April 2003.

[32] Valenzuela R .A. , Chizhik D. , and Ling J., "Measured and predicted correlation between local average power and small scale fading in indoor wireless communication channels," 48th IEEE Vehicular technology Conference, Vol. 3, pp. 2104-2108 , May 18-21, 1998.

[33] Walker E., Zepernick H., Wysocki T., "Fading Measurements at 2.4 GHz for The Indoor Propagation Channel," Broadband Communications, 1998, Accessing Transmission, Networking proceedings, International Zurich Seminar, pp. 171-176, February 17,1998.

[34] Wysocki T.A., Zepernick H., "Characterization of the Indoor Radio Propagation Channel at 2.4 GHz," Journal of Telecommunications and Information Technology, Vol. 1 , No. 3-4 , pp. 84-90, 2000.

[35] Zhang Y.P., Hwang Y., "Characterizations of UHF Radio Propagation Channels in Tunnel Environments for Microcellular and Personal Communications," IEEE Transactions on Vehicular Technology, Vol. 47, No.1, pp.283-296, February 1998.

[36] Afzal I., Venkat M., Lobo R., "E-Field Intensity Measuring Robot," ELEC 490 report, Department of Electrical and Computer Engineering, Concordia University, Montreal, Quebec, March 2005.

[37] Hsieh G., "Phased–Locked Loop Techniques-A Survey," IEEE Transactions on Industrial Electronics, Vol. 43, No.6, pp. 609 – 615, December 1996.

[38] Valenzuela R.A., Landron O., Jacobs D.L., "Estimating Local Mean Signal Strength of Indoor Multipath Propagation," IEEE Transactions on Vehicular Technology, Vol. 46 , No. 1, pp. 203-212, February 1997.

[39] Policarpio R., Sarine G., Kostyk A. " Prediction and Measurement of WLAN Signal Propagation," ELEC 490 report, Department of Electrical and Computer Engineering, Concordia University, Montreal, Quebec, March 2006.

[40] Schafer T., Maurer J., Hagen J." Experimental Characterization of Radio Wave Propagation in Hospitals," IEEE Transactions on Electromagnetic Compatibility, Vol. 47, No.2, pp. 304-311. May 2005.

Appendix A: LabVIEW programs (Front Panel, Block Diagram and Icon)

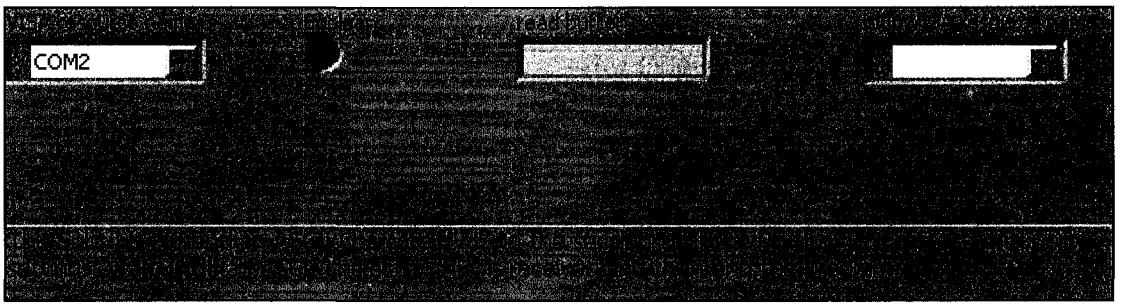

Figure A1 The LabVIEW Front Panel for A-AB VI.

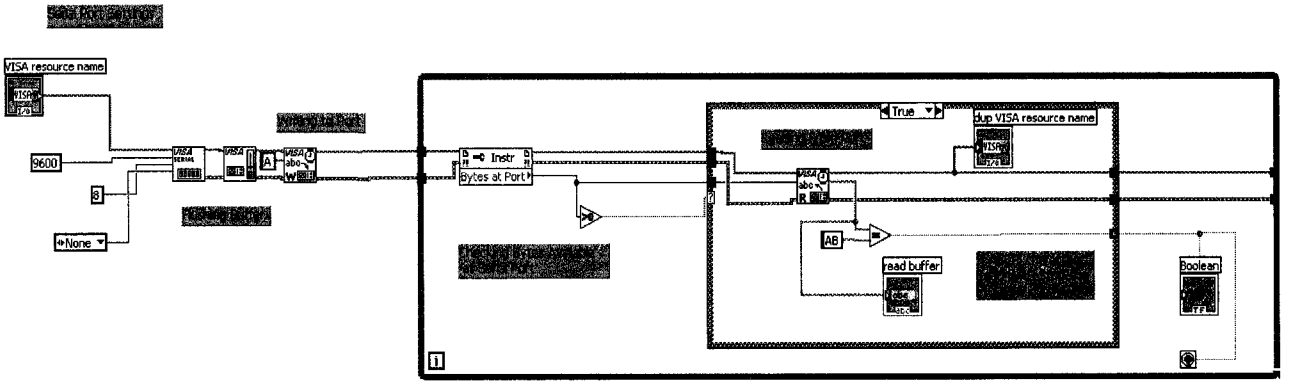

Figure A2 The LabVIEW Block Diagram for A-AB VI.

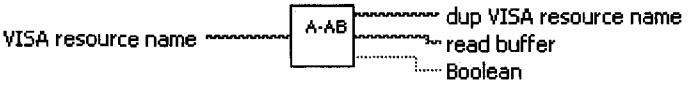

Figure A3 The LabVIEW Icon for A-AB VI.

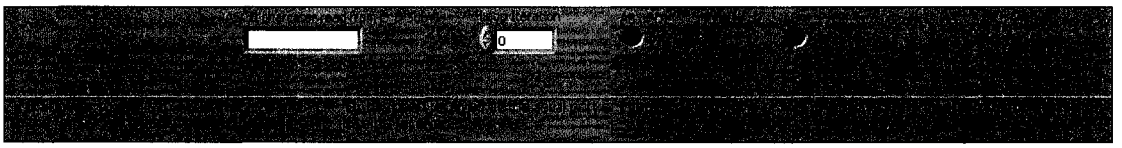

Figure A4 The LabVIEW Front Panel for AB_OR_D VI.

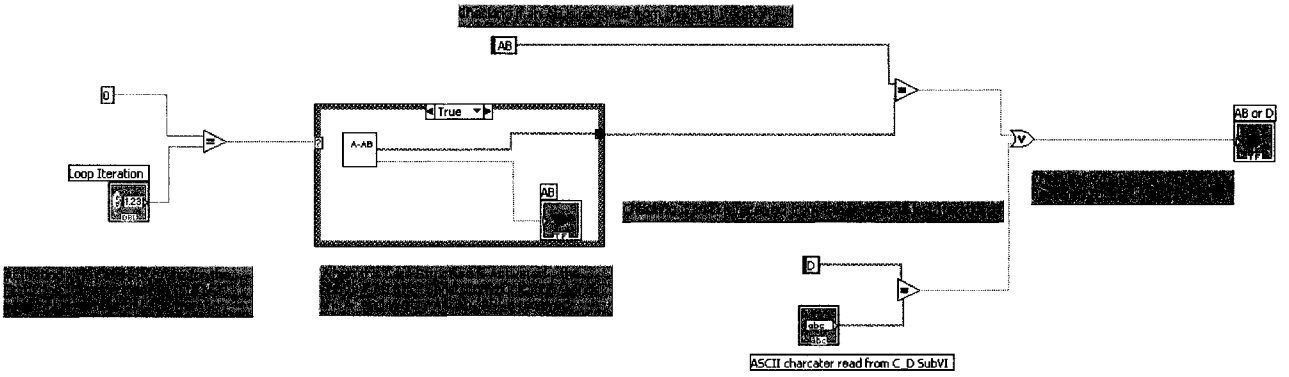

Figure A5 The LabVIEW Block Diagram for AB_OR_D VI.

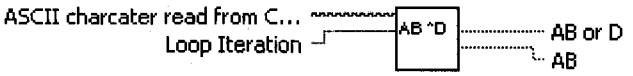

Figure A6 The LabVIEW Icon for AB_OR_D VI.

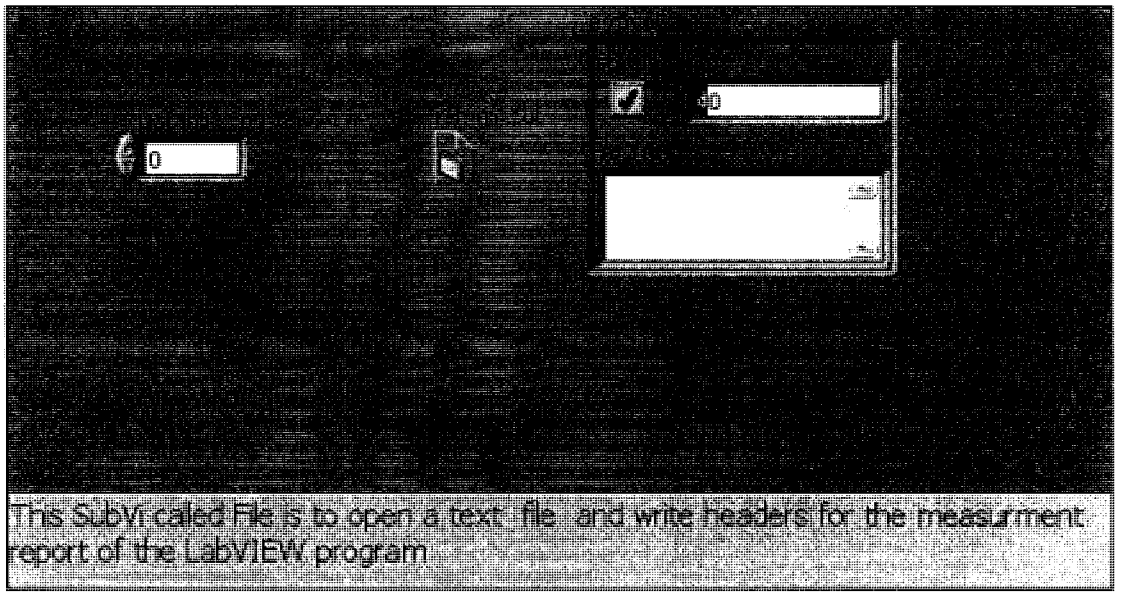

Figure A7 The LabVIEW Front Panel for File VI.

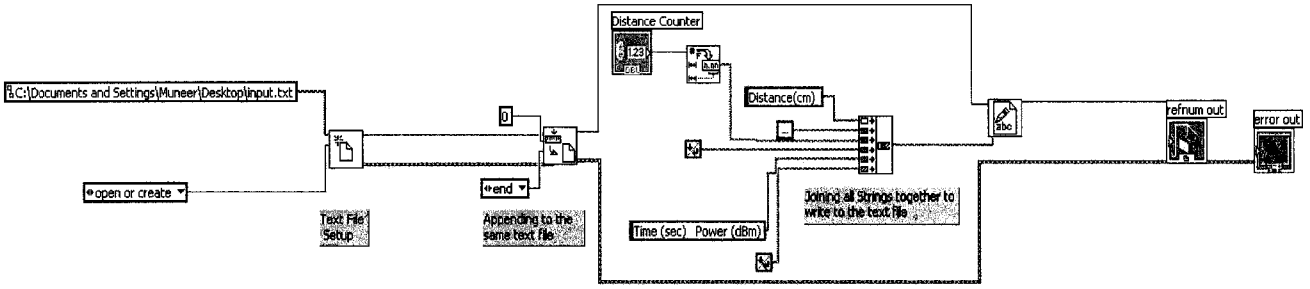

Figure A8 The LabVIEW Block Diagram for File VI.

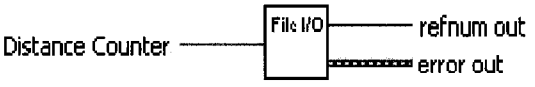

Figure A9 The LabVIEW Icon for File VI.

Figure A10 The LabVIEW Front Panel for Scale Constants VI.

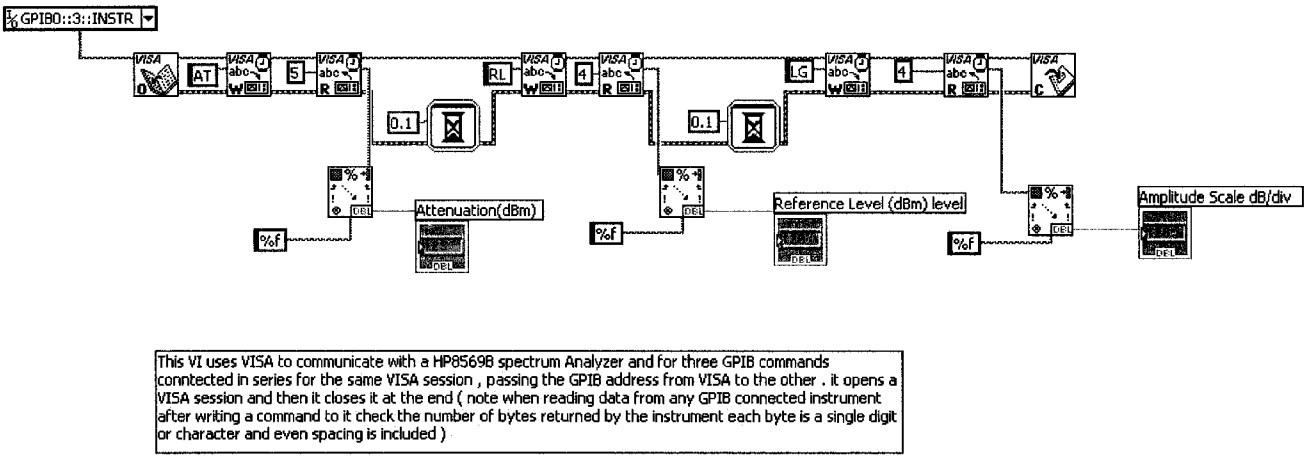

Figure A11 The LabVIEW Block Diagram for Scale Constants VI.

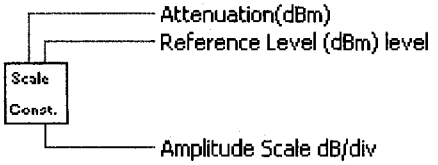

Figure A12 The LabVIEW Icon for Scale Constants VI.

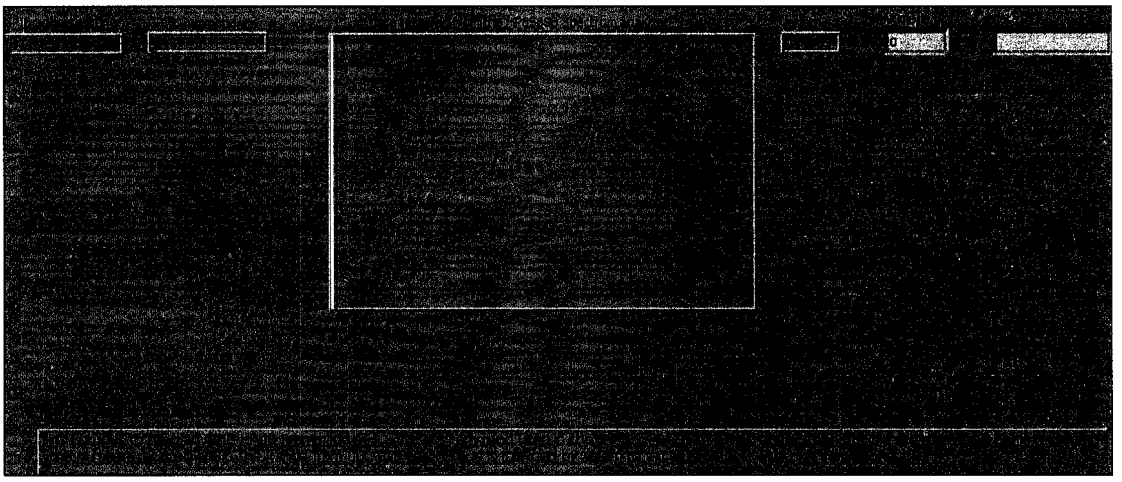

Figure A13 The LabVIEW Front Panel for GPIB VI.

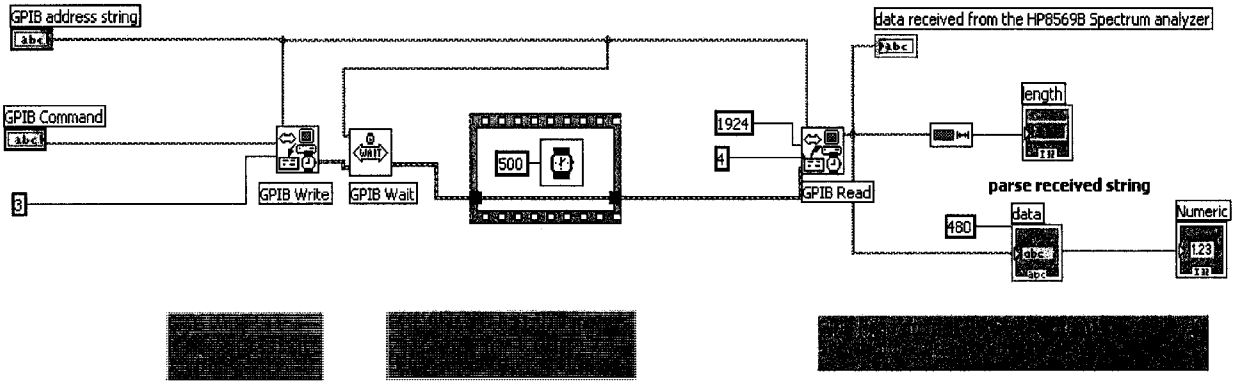

Figure A14 The LabVIEW Block Diagram for GPIB VI.

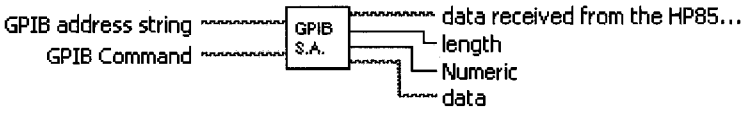

Figure A15 The LabVIEW Icon for GPIB VI.

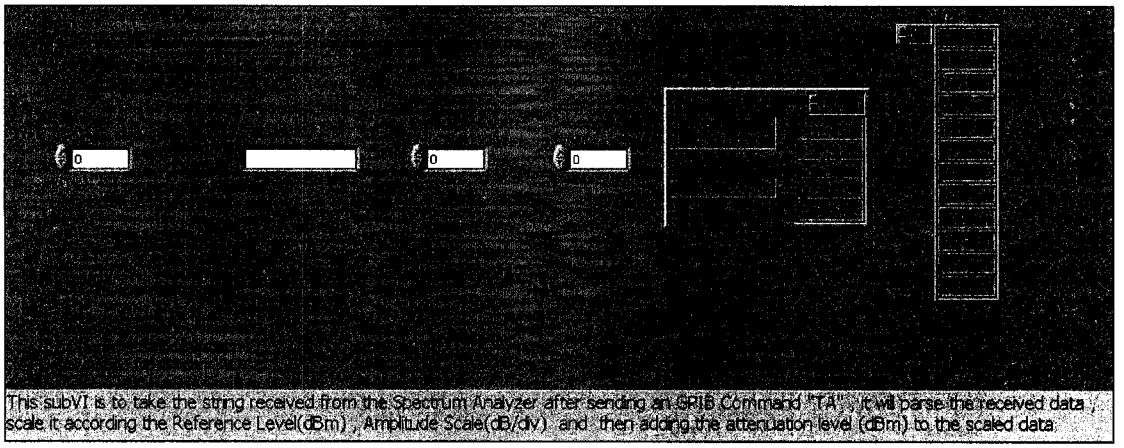

Figure A16 The LabVIEW Front Panel for Parsing VI.

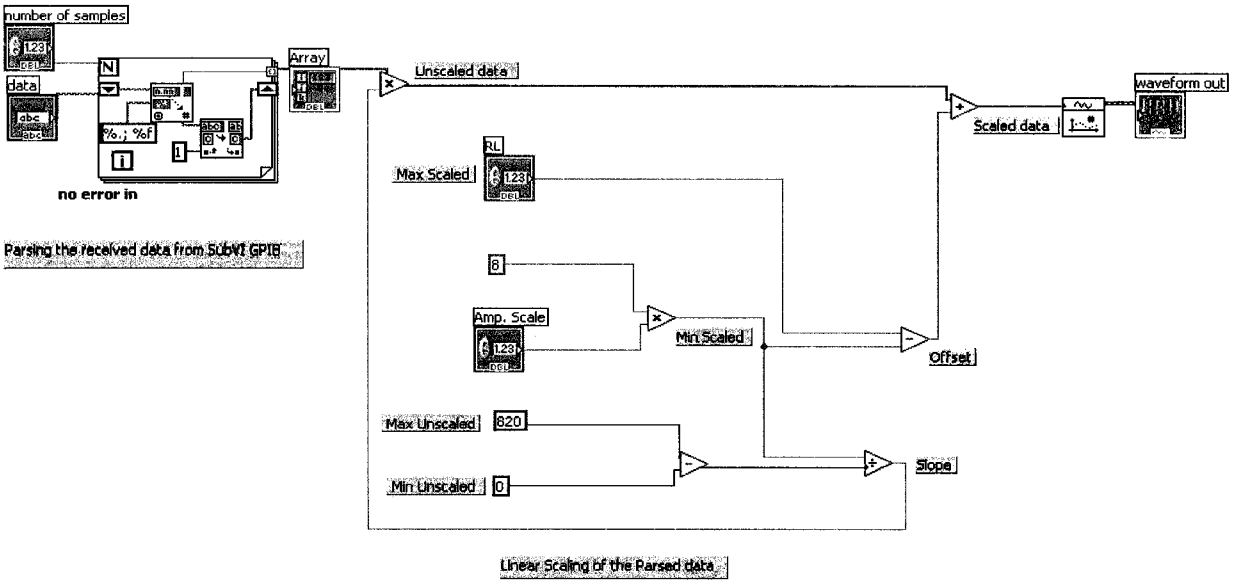

Figure A17 The LabVIEW Block Diagram for Parsing VI.

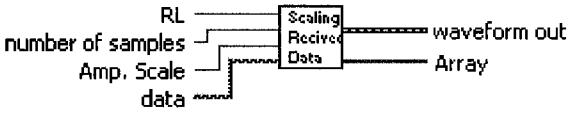

Figure A18 The LabVIEW Icon for Parsing VI.

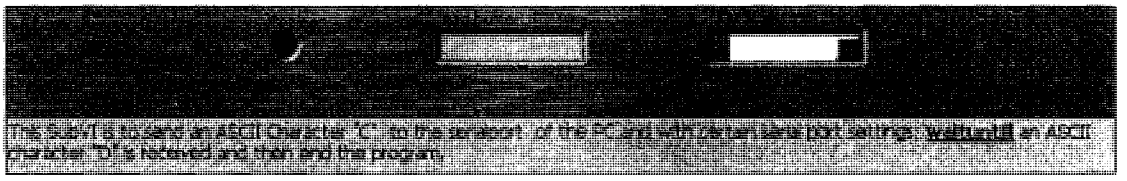

Figure A19 The LabVIEW Front Panel for C-D VI.

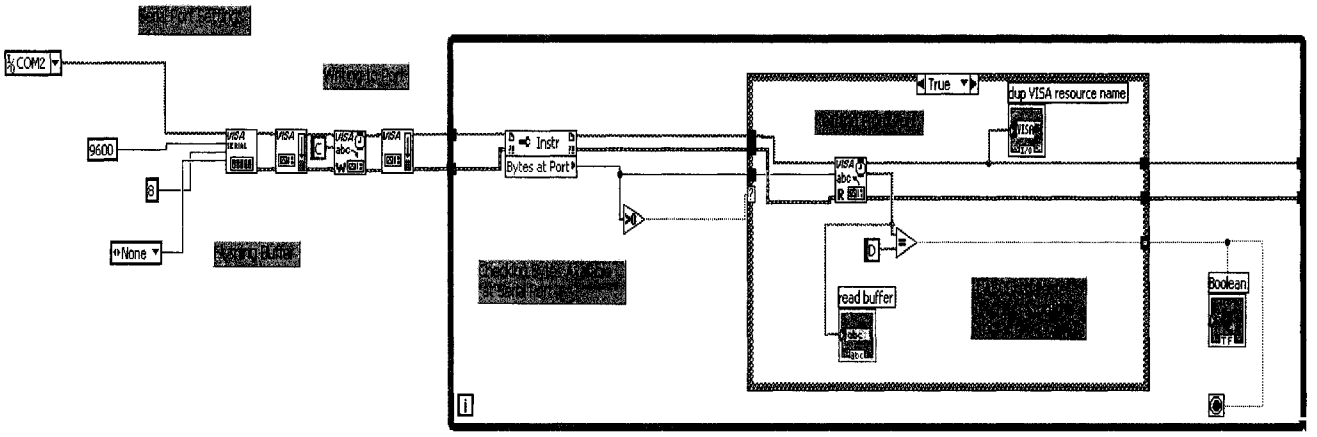

Figure A20 The LabVIEW Block Diagram for C-D VI.

Figure A21 The LabVIEW icon for C-D VI.

Figure A22 The LabVIEW Front Panel for Serial_com2E VI.

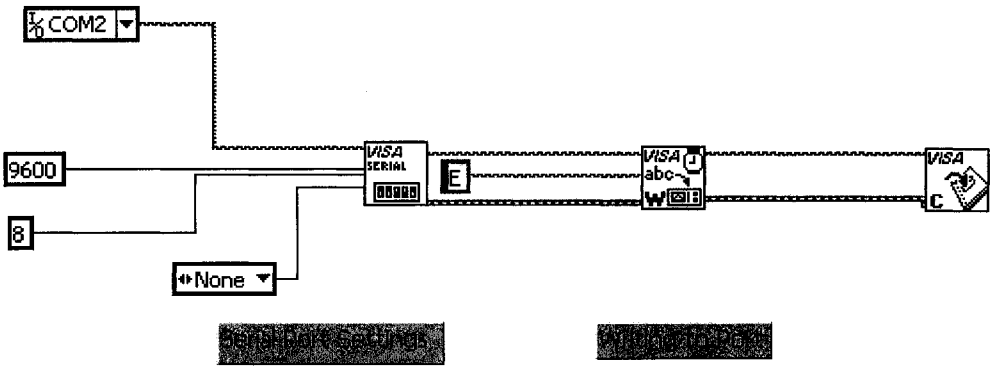

Figure A23 The LabVIEW Block Diagram for Serial_com2E VI.

Figure A24 The LabVIEW Icon for Serial_com2E VI.

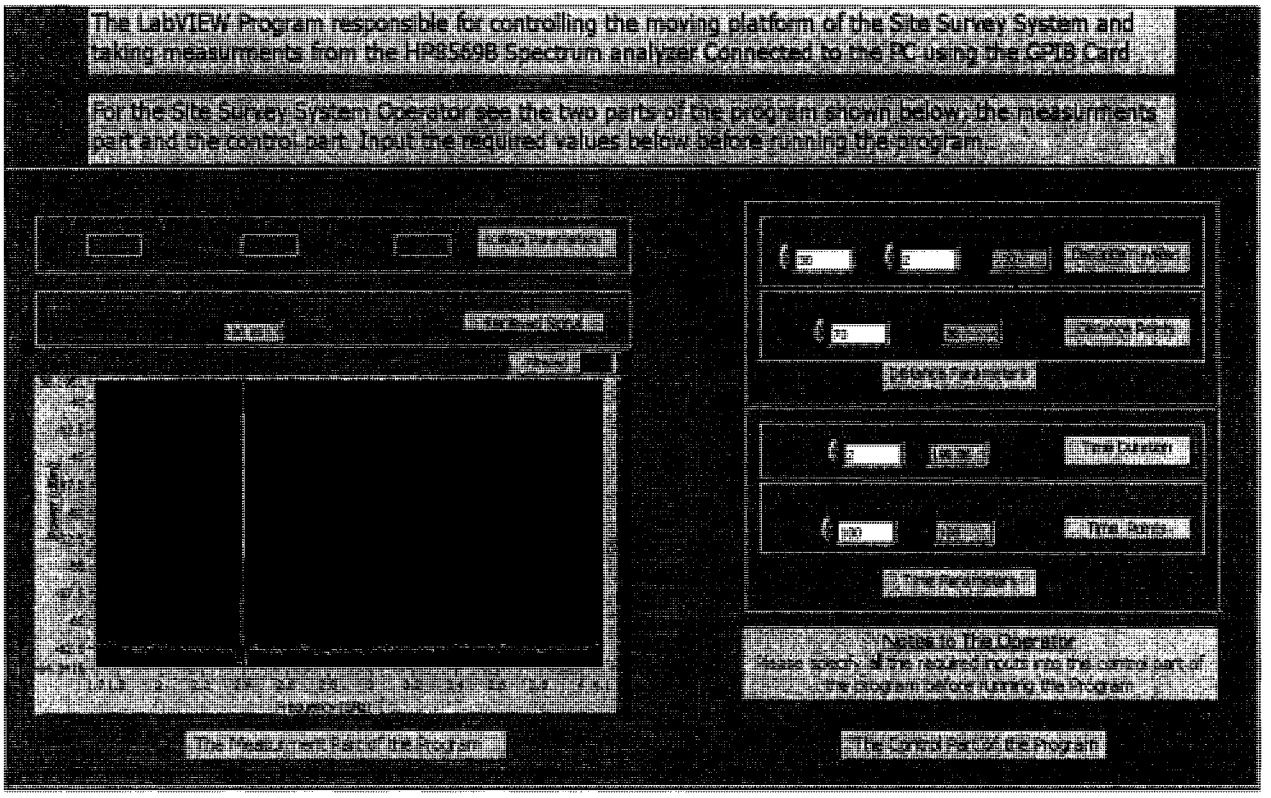

Figure A25 The LabVIEW Front Panel for control_measurments VI.

Figure A26 The LabVIEW Icon for control_measurments VI.

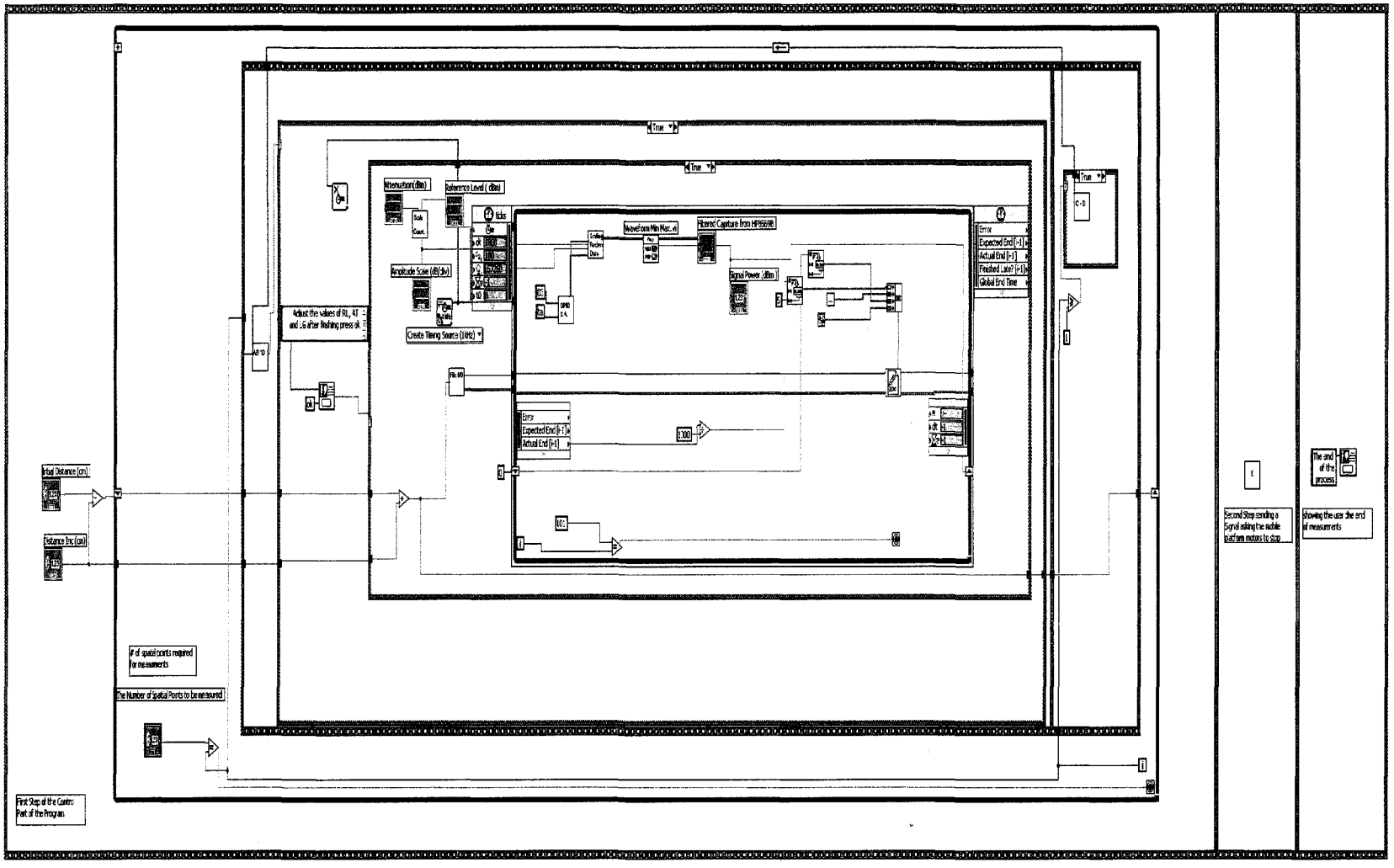

Figure A27 The LabVIEW block diagram for control_measurments.vi.

Appendix B: Moving Platform Program (using Cricket Logo Language)

```
;*********************************************************************
; Driver program required to use the sensor ports on the expansion board
;*********************************************************************
global [x]
to sensor1
output sens 1
end
to sensor2
output sens 2
end
to sensor3
output sens 3
end
to sensor4
output sens 4
end
to switch1
output (sens 1) < 128
end
to switch2
output (sens 2) < 128
end
to switch3
output (sens 3) < 128
end
to switch4
output (sens 4) < 128
end
```

```
to sens :n
bsend $112
setx bsr :n - 1
output x * 256 + bsr 0
end
to counts :n
bsend $112
setx bsr :n + 7
output x * 256 + bsr 0
end
to resetc :n
bsend $112
bsend $f + :n   ; counter 1 is at $10
bsend 0
end
to velo :n
bsend $112
setx bsr :n + 3
output x * 256 + bsr 0
end
to quad12
bsend $112
setx bsr 12
output x * 256 + bsr 0
end
to resetq12
bsend $112 bsend $14 bsend 0
end
to quad34
bsend $112
setx bsr 13
```

```
output x * 256 + bsr 0
end
to resetq34
bsend $112 bsend $15 bsend 0
end
;*********************************************************************
; end of the driver program
;*********************************************************************
;*********************************************************************
; Procedure tracksensor  used to make the  robot follow the tape
; a program used to make the robot follow the black tape
; motor c is the right motor (s4 sensor is the  right sensor)
; motor d is the left  motor  (s1 sensor  is the  left   sensor)
;*********************************************************************
;this is to define variables s1 s4 and choice
global [s1  s4 choice]
to tracksensor  ;procedure tracksensor is the function
; this set the value of the variables , if it this it is true=1 , otherwise it is  false =0
;*********************************************************************; To
make the moving platform follow a black tape on ground using  left and right
;  sensors,  if  you want to make the robot  follow a white tape just change every < 30
; to > 100
;*********************************************************************
sets1 sensor1  <  30
sets4 sensor4  <  30
;*********************************************************************
; This is used to identify the s1 sensors as the most signifcant bit (MSB)
;and the s3 as the least significant bit(LSB) ,  and  replacing them with one parameter
; called "choice"
;*********************************************************************
```

```
setchoice (s1  *  2)  +  s4
;*********************************************************************
; The value of choice (3 Decimal) (11 Binary)  means s1=1  and s4 =1
; This happens when the s1 and S4 are in the black tape
; make the power level 2 for both motors
; make them both on for 0.1 second
;*********************************************************************
if choice = 3 [ cd, setpower 2 cd, onfor 1]
;
;*********************************************************************
;The value of  choice (2 decimal) ( 10 binary  ) means  s1=1 and s4 =0
; in other words s4 is outiside the blacktape and s1 is  inside the black tape
; This happens when the robot is shifted to the right
; it asks the robot to stop the left  motor(d) and move the right motor(c) for 0.1 sec
; power level 5 for right motor c
; till it reads all sensors are one
;*********************************************************************
if choice = 2 [ d, off
    c, setpower 5  c, onfor 1 ]
;*********************************************************************
; The value of  choice (1 decimal) ( 01 binary  ) means  s1=0 and s4 =1
; in other words s1 is outside the black tape and s4 is  inside the black tape
; This happens when the robot is shifted to the left
; it asks the robot to stop the right  motor(c) and move the left motor(d) for 0.1 sec
; power  level 5 for left motor d
; till it reads all sensors are one
;*********************************************************************
 if choice = 1 [ c, off   d, setpower 5   d, onfor 1]
*********************************************************************
; this value of the variable zero means the robot is outside the track s1=0 and s4 =0
;*********************************************************************
```

```
if choice = 0 [cd, off]
end
;*********************************************************************
; End of the procedure tracksensor
;*********************************************************************
;The Start of The Program
;*********************************************************************
;*********************************************************************
;Thee program will wait until an ASCII Character is received from the serial port
; and act accordingly
;*********************************************************************
 to main
loop
[waituntil [newir?]
;*********************************************************************
;If an ASCII character A is received when this means the LabVIEW program has been
; ON and the Moving platform will send in response B (initialization of the Process)
;*********************************************************************
if  ir = 65  [send 66]
;*********************************************************************
;  If an ASCII Character B is received The  Robot will go to  Procedure main1
;*********************************************************************
if ir = 67 [ main1]
;*********************************************************************
;  If an ASCII Character E is received this acknowledges the end of the measurement
;  Campaign and Both motors C and D will stop
if ir = 69 [cd, off] ]
end
;*********************************************************************
;  Procedure main1 to move the  moving platform to the next step
;*********************************************************************
```

```
to main1
 cd, setpower  2 ;powerlevel 6 corresponds to voltage = 6x1.5=9v
loop
[ encoder
  send  68
  stop
   ]
end
;*****************************************************************
; Procedure Encoder,  reads the value of  the encoders as the robot is moving
to  encoder
; seeing the white  sector
if  sensora  >  180
[  loop [ tracksensor
       if sensora  <  180 [ stop ] ] ]
; seeing the black sector
if  sensora  <  180
 [ loop [ tracksensor
         if sensora  > 180  [ stop ] ] ]
stop
```

Appendix C Format of text file generated by the LabVIEW program

This file contains a received power at a distance of 30 cm from the receiver every 2 seconds for period of 58 seconds

```
Distance(cm)  30.000000
Time (sec)    Power (dBm)
0.00000 0.000000
1.08300 -34.736585
2.82500 -35.009756
4.87900 -34.951220
6.94200 -34.931707
8.79400 -34.931707
10.94700 -35.029268
12.82000 -35.048780
14.96300 -35.185366
16.76600 -35.146341
18.90900 -34.892683
20.81200 -35.068293
22.96500 -35.068293
25.01800 -34.736585
26.79000 -35.087805
28.94400 -34.834146
30.79600 -35.068293
32.91900 -34.814634
34.82100 -34.834146
36.97500 -34.756098
38.76700 -34.853659
40.92100 -34.912195
42.98400 -34.814634
44.75600 -35.263415
46.91900 -34.892683
48.98300 -34.931707
50.77400 -34.970732
52.89800 -35.048780
54.98100 -34.951220
56.76300 -35.048780
58.92600 -35.185366
```

Appendix D: Proof of K_G and K_{24} Having Identical Formulas

This appendix gives a proof to show that the K_G formula can be derived from the K_{24} formula, showing that both are identical. The K_G formula is (3.5)

$$K_G = \frac{\left(2\mu_2^2 - \mu_4\right)^{0.5}}{\mu_2 - \left(2\mu_2^2 - \mu_4\right)^{0.5}}. \tag{D.1}$$

Multiplying the numerator and denominator of the (D.1) by $\mu_2 + \left(2\mu_2^2 - \mu_4\right)^{0.5}$ and rearranging them results in

$$K_G = \frac{2\mu_2^2 - \mu_4 + \mu_2\left(2\mu_2^2 - \mu_4\right)^{0.5}}{\mu_4 - \mu_2^2}. \tag{D.2}$$

To make (D.2) identical to the K_{24} formula, we multiply the numerator and the denominator of (D.2) by -1 this gives

$$K_G = \frac{-2\mu_2^2 + \mu_4 - \mu_2\left(2\mu_2^2 - \mu_4\right)^{0.5}}{\mu_2^2 - \mu_4}, \tag{D.3}$$

This is the formula for K_{24} given by (3.13)

Appendix E: Path Loss Index Derivation

The square error is given by

$$Q = \sum_{i=1}^{m} \left(V_{dBi} - \left(V_{dB0} - n20\log r_i\right)\right)^2 . \tag{E.1}$$

To find the values for V_{dB0} and n that make Q minimized, taking the partial derivative of Q with respect to V_{dB0} and set it equal to zero and taking the partial derivative of Q with respect to n and set it equal to zero results in

$$\frac{\partial Q}{\partial V_{dB0}} = 2\sum_{i=1}^{m} \left(V_{dBi} - V_{dB0} + n20\log r_i\right)(-1) = 0 \tag{E.2}$$

$$\frac{\partial Q}{\partial n} = 2\sum_{i=1}^{m} \left(V_{dBi} - V_{dB0} + n20\log r_i\right)(20\log r_i) = 0 . \tag{E.3}$$

Arranging (E2) results in

$$\sum_{i=1}^{m} \left(V_{dB0} - V_{dBi} - n20\log r_i\right) = 0 . \tag{E.4}$$

Expressing V_{dB0} in terms of other quantities results in

$$V_{dB0} = \frac{\sum_{i=1}^{m} V_{dBi} + n\sum_{i=1}^{m} 20\log r_i}{m}. \tag{E.5}$$

Arranging (E3) results in

$$\sum_{i=1}^{m} V_{dBi}\, 20\log r_i - V_{dB0}\sum_{i=1}^{m} 20\log r_i + n\sum_{i=1}^{m} (20\log r_i)^2 = 0. \tag{E.6}$$

Substituting (E.5) in (E.6) and arranging to find n in terms of other quantities results in

$$n = \frac{\sum_{i=1}^{m} V_{dBi}\sum_{i=1}^{m} 20\log(r_i) - m\sum_{i=1}^{m} V_{dBi}\, 20\log(r_i)}{m\sum_{i=1}^{m} (20\log(r_i))^2 - \left(\sum_{i=1}^{m} 20\log(r_i)\right)^2}. \tag{E.7}$$